University of Alberta

Development of Valve-based Microchip for Proteomics

by

Qingye Lu

A thesis submitted to the Faculty of Graduate Studies and Research
in partial fulfillment of the requirements for the degree of

Doctor of Philosophy

Department of Chemistry

Examining Committee

Professor D. Jed Harrison, Chemistry

Professor Mark T. McDermott, Chemistry

Professor Mariusz Klobukowski, Chemistry

Professor Liang Li, Chemistry

Professor Joel Weiner, Biochemistry

Professor Aaron Wheeler, Chemistry, University of Toronto

Dedicated to my dearest

Parents, Jingxing and Wansu
Husband, Weibing
Daughter, Jessica

Abstract

Interest in microfluidic platforms has surged as an alternative for sample preparation in the past two decades, with the potential for miniaturization, portability, automation, integration and parallelism driving this research. However, it is still very challenging to develop an integrated microfluidic device for proteomic preparation for mass spectrometry analysis.

My thesis work is focused on the development of a valve-based microfluidic platform interfaced with electrospray ionization mass spectrometry for multiplexed proteomic analysis. First, techniques are developed for the fabrication and packing of multiple beds in a polydimethylsiloxane (PDMS) microdevice, which is compatible with the integration of multilayer microvalves. A soft lithography technique was used to fabricate stable weirs in microchips and new bead introduction techniques were explored for the elimination of bead introduction channels in the design. Such a combination provides a convenient, efficient and effective way for multiple bed preparation in a complex design. Next, detailed studies were carried out on the design parameters and performance of multilayer PDMS microvalves in the presence of high electric fields. These studies guided the integration of electrophoresis methods with valve-based fractionation. Finally, a coupled CE-fractionation-SPE-ESIMS peptide analysis on a totally integrated valve-based microchip is presented. We show the design and operation of a system that performs electrokinetic separation, followed by

fractionation into multiple channels, SPE extraction and sample cleanup on packed reaction beds, using a multiplexed, hydraulically valved system, with subsequent mass spectral (MS) analysis. This coupled multiple channel CE-Fractionation-SPE-ESIMS platform on valve-based microchip was successfully applied to peptide analysis.

Acknowledgements

There are many people I would like to thank for their help during my PhD study in Edmonton and I feel it is so difficult to fully express my sincere gratitude.

First and foremost, I would like to thank my supervisor, Prof. Jed Harrison, who provided me financial support, insightful guidance, enthusiastic encouragement and patience. Without his help, I could not accomplish my PhD thesis. I had no experience in microfluidics or microchip before I joined the group. I really appreciate that Prof Jed Harrison introduced me to such a wonderful and exciting field and helped me overcome so many difficulties. He taught me a lot, academically and personally. This experience will make me stronger, maturer and more confident in my future life. I am also deeply indebted that he gave me generous financial support, patience, encouragement and help during my time as a mother and a graduate.

I would like to thank all the support from my committee members, Professors Mark T. McDermott, Mariusz Klobukowski, Liang Li, Joel Weiner, Wolfgang Jäger, and thank Professor Aaron Wheeler for serving as my external committee member. I would like to say thanks to the support staff in the general office, nanofab, electronics, biological, glass shop and machine shop. Without their help, I could not accomplish my thesis. Specially, thanks for the help from Mr Paul Crothers for pressure system setup; Mr Dieter Starke for metal puncher fabrication; Dr. Ken Westra, Mrs. Stephanie Bozic, Mr. Les Schowalter, and Mr.

Table of Contents

Chapter 3 Application of Polydimethylsiloxane (PDMS)

Microvalves as Electric Switches

Chapter 4   Coupled CE-Fractionation-SPE-ESIMS Peptide Analysis on Valve-Based Microchip

Chapter 5   Conclusions and Future Thoughts

Appendix

List of Tables

List of Figures

List of Abbreviations

BSA   bovine serum albumin

CCW   control channel width

CE   capillary electrophoresis

CEC   capillary electrochromatography

CGE   capillary gel electrophoresis

COC   cyclic olefin copolymer

CP   control pressure

CZE   capillary zone electrophoresis

2DCC   two-dimensional column chromatography

DDM n-dodecyl-β-D-maltoside

2D-PAGE   two-dimensional polyacrylamide gel electrophoresis

EOF   electroosmotic flow

ESI   electrospray ionization

ESIMS   electrospray ionization mass spectrometry

FCW   fluidic channel widths

IEF   isoelectric focusing

LIF   laser induced fluorescence

LSI   large scale integration

MALDI   matrix-assisted laser desorption/ionization

MC   methylcellulose

MC	missed cleavages
MEKC	micellar electrokinetic chromatography
MS	mass spectrometry
MSL	multilayer soft lithography
MW	molecular weight
3P	punch-pack-plug
PAAm	polyacrylamide
PC	polycarbonate
PCR	polymerase chain reaction
PDMS	polydimethylsiloxane
PEG	polyethylene glycol
PFPEs	perfluoropolyethers
pI	isoelectric point
PMMA	polymethyl methacrylate
RPC	reversed-phase column
SDS	sodium dodecyl sulfate
SDS-μCGE	sodium dodecyl sulfate microcapillary gel electrophoresis
SPE	solid phase extraction
TI	trypsin inhibitor
TIC	total ion count
μCE	microchip capillary electrophoreis
μTAS	micro total analysis system
XIC	extracted ion counts

Chapter 1

Introduction

1.1 Background and Motivation

1.1.1 Proteomics

Proteomics involves the large scale study of proteins, including identification and quantification of all proteins in a biological sample (profiling proteomics), exploring protein function (functional proteomics) and tertiary protein structure (structural proteomics). Profiling proteomics is an overwhelming challenge, considering the complexity of proteins as analytes: there are about 20,000 different proteins in mammalian samples, a wide range of isoelectric points (pI), polarity, solubility and abundance, existence of post-translational modifications, nonspecific adsorption onto many surfaces, and so on.

The analytical techniques for the proteome study require high throughput, automation and multiplexed capabilities. There are two conventional methods for proteome analysis/protein identification by mass spectrometry (MS). One is a top-down method, which is performed by separating the proteins in a proteomic sample, and then identifying individual protein or its digests by mass spectrometry.[6, 7] The separation of proteins is commonly done by two-dimensional (slab) polyacrylamide gel electrophoresis (2D-PAGE) with separation in one dimension by pI and in the other dimension by molecular weight (MW), so as to provide high separation efficiency (as many as 3000-5000

different protein spots detected in a single 2D-PAGE image). The process involves a series of steps that require several days of labor-intensive laboratory work. The throughput of the 2D-PAGE based method is low since the individual extraction, digestion, and analysis of each spot from 2D-PAGE is tedious and time-consuming. It also has a limited dynamic range and relatively low sensitivity because of the types of visualization methods. The system is biased since proteins exhibiting more extreme characteristics (i.e. high or low pI, high MW, low abundance, low solubility such as membrane proteins) are often not seen.

Another method is called the bottom-up/shotgun method, which uses a chemical or an enzyme to degrade/digest all of the proteins present in the sample and then uses multi-dimensional liquid chromatography to separate peptides for tandem MS sequencing.[12, 13] This system is relatively unbiased, since some proteins with extremes can be identified. It is relatively faster, more sensitive and more amendable to automation compared to 2D-PAGE based method. However, the peptides need to be analyzed using a combination of tandem MS sequencing and very complex data analysis technique (SEQUEST), leading to limitations of system throughput.

In this context, new methods with high throughput, automation and multiplexed capabilities could be developed for proteomics, just as DNA microarrays and multiplexed sequencing for the era of high-throughput genomics. Microfluidics is one of the potentially new proteomics tools.[14]

1.1.2 Microfluidics in Proteomics

Scaling down fluidics to the microscale provides many significant advantages:[15, 16] reduced sample consumption due to the ultra-low volume used, rapid heat transfer from low thermal mass and large surface to volume ratio, faster reaction rates from large surface to volume ratio, portability, experiment parallelization without rooms of massive equipment, high speed analysis (e.g. capillary electrophoresis, CE), high sensitivity, capacity to integrate multiple components with different functionalities, the ability to arrange full automation and so on. A single integrated chip can perform all the chemical processing like sampling, pre-processing, and measurement in one assay. Such advantages, especially the automation, integration and parallelism can increase screening throughput.

Researchers have been exploring the application of microchips for proteomic analysis,[14, 17-19] such as chemical processing (e.g. enzymatic digestion), sample concentration and cleanup, separation and interfacing with mass spectrometry. To build an applicable microfluidics platform for proteomics, high peak capacity methods with fast speed for proteins or peptides separation must be devised to replace the slab-gel-based 2DGE or shotgun-based 2D column chromatography (2DCC). Impressive progresses have been made in microfluidics-based 2D separations.[18, 20] Some examples are listed in Figure 1.1. Ramsey's group plays a pioneer role in the development of multidimensional microfluidic separations by on chip hyphenation of capillary electrochromatography (CEC) or micellar electrokinetic chromatography (MEKC) with CE, using laser induced

fluorescence (LIF) detection.[21-23] The analysis of the fluorescently-labeled tryptic digest of bovine serum albumin (BSA) in an optimized MEKC-CE system within 15 min produced an impressive peak capacity of 4,200,[21] which is comparable to that of 2DGE. There are some disadvantages for this system, e.g., inconvenience for stepwise elution between the first and the second dimensions, and
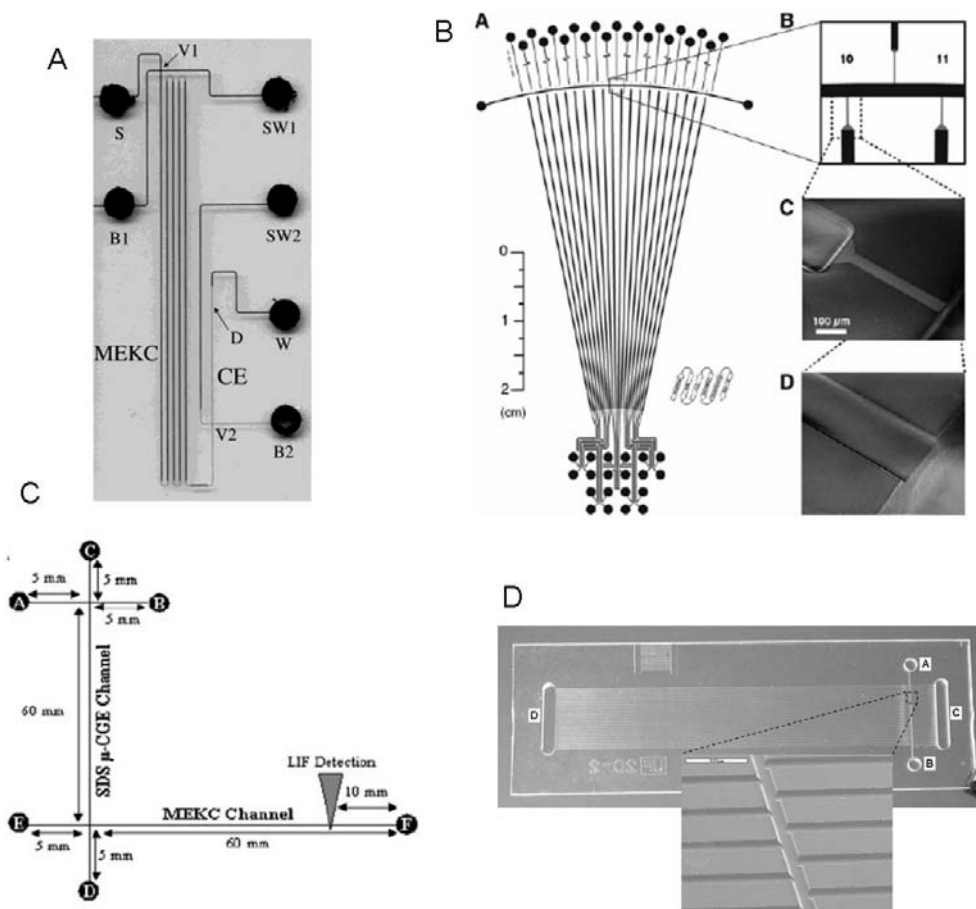
Figure 1.1 Microfluidic devices for 2-D protein separation: (A) MEKC-CE glass chip in Ramsey's group;[2, a] (B) IEF-CGE glass chip in Mathies's group;[5, a] (C) SDS-μCGE-MEKC PMMA chip in Soper's group;[10, b] (D) IEF-PAGE COC chip in Fan's group.[13, c]

---

incompatibility with MS detection from running buffers. Shadpour and Soper [24, 25] incorporated sodium dodecyl sulfate microcapillary gel electrophoresis (SDS-μCGE) with MEKC in polymethyl methacrylate (PMMA) device for proteins separation with LIF detection. A device with 11 cm separation length in both dimensions can generate peak capacities of 2600 for a biological serum sample in less than 30 min, nearly three times larger and ~ 60 times faster than that obtained using conventional isoelectric focusing (IEF)/SDS-PAGE. Other work is focused on the integration of IEF and CE, in two intersected channels,[26-28] and in numerous intersected channels with IEF solution,[29-33] immobilized pH gradients strip,[34-36] and polymerized gel plugs as pseudovalves.[37-39] Fan's group developed cyclic olefin copolymer (COC) chips for IEF-PAGE separations, using in-situ gel polymerization as pseudovalves to eliminate cross contamination. 2-D separations of four model proteins were demonstrated.[37] The device developed in Mathies' group[29] was used to perform differential separations of complex, cellular protein mixtures obtained by induced protein expression in E. coli. Other devices were tested for limited number of model protein samples. All of them used fluorescence detection and MS coupling remains questionable.

The ultimate goal of microfluidics in proteomics is to develop fully integrated platforms, including chemical processing, sample preconcentration and cleanup, separations, and interfaces with mass spectrometry, with the ability to deal with real proteomic samples and problems. Very few efforts succeeded in integrating several processes on the same device, with either column chromatography based[5, 9, 10, 40] or CE based separations.[3, 11, 41] Some examples are shown in Figure 1.2.

Harrison's group[3] developed the first fully integrated miniaturized platform for proteomic analysis, by integrating solid phase extraction (SPE) bed for sample pretreatment, a narrow channel for CE separation and a glued low-dead-volume
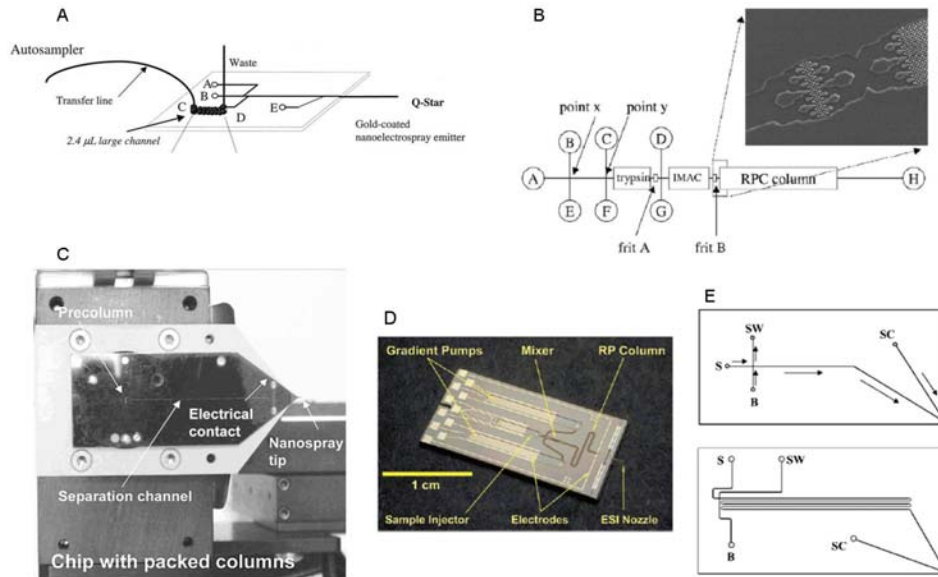
Figure 1.2 The integrated microfluidic devices for proteomics: (A) The glass chip developed in Harrison's group integrating SPE bed, CE separation, ESI tip and interfacing with an autosampler and the MS for tryptic digest analysis;[3, d] (B) The PDMS chip developed in Regnier's group integrating digestion bed, affinity chromatography bed and reversed-phase capillary electrochromatography bed;[5, e] (C) The polyimide chip developed by Agilent Technologies integrating precolumn, separation column and in-line nanospray tip;[9, a] (D) The hybrid chip made of parylene, silicon and PDMS developed by Xie *et al*., integrating gradient pump, injector, mixer, reversed-phase column, electrodes and ESI nozzle;[10, a] (E) The glass chip developed in Ramsey's group integrating CE separation and in-line ESI tip from the corner of the rectangular chip.[11, a]

_____

nanospray emitter for electrospray ionization mass spectrometry (ESIMS) coupling, using a transfer line to off-chip autosampler. The device performed a

sequential injection, preconcentration, and separation of peptide standards and tryptic digests at a rate of 12 samples per hour with a detection limit of 5 nM (25 fmol on chip), and was used for identification of 72 proteins of human prostatic cancer LNCap cells obtained from 2DGE spots. Another work presented by the same group[41] involved an integration of immobilized trypsin bead beds for on line protein digestion, CE separation of digests, and an electrospray mass spectrometry interface for automated sample processing. Rapid digestion, separation and identification of proteins were demonstrated. Regnier's group[5] developed a multicolumn polydimethylsiloxane (PDMS) chip, incorporating trypsin-derivatized bead packed column for trypsin digestion, immobilized metal affinity capture bead packed column for selection of histidine-containing tryptic peptides, and microfabricated collocated monolithic support structures for reversed-phase column (RPC) for CEC of the trapped peptides. The device was tested by running fluorescently-labeled BSA sample and its compatibility with MS detection remains unknown. Xie *et al.* developed a chip fabricated from parylene, silicon and PDMS, integrating gradient pumps, an injector, mixer, reversed-phase separation column, electrodes and ESI nozzle.[10] The system performance is similar to that of commercial nanoflow LC system, when comparing the analysis of digested BSA. Agilent Technologies developed a compact commercialized polyimide microdevice composed of a sample enrichment loop, bead-based liquid chromatography column and laser-ablated in-line nanoflow ESI emitter.[40] This system performance was verified by the analysis of BSA digest and was comparable to standard state-of-the-art nano-LC-MS. The device was further

developed for 2-Dimensional LC separation of tryptic digests and plasma samples.[9] Ramsey's group previously developed an integrated device for digestion, separation and postcolumn labeling of proteins and peptides.[42] Recently, they reported an integrated compact glass chip, including CE separation and an in-line direct ESI spray from the corner of a rectangular device.[11] CE-MS analysis of peptides and proteins were performed with the efficiencies over 10^6 plates/m.
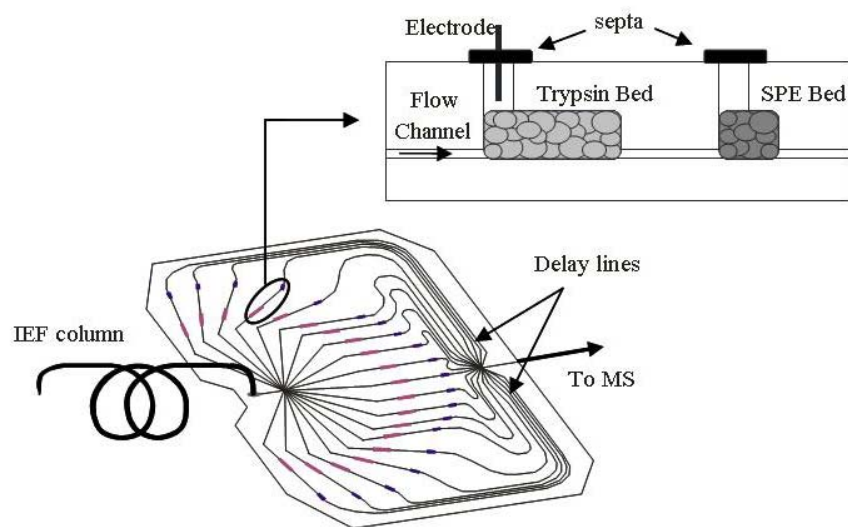
Figure 1.3 Microfluidics platform for multiplexed protein analysis explored in our group, including capillary IEF separation, sequential grounding of the electrode to drive protein fractions into 20 separate channels, online trypsin digestion and SPE of resulting peptides, and discrete fraction release to ESIMS via delay lines control. Adapted from Taylor *et al.*[1]

A fully integrated, multiplexed, automated microfluidic platform for protein processing interfaced to MS detection might be beneficial, since multiplexing of microfluidic systems for protein analysis provides a powerful route to more rapid, less costly proteomics research. Our group has been working on the integration of several protein processes together in one microchip before ESI mass spectrometry

detection, to make it compact and multifunctional. Single channel device developed by C. Wang *et al* was further developed to the two-bed system, where one bed contained trypsin digestion beads, a second bed is filled with reverse-phase beads for solid phase extraction of the eluting peptides, followed by CE-ESIMS detection for peptides elution.[43] J. Taylor tried to further develop the two-bed system into a multiplexed platform with 20 channels via delay line control, each containing the trypsin and SPE beds,[1] as shown in Figure 1.3. However, due to poor bead packing reproducibility, elution to the mass spectrometer was not directly correlated with channel length and could not be reliably foreseen. This has driven us to explore different strategies for multiplex integration, e.g., making multiple uniform columns, optimizing electrically controlled fractionation. Valve-based microchip is another attractive choice.

1.1.3 Valve-based Microchip for Integration and Multiplex Analysis

The fluid delivery and control mechanism is an important element in the design of integrated microfluidic devices. Among the methods developed to control fluid flow in microfluidics, electroosmotic flow (EOF) is the most commonly used, effective and low-dispersion method to manipulate fluids between different on-chip components, by application of an axial electric field.[44, 45] The popular integration of microchip CE based separation makes EOF control especially unique in micro total analysis system (μTAS).[46] It has some disadvantages, like susceptibility to the physicochemical properties of the fluids

(pH, ionic strength), difficulties in control due to the variability of surface properties, and limited flow rate.[44, 47]

In addition to EOF control, mechanical valves and pumps have been shown to be an alternative, potent actuation system to switch between different on-chip components. Unlike other controls, mechanical valves and pumps are completely independent of fluid properties and can be actuated individually to manipulate fluid. However, miniaturization and integration of mechanical valves and pumps on chip are challenging. Various kinds of microvalves have been explored in microfluidics for applications including flow regulation, on/off switching and sealing of liquids, gases and vacuums.[48] Among them, thin monolithic membranes[49] and in-line microvalves,[4, 50] actuated by external pneumatic pressure or vacuum, are especially applicable and suitable for large scale integration and automated multiplex analysis on chip, even though the additional external actuation system needs to be further optimized for miniaturization. These microvalves are based on a thin monolithic elastomeric silicone membrane, which can be deflected easily by pressure/vacuum to close/open the channels. In thin membrane microvalves, the features for fluidic channels and pneumatic control channels were etched separately into glass wafers, and then the wafers were coupled through a thin PDMS membrane to form normally-closed valves. The valve chamber volume can be reduced to approximately 60 nL with a chamber diameter of 1 mm. In-line microvalve devices are made of multilayered PDMS using multilayer soft lithography (MSL); basically two channels from different layers crossing each other with a thin membrane in between, and overlapping

regions forming a normally-opened valve. The valve areas can be as small as 100 μm^2. Multiplexing strategies have been explored to minimize the valve control pin-outs, a key component is named a "multiplexer" on chip.[4, 51, 52] One of the multiplexers uses 2log$_2$N horizontal valve control channels to control N vertical flow channels, called a binary tree design. Small dimensions, the relative ease of fabrication, and the successful performance of multiplexer controls with these kinds of microvalves facilitate large scale integration (LSI) on a chip.[51]

There are various application examples of the monolithic membrane microvalve-based microchip for full integration and multiplex analysis. Thin membrane microvalves in a glass device developed in Mathies' group[49] are used for fully integrated polymerase chain reaction (PCR)-CE system,[53, 54] complex DNA-based computing,[55] primarily electrophoresis-based separations for genotyping[53] and sequencing of DNA,[2] and amino acid analysis systems for space exploration.[56] Figure 1.4A gives one set of the bioprocessor for Sanger DNA sequencing,[2] integrating 250-nL thermal cycling reactors, affinity-capture sample purification chambers, high-performance capillary electrophoresis channels, and pneumatic valves and pumps onto a single device. A 10 cm wafer includes two independent sequencing systems with the microvalves for sealing and pumping. Such a system enables complete Sanger sequencing from only 1 fmol of DNA template. In-line microvalves developed in Quake's group are used for various biochemical micro total analysis, such as single cell analysis,[57-59] DNA sequencing,[60] PCR,[61] protein crystallization,[62, 63] nucleic acid extraction,[64] cell culture.[63, 65] These platforms based on multilayer soft lithography technique
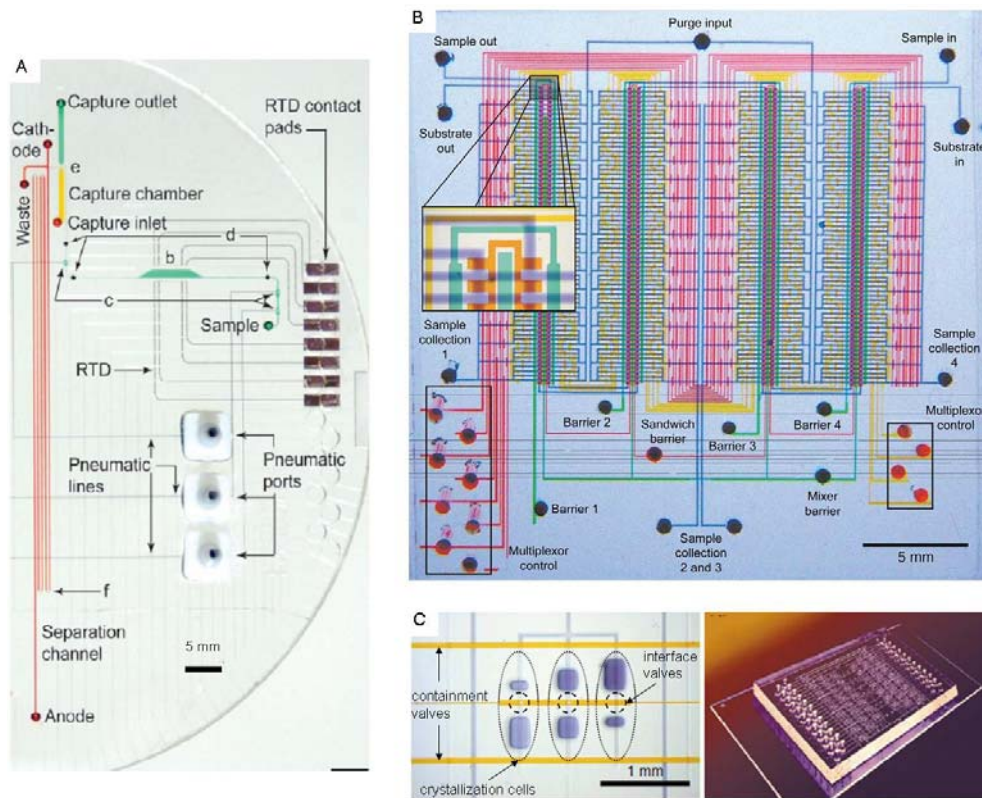
Figure 1.4 Valve-based devices for integration and multiplex analysis: (A) One set of the integrated bioprocessor[2, f] for Sanger DNA sequencing developed in Mathies' group, consisting of thermal cycling reactors, purification chambers, CE channels, resistive temperature detectors (RTDs), microvalves/pumps, pneumatic manifold channels and surface heaters; (B) A microfluidic comparator[4, g] containing 2056 microvalves and 256 subnanoliter reaction chambers in a 2.5 cm × 2.5 cm area; (C) The microfluidic protein crystallization platform, one unit cell (left) and the chip with 480 valves and 48 unit cells to perform 144 reactions in parallel (right)[8, e], adapted.

---

f.   Copyright © by the National Academy of Sciences
g.   Copyright © by the American Association for the Advancement of Science

are very unique and inspiring, due to the possibility to easily integrate mechanical

microvalves at extremely high densities and application for serial and parallel

analysis. As shown in Figure 1.4B, a device containing 2056 valves and 256 subnanoliter reaction chambers in an area of a few square centimeters was designed as a microfluidic comparator.[4] Multiplexers made with combinatorial arrays of binary valve patterns allow complex fluid control with limited number of control inputs. Quake's device was tested for the screening and selection, by loading cell mixtures, partitioning into 256 chambers with ~ 1 cell/chamber, introducing a specific substrate which becomes fluorescent by enzyme expressed in each cell, and selectively recovering cells from the addressable chambers for future analysis. Some technologies based on the MSL fabricated devices have been commercialized by the company Fluidigm, e.g., the protein crystallization platform (TOPAZ[®]). As shown in Figure 1.4C, a single device with 480 valves and 48 unit cells was designed to perform 144 parallel protein crystallization reactions.[8, 62] The key component is the simple unit cell, which consists of three pairs of microfluidic chambers with precise volumes for different reagent mixing ratios. The reagents were separated by closing interface valves and mixed via free interface diffusion by opening interface valves. Compared to conventional techniques, the platform can ensure metering and mixing of nanoliters of reagents in highly scalable fashion, faster crystal growth with a higher hit rate, and faster screening for crystallization conditions by the consumption of less sample amounts.

The challenge of making electroosmotically driven multichannel device containing SPE or chromatographic beds with identical flow resistance and the successful integration of easy-to-use pneumatic microvalves into microfluidic

system, has encouraged us to explore mechanical valve-based platform for the proteomics project. Before going into the brief introduction of the progress made in our work, some background information needs to be reviewed.

1.2 PDMS Microfluidic Devices

PDMS is a flexible polymer with repeated units of -(O-Si-(CH$_3$)$_2$)-. It has become the most popular polymer material for microchip fabrication due to several characteristics:[66, 67] low cost, low-temperature polymerization, elasticity, transparency in the visible/UV region (UV cutoff ~240 nm), biological inertness, high replication fidelity, easy sealing with smooth plastic or glass materials, and low electrical conductivity.

Soft lithography techniques have been well developed for the fabrication of PDMS devices using elastomeric polymer molding, which allows rapid prototyping of microfluidic structures.[68-71] The polymer properties (eg. easy-sealing, softness, elasticity) make the fabrication and integration of components (mixers, pumps, valves and others) particularly easy in PDMS-based system.[66] Multilayer soft lithography (MSL)[50, 72] was developed to combine soft lithography with the ability to bond multiple patterned layers of elastomer (mainly PDMS). Using this technique, valves, pumps, mixers and multiplexers can be built in the microfluidic systems to accomplish complex large scale integration.[4] The basic process of MSL is illustrated in Figure 1.5A. Two layers of elastomer with different patterns, obtained by separate replica molding, are irreversibly bonded together to create a monolithic three-dimensionally patterned structure

14
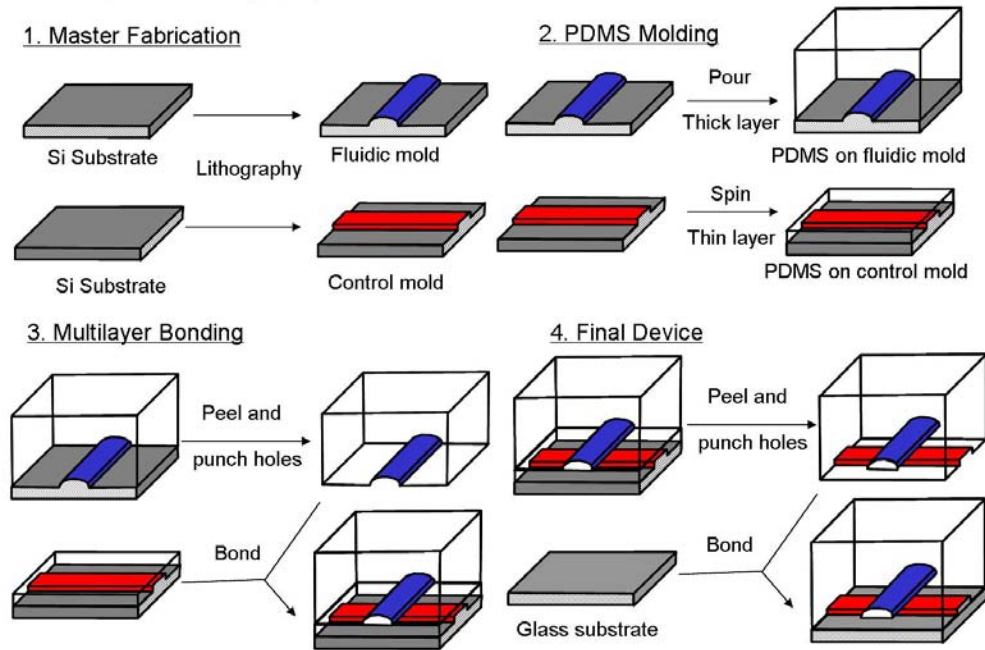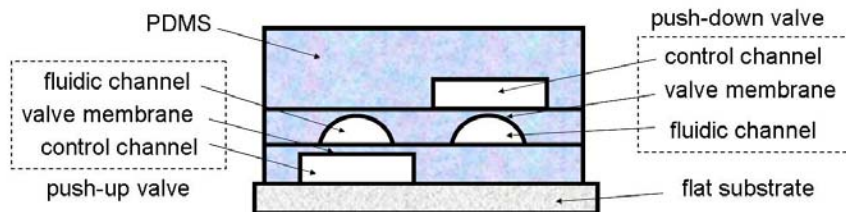
Figure 1.5 (A) The basic process flow of multilayer soft lithography and (B) the schematic side view of fabricated three-layer device with both in-line push-up valve and push-down valve.

composed entirely of elastomer. For off-ratio bonding, one layer is made with the excess of vinyl groups and the other with the excess of Si-H groups. Other techniques, which can be used for bonding, are: intermediate layers of uncured PDMS, UV-curable glue, curing agent, partial curing of PDMS, and surface oxidation of PDMS by corona discharge or plasma oxidation.[73] For oxidative bonding, silanol groups are formed and exposed at the surface, and form covalent siloxane bonds when two surfaces are put together. Multiple layers are obtained

by the repetition of the two layer fabrication process. Valves are fabricated by using crossed-channel architecture with rounded flow channels, as shown in Figure 1.5B, a three-layer device with both push-up and push-down valves. A thin layer of membrane is formed in between the two channels, where the flow channel is positioned orthogonal to the control channel. The flow channel is naturally open; it closes, when sufficient pressure is applied in the control channel, through deformation of the thin membrane, which pinches off flow in the flow channel. The flow channel must be rounded to enable complete valve closure.

Despite the many advantages of PDMS, its hydrophobicity restrains its applicability in microfluidics, especially in electrophoresis-based analysis. It has poor wettability by aqueous solutions. It swells in some organic solvents,[74] absorbs some small molecules,[75] and adsorbs some hydrophobic analytes (eg. proteins) on the channel walls.[76]

Some efforts have been made to modify PDMS to suppress nonspecific protein adsorption in electrophoresis.[76-98] There are two main approaches, dynamic coatings and permanent surface modifications. Typically, dynamic coatings are accomplished by the addition of surface-active coating materials or surface modifiers, such as polymers, charged low-MW compounds, detergents, into a background electrolyte. The hydrophobic tail of the modifiers can be adsorbed on the hydrophobic PDMS surface, which changes surface properties and suppresses analyte adsorption. It is a relatively simple and convenient process. However, it usually needs to be avoided due to the eventual desorption of the modifiers from the surface and/or detrimental effects when coupling to MS or

miniaturized chemical reactors. It may cause denaturing or destruction of protein-based analytes. There are some examples of dynamic coating of PDMS for protein or peptide analysis including using charged surfactants without the demonstration of separation (sodium dodecyl sulfate (SDS) and tetrabutylammonium chloride (TBACl)),[79] SDS for separation of two proteins,[80] a combination of *n*-dodecyl-β-D-maltoside (DDM) and SDS,[59, 81, 82] methylcellulose (MC) coating for IEF separation of proteins,[83] ionic liquid and nonionic surfactant (Imidazolium melts and Triton X-100),[84] Brij35,[85] PolyE-323,[86] in-situ grafting of polyethylene glycol (PEG) to Chitosan coated PDMS surface,[96] polyelectrolyte multilayers[78] and so on. The separations are either not satisfactory or not compatible with ESIMS detection.

Permanent modification of PDMS is preferred for MS opportunities. However, modification usually needs tedious multistep physical/chemical processing to permanently attach functional groups to the channel surface, which complicates preparation of the microchip. Typically the channel surface is activated by relatively harsh chemical reactions or high-energy sources (eg. light irradiation, corona, plasma), followed by covalent anchoring of protein-resistant polymers. Below are some examples for surface grafting in PDMS channel. Han's group reported a grafting of polyacrylamide (PAAm) by chemically initiated free radical polymerization in a microfabricated 2-D IEF-CE/CGE PDMS device,[28] through a series of steps with initial activation of the microchannel by oxygen plasma, followed by attachment of 3-methacryloxypropyl trimethoxysilane as adhesion promoter. A mixed solution containing monomer (acrylamide (AAm)) and

catalysts (ammonium persulfate and tetramethylethylenediamine) (chemical initiator) was injected into the microchannels in a nitrogen purged vacuum chamber to eliminate oxygen quenching. Finally, a dynamic coating with 0.5% MC decreased the protein adsorption further. The IEF separation test on fluorescent IEF markers in viscous solution shows better signal-to-noise ratio and separation properties compared to short fused silica cIEF. Allbritton's group developed UV-induced surface grafting of various hydrophilic homopolymers or copolymers by one step grafting,[87, 98, 99] or "surface-directed" grafting,[88, 89] Peptides separation was tested with the good theoretical plates/m (4.8 – 7.4 × 10^5 plates/m) values,[87] while no demonstration for protein separation was shown. Xiao *et al.*[90, 91] used atom-transfer radical polymerization (transition-metal-catalyzed free radical polymerization) to graft PAAm on PDMS surface. Open-channel electrophoresis for BSA labeled with fluorophor shows that nonspecific adsorption of proteins was reduced and an efficiency of 3. 3 × 10^4 plates/m was obtained. Some researchers used a sol-gel method to form a glasslike layer on a PDMS surface.[92, 93] Electrophoretic separation of tetramethylrhodamine succidimidyl ester and fluorescein-5-isothiocyanate derivatized amino acids gives efficiencies of 2.2 – 2.9 × 10^6 plates/m.[92] Lin's group developed the idea of grafting[95] or self-assembling[100] epoxy-modified polymers on PDMS, through plasma oxidation of PDMS, adsorption of epoxy-modified polymers based on H-bond interaction, and crosslinking of epoxies of polymer and silanols on oxidized PDMS surface by heating at 110 ℃. Satisfactory separations of basic proteins, peptides and DNA fragments were obtained, with an efficiency of 10^6 plates/m

for lysozyme. Other techniques used silanization as well to graft polyethylene glycol (PEG) for protein patterning,[94] though no separations were demonstrated.

Considering the challenge of PDMS surface property modification, rigid non-porous materials like glass or silicon may be a better choice for proteomic analysis, since there are well known surface properties control methods that have well established separation results. However, PDMS is an appropriate choice for the development of a complex total integration design for proteomic processing, since currently PDMS is the most widely used and easiest material for microvalve actuation. The surface problems may be resolved with the development of new materials, such as solvent-resistant soft fluoropolymers.[101, 102] The photocurable perfluoropolyethers (PFPEs) have many attractive physical properties of PDMS, but do not swell in many organic solvents. Their chemical compatibility extends the use of soft polymer microfluidic devices to organic chemical reactions, such as oligonucleotides synthesizer. The fabrication of PFPEs is relatively difficult and further exploration of solvent resistant devices in thiolene allows rapid, simple and low cost fabrication.[103]

1.3 Electrospray Ionization Mass Spectrometry

Mass spectrometry coupled with conventional separation methods is a powerful tool for protein identification. Electrospray ionization (ESI) and matrix-assisted laser desorption/ionization (MALDI) are two commonly used ionization interfaces developed for high molecular weight compounds like peptides or proteins. The compatibility with liquid separation methods (HPLC or CE) and the

fluidics in the microchannel (nL/min to µL/min) brought popularity to microchip ESI MS coupling. To build fully integrated microfluidic devices for proteomic analysis, a stable and robust microfluidic ESI MS coupling interface is essential. Several microfluidic ESI MS coupling techniques have been described [18, 104-106]: spraying directly from the edge of the chip, spraying with an inserted tapered capillary tip, spraying from micromachined/integrated tapered tips and multiplexed ESI MS. The totally integrated, no-dead-volume in-line spray seems to be most attractive. Currently, none of the coupling methods are robust. We chose to use the inserted tapered capillary tip, which is relatively good. This kind of tip has been commercialized and gives sufficiently stable spray.

ESI can be operated either in positive mode for the generation of positive gas phase ions or in negative ion mode for the generation of negative ions. The basis of the technique involves a number of steps: the formation of charged droplets, desolvation, ion generation, declustering, and ion sampling. During the formation of charged droplets in ESI, analytes and other chemical species such as salts and surfactants will compete for the limited surface space. One type of ion can dominate in the mass spectrum, while reducing the probability of detecting other types of ions in mixture, which is called ion suppression. Surfactants, such as SDS, PEG derivatives, urea and so on, can easily suppress the detection of proteins. Thus, the selection of sample preparation and separation conditions is critical. In addition, it is necessary to integrate sample preconcentration and cleanup before MS detection.

Several approaches (e.g., sample stacking, dialysis, and SPE) have been explored to conduct sample preconcentration and cleanup in microfluidic devices.[18, 107] The most common method is solid phase extraction (SPE), where hydrophobic analytes (most peptides and proteins) are adsorbed onto a solid hydrophobic medium allowing hydrophilic contaminants to be washed away. After the elimination of unwanted constituents, such as non-protein biomolecules, surfactants, and buffers, the detection sensitivity can be significantly increased. SPE also allows some flexibility in the selection of sample preparation and separation parameters. There are examples of integrating SPE on a chip, with packed bed of SPE beads,[86, 108-112] in-situ polymerized porous monolith,[113-116] and pre-formed porous membrane.[117, 118] Among them, bead packing is an amenable and straightforward way to introduce stationary phase on a chip. Lindberg et al.[86] developed a microbead-packed PDMS microchip with an integrated electrospray emitter prior to ESIMS, giving an estimated LOD of 20 fmol for angiotensin II from a sample of neuropeptides dissolved in physiological salt solution. Laurell's group[108] explored a weir based silicon microextraction chip packed with reversed phase beads for MALDI-TOF MS, succeeding in analysis of 10 nM peptide mixture, containing 2 M urea in 0.1 M phosphate-buffered saline. Performance was improved by optimizing the design from a weir to a grid structure to constrain the beads.[109] Ramsey's group[110] integrated SPE with the in-situ polymerized plug for bead trapping in microchannels coupled to micellar electrokinetic chromatography separation, capable of LIF detection of 100 pM analyte. Harrison's group[111, 112] explored a 1-μm constriction for bead trapping in a glass

microchannel, obtaining a detection limit of 70 fM for the extraction of Bodipy dyes with LIF detection. Alternate selectivity instead of mainly hydrophobic interactions (SPE) can also be used to develop integrated chip for specific purposes (selection/removal of specific proteins/peptides), e.g., immobilized metal affinity chromatography beads for the selective concentration of histidine-rich peptides[5] and porous monolith-based methods for the concentration of phosphorylated and glycosylated peptides.[119] This strategy is explored in the thesis for the fabrication of valve-based PDMS devices with double weirs for large SPE bead packing.

1.4 Microchip Capillary Zone Electrophoresis and Isoelectric Focusing

Capillary zone electrophoresis (CZE) is a popular technique in separation, based on the different migration speed of the molecules in the electric field, due to the motion of bulk solution and differential electrophoretic movement of ions or charged particles, named as electroosmotic flow (EOF) and electrophoresis respectively. EOF is the bulk solution flow in the capillary caused by the surface charges near the solution/solid interface under an axially applied electric field. The mechanism of EOF is shown in Figure 1.6. Most of solid surfaces will become charged in solution due to the ionization of the surface and/or adsorption of ionic species on the surface. When silica capillary is filled with buffer at pH above 3.0, the interior wall of the capillary will become negatively charged due to the deprotonation of silanol groups on the surface. Counterions are attracted to the

22

surface by electrostatic interactions to balance the surface charge. According to Stern's model, it forms a static Stern layer of adsorbed ions near the surface,
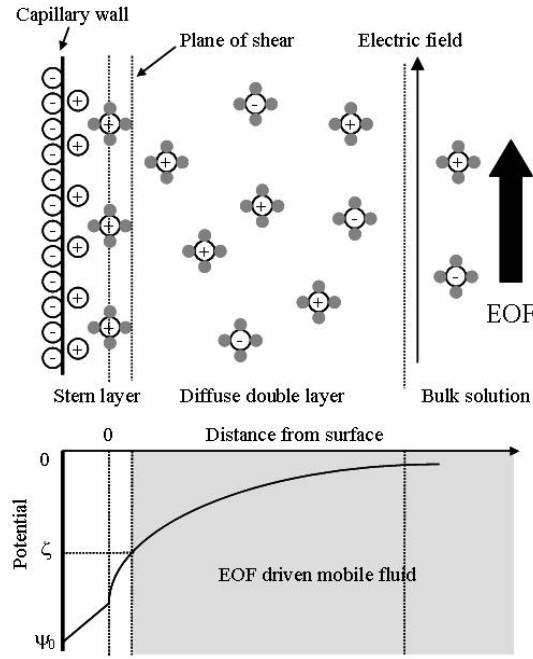
Figure 1.6 Schematic illustration of electroosmotic flow.

followed by a diffuse layer. This double layer system causes a potential difference between the wall and the solution. When electric field is applied axially, the cations in the diffuse double layer move towards the cathode. Since the cations are solvated, their movement drags the bulk solution through viscous media, which is called EOF. The velocity of EOF (v_{eof}) is defined by

$$v_{eof} = \mu_{eof} E = \frac{\varepsilon \varepsilon_o \zeta}{\eta} E \qquad (1.1)$$

where μ_{eof}, E, ε, ε_o and η are electroosmotic mobility, electric field, the permittivity of vacuum, dielectric constant and viscosity of the solution, respectively. ζ is the potential at the plane of shear in the diffuse layer, called the

23

zeta potential, which drops exponentially with distance from the surface. The zeta potential is affected by surface charge and ion concentration. Buffer ionic strength and pH can be used for zeta potential adjustment, which affects the electroosmotic mobility. Coating can influence zeta potential as well through the surface charge change.

In addition to EOF, ions or charged particles are also driven by electrophoretic forces under electric field. The electrophoretic velocity (v_{ep}) is given by

$$v_{ep} = \mu_{ep}E = \frac{q}{6\pi\eta r}E \tag{1.2}$$

where μ_{ep}, q and r are electrophoretic mobility, charge on the particle and the radius of the particle, respectively. According to the relationship, small, highly charged analytes have high electrophoretic mobilities. The effective velocity of analytes in capillary electrophoresis depends on both the EOF and the electrophoretic flow.

Microchip capillary electrophoresis, first introduced by Harrison *et al.*[120, 121] performs capillary electrophoresis on microfluidic devices. Microchip CZE has become a powerful tool in separation science, since it allows high performance separation for a variety of biomolecules with higher speed and less sample consumption, the easiness of implementation and integration, the capability to generate EOF on chip without extra mechanical pumps or valves, and parallel high throughput sample analysis by incorporation of multiple channels. Various CE schemes have been adapted on microfluidic devices for protein separation,[20, 122-124] capillary gel electrophoresis (CGE), zone electrophoresis (CZE), isoelectric

focusing (cIEF), micellar electrokinetic chromatography (MEKC) and so on, in single- or multi- dimensional way.

CZE is one of the most widely employed techniques for protein separations based on their differences in electrophoretic mobility (i.e., differences in mass-to-charge ratio). It is especially amenable to miniaturization and integration, since it does not require any stationary phases filling of the capillary. CZE has good compatibility with ESI MS, allowing fast and automatic analysis. Various chip CZE-MS interfaces were explored on glass[125-128] and PDMS[129, 130] as well, with demonstration of peptide analysis. CZE separations of proteins or peptides are run in a simple buffer, with additives/surfactant, or with wall coating to decrease the adsorption on the wall. Hauser's group developed CZE separation of proteins and peptides on a PMMA microchip with a contactless conductivity detection in an acetic buffer containing 0.05% Tween 20.[131] Shadpour *et al*. developed a 16-channel polycarbonate (PC) chip with integrated conductivity sensor array for protein separation and detection in a phosphate buffer containing 0.5 mM SDS and 0.05% methylhydroxyethycellulose.[132] Fruetel *et al*. developed a μChemlab system, where CZE separation of proteins in buffer containing 10 mM phytic acid and 2 mM N-dodecyl-N,N-dimethyl-3-ammonio-1-propanesulfonate by LIF detection.[133] Ramsey's group used MEKC-CZE separation of protein digests, where CZE is run in boric acid buffer.[21] Free solution separations of peptides were also demonstrated in PDMS devices, with acceptable efficiencies of $\sim 2{\times}10^5$ plates/m.[134] CZE separations of peptides in free solution without additives were carried out in the thesis.

IEF is a very unique electrophoretic separation technique, that can separate amphoteric molecules (e.g., proteins, peptides) based on their isoelectric points (pI) and focus them into highly resolved bands. Capillary-IEF was forecast to have peak capacity as high as 1000 for a single one dimensional run. Herr *et al.*[26] reported a peak capacity of 175 for a 2.54-cm long PMMA channel at 495 V/cm. With basic buffer (catholyte) and acidic buffer (anolyte) at the cathode and anode respectively, a mixture of ampholytes and analytes (e.g. proteins) are loaded into the separation capillary/channel. Ampholytes are used to quickly establish a stable and high-resolution pH gradient in the channel by applying an external electric field. Proteins move to the positions of their own pI values and are focused at those positions into narrow zones. The proteins may be mobilized for detection or collection through chemical mobilization, hydrodynamic mobilization or EOF driven mobilization. The first two steps are carried out after focusing, while the last one is accomplished during the focusing step. Static IEF with full elimination of EOF can provide better resolution though it is difficult to fully suppress EOF in the channel. Highly viscous solutions are usually used for further suppression of EOF. Since the first adaptation of capillary IEF to microchannels on a glass chip[135] there is abundant work on microchip IEF separations of proteins and peptides,[20, 122-124, 136, 137] which is particularly well adapted as a first dimension for 2-D separation on chips. Some work has been done in PDMS devices,[28, 83, 138-140] with the addition of methylcellulose to restrict EOF and decrease protein adsorption.

Microchip IEF has such advantages as very high resolution, low detection limit, high loading capacity and short focusing time, yet it is difficult to couple an IEF chip with ESIMS detection due to the more complicated background interferences, such as ampholytes, buffers or other coating/viscous reagents. The mobilization required for direct coupling of IEF to MS may also cause some loss of band resolution. Wen *et al*.[141] demonstrated a feasible μIEF-MS system in a polycarbonate device with an in-line ESI emitter tip. After IEF separation, the pressure driven focused bands were sprayed into the MS with the help of the sheath flow of gas and liquid along the separation channel. In this thesis, IEF separation of proteins in PDMS channel with the dynamic coating of MC was tested to illustrate the feasibility of the device's performance.

Protein sample preparation before MS includes key fractionation steps to reduce the high complexity of the samples (e.g., serum/plasma). All the separations can be considered as fractionation tools. Fractionations have been used to generate some fractions from the samples (e.g., CE, LC), or to selectively enrich/isolate/remove a particular fraction of proteins/peptides (e.g., SPE). A favorable MS detection dynamic range for the samples may be obtained by the combination of different fractionation strategies, depletion of high abundance sample, enrichment of low abundance sample and multidimensional separation. Several strategies have been developed on microchip for fractionation and collection, multidimensional electrophoresis switched by electrokinetically driven flow,[20] microvalve isolation,[28, 80] free flow electrophoresis,[142] separation fractionation and collection to multiple reservoirs/SPE columns using centrifugal

force,[143] electrokinetic sorting and collection,[144-146] and so on. An online fractionation and collection design is developed in the thesis, and it utilizes CE separation modes, multiple microvalve isolation and SPE collection.

1.5 Scope of the Thesis

The following thesis represents the development of a PDMS microfluidics platform using multilayer microfabricated valves for multiplexed proteomics analysis.

In chapter 2, we discuss technique development for fabrication and packing of multiple beds in a PDMS device, which is compatible with the integration of multilayer valves. A soft technique was used to fabricate stable weirs in PDMS, which is compatible with the multi-layered valve device used for bead trapping. New bead introduction techniques were explored for the elimination of bead introduction channels in the design. Such a combination provides a convenient, efficient and effective way for multiple bed preparation in a complex design. The packed beds were tested for solid phase extraction (SPE), in-situ protein digestion, as well as for acceptable chromatographic effects for peptides, using ESIMS detection.

In chapter 3, we present detailed studies on the design parameters and performance of multilayer PDMS microvalves in the presence of high electric fields. These studies guided the integration of electrophoresis methods with valve-based fractionation. The pressure-actuated in-channel microvalves in a push-up valve scheme are described, with a high closed-valve resistance $(100 - 1000 \text{ G}\Omega)$,

and high enough flow resistance to stop pressure-driven flow. The phenomenon of current breakthrough and electrical damge to the valves (under certain applied voltage and valve dimensions) is presented. The breakthrough mechanism was studied and the key parameters for control of the performance of the valves in strong field are discussed, specifically, the thickness of the membrane, the valve dimensions, and the surface roughness.

In chapter 4, coupled CE-fractionation-SPE-ESIMS peptide analysis on a valve-based microchip is presented. We show the design and operation of a system that performs electrokinetic separation, followed by fractionation into multiple channels, SPE extraction and sample cleanup on packed reaction beds, using a multiplexed, hydraulically valved system, with subsequent mass spectral analysis. This coupled multiple channel CE-Fractionation-SPE-ESIMS platform on valve-based microchip was successfully applied to peptide analysis.

Chapter 5 discusses future work.

1.6 References

(1)   Taylor, J. PhD theses, University of Alberta (Canada), Edmonton, 2004.

(2)   Blazej, R. G.; Kumaresan, P.; Mathies, R. A. *Proc. Natl. Acad. Sci. U. S. A.* **2006**, *103*, 7240-7245.

(3)   Li, J. J.; LeRiche, T.; Tremblay, T. L.; Wang, C.; Bonneil, E.; Harrison, D. J.; Thibault, P. *Molecular & Cellular Proteomics* **2002**, *1*, 157-168.

(4)   Thorsen, T.; Maerkl, S. J.; Quake, S. R. *Science* **2002**, *298*, 580-584.

(5)   Slentz, B. E.; Penner, N. A.; Regnier, F. E. *J. Chromatogr. A* **2003**, *984*, 97-107.

(6)   Gevaert, K.; Vandekerckhove, J. *Electrophoresis* **2000**, *21*, 1145-1154.

(7)   Baggerman, G.; Vierstraete, E.; De Loof, A.; Schoofs, L. *Comb. Chem. High Throughput Screening* **2005**, *8*, 669-677.

(8)   Hansen, C.; Quake, S. R. *Curr. Opin. Struct. Biol.* **2003**, *13*, 538-544.

(9)   Fortier, M. H.; Bonneil, E.; Goodley, P.; Thibault, P. *Anal. Chem.* **2005**, *77*, 1631-1640.

(10)   Xie, J.; Miao, Y. N.; Shih, J.; Tai, Y. C.; Lee, T. D. *Anal. Chem.* **2005**, *77*, 6947-6953.

(11)   Mellors, J. S.; Gorbounov, V.; Ramsey, R. S.; Ramsey, J. M. *Anal. Chem.* **2008**, *80*, 6881-6887.

(12)   Washburn, M. P.; Wolters, D.; Yates, J. R. *Nat. Biotechnol.* **2001**, *19*, 242-247.

(13)   Wolters, D. A.; Washburn, M. P.; Yates, J. R. *Anal. Chem.* **2001**, *73*, 5683-5690.

(14)   Lion, N.; Reymond, F.; Girault, H. H.; Rossier, J. S. *Curr. Opin. Biotechnol.* **2004**, *15*, 31-37.

(15)   Manz, A.; Harrison, D. J.; Verpoorte, E. M. J.; Fettinger, J. C.; Ludi, H.; Widmer, H. M. *Chimia* **1991**, *45*, 103-105.

(16)   Jensen, K. F. *Chem. Eng. Sci.* **2001**, *56*, 293-303.

(17)   Figeys, D.; Pinto, D. *Electrophoresis* **2001**, *22*, 208-216.

(18)   Freire, S. L. S.; Wheeler, A. R. *Lab Chip* **2006**, *6*, 1415-1423.

(19)   Lion, N.; Rohner, T. C.; Dayon, L.; Arnaud, I. L.; Damoc, E.; Youhnovski, N.; Wu, Z. Y.; Roussel, C.; Josserand, J.; Jensen, H.; Rossier, J. S.; Przybylski, M.; Girault, H. H. *Electrophoresis* **2003**, *24*, 3533-3562.

(20)   Chen, H.; Fan, Z. H. *Electrophoresis* **2009**, *30*, 758-765.

(21)   Ramsey, J. D.; Jacobson, S. C.; Culbertson, C. T.; Ramsey, J. M. *Anal. Chem.* **2003**, *75*, 3758-3764.

(22)   Rocklin, R. D.; Ramsey, R. S.; Ramsey, J. M. *Anal. Chem.* **2000**, *72*, 5244-5249.

(23)   Gottschlich, N.; Jacobson, S. C.; Culbertson, C. T.; Ramsey, J. M. *Anal. Chem.* **2001**, *73*, 2669-2674.

(24)   Osiri, J. K.; Shadpour, H.; Park, S.; Snowden, B. C.; Chen, Z. Y.; Soper, S. A. *Electrophoresis* **2008**, *29*, 4984-4992.

(25)   Shadpour, H.; Soper, S. A. *Anal. Chem.* **2006**, *78*, 3519-3527.

(26)   Herr, A. E.; Molho, J. I.; Drouvalakis, K. A.; Mikkelsen, J. C.; Utz, P. J.; Santiago, J. G.; Kenny, T. W. *Anal. Chem.* **2003**, *75*, 1180-1187.

(27)   Cong, Y. Z.; Zhang, L. H.; Tao, D. Y.; Liang, Y.; Zhang, W. B.; Zhang, Y. K. *J. Sep. Sci.* **2008**, *31*, 588-594.

(28)   Wang, Y. C.; Choi, M. N.; Han, J. Y. *Anal. Chem.* **2004**, *76*, 4426-4431.

(29)   Emrich, C. A.; Medintz, I. L.; Chu, W. K.; Mathies, R. A. *Anal. Chem.* **2007**, *79*, 7360-7366.

(30)   Chen, X. X.; Wu, H. K.; Mao, C. D.; Whitesides, G. M. *Anal. Chem.* **2002**, *74*, 1772-1778.

(31)   Becker, H.; Lowack, K.; Manz, A. *J. Micromech. Microeng.* **1998**, *8*, 24-28.

(32)   Li, Y.; Buch, J. S.; Rosenberger, F.; DeVoe, D. L.; Lee, C. S. *Anal. Chem.* **2004**, *76*, 742-748.

(33)   Yang, S.; Liu, J.; DeVoe, D. L. *Lab Chip* **2008**, *8*, 1145-1152.

(34)   Griebel, A.; Rund, S.; Schonfeld, F.; Dorner, W.; Konrad, R.; Hardt, S. *Lab Chip* **2004**, *4*, 18-23.

(35)   Usui, K.; Hiratsuka, A.; Shiseki, K.; Maruo, Y.; Matsushima, T.; Takahashi, K.; Unuma, Y.; Sakairi, K.; Namatame, I.; Ogawa, Y.; Yokoyama, K. *Electrophoresis* **2006**, *27*, 3635-3642.

(36)   Hiratsuka, A.; Kinoshita, H.; Maruo, Y.; Takahashi, K.; Akutsu, S.; Hayashida, C.; Sakairi, K.; Usui, K.; Shiseki, K.; Inamochi, H.; Nakada, Y.; Yodoya, K.; Namatame, I.; Unuma, Y.; Nakamura, M.; Ueyama, K.; Ishii, Y.; Yano, K.; Yokoyama, K. *Anal. Chem.* **2007**, *79*, 5730-5739.

(37)   Das, C.; Zhang, J.; Denslow, N. D.; Fan, Z. H. *Lab Chip* **2007**, *7*, 1806-1812.

(38)   Das, C.; Fredrickson, C. K.; Xia, Z.; Fan, Z. H. *Sens. Actuators A* **2007**, *134*, 271-277.

(39)   Liu, J. K.; Yang, S.; Lee, C. S.; Devoe, D. L. *Electrophoresis* **2008**, *29*, 2241-2250.

(40)   Yin, N. F.; Killeen, K.; Brennen, R.; Sobek, D.; Werlich, M.; van de Goor, T. V. *Anal. Chem.* **2005**, *77*, 527-533.

(41)   Wang, C.; Oleschuk, R.; Ouchen, F.; Li, J. J.; Thibault, P.; Harrison, D. J. *Rapid Commun. Mass Spectrom.* **2000**, *14*, 1377-1383.

(42)   Gottschlich, N.; Culbertson, C. T.; McKnight, T. E.; Jacobson, S. C.; Ramsey, J. M. *J. Chromatogr. B* **2000**, *745*, 243-249.

(43)   Wang, C. Ph.D. theses University of Alberta (Canada), Edmonton, 2001.

(44)   Pennathur, S. *Lab Chip* **2008**, *8*, 383-387.

(45)   Shui, L.; Pennathur, S.; Eijkel, J. C. T.; van den Berg, A. *Lab Chip* **2008**, *8*, 1010-1014.

(46)   Haeberle, S.; Zengerle, R. *Lab Chip* **2007**, *7*, 1094-1110.

(47)   Jeon, N. L.; Chiu, D. T.; Wargo, C. J.; Wu, H. K.; Choi, I. S.; Anderson, J. R.; Whitesides, G. M. *Biomedical Microdevices* **2002**, *4*, 117-121.

(48)   Oh, K. W.; Ahn, C. H. *J. Micromech. Microeng.* **2006**, *16*, R13-R39.

(49)   Grover, W. H.; Skelley, A. M.; Liu, C. N.; Lagally, E. T.; Mathies, R. A. *Sens. Actuators B* **2003**, *89*, 315-323.

(50)   Unger, M. A.; Chou, H. P.; Thorsen, T.; Scherer, A.; Quake, S. R. *Science* **2000**, *288*, 113-116.

(51)   Melin, J.; Quake, S. R. *Annu. Rev. Biophys. Biomol. Struct.* **2007**, *36*, 213-231.

(52)   Grover, W. H.; Ivester, R. H. C.; Jensen, E. C.; Mathies, R. A. *Lab Chip* **2006**, *6*, 623-631.

(53)   Lagally, E. T.; Scherer, J. R.; Blazej, R. G.; Toriello, N. M.; Diep, B. A.; Ramchandani, M.; Sensabaugh, G. F.; Riley, L. W.; Mathies, R. A. *Anal. Chem.* **2004**, *76*, 3162-3170.

(54)   Thaitrong, N.; Toriello, N. M.; Del Bueno, N.; Mathies, R. A. *Anal. Chem.* **2009**, *81*, 1371-1377.

(55)   Grover, W. H.; Mathies, R. A. *Lab Chip* **2005**, *5*, 1033-1040.

(56)   Skelley, A. M.; Scherer, J. R.; Aubrey, A. D.; Grover, W. H.; Ivester, R. H. C.; Ehrenfreund, P.; Grunthaner, F. J.; Bada, J. L.; Mathies, R. A. *Proc. Natl. Acad. Sci. U. S. A.* **2005**, *102*, 1041-1046.

(57)   Zhong, J. F.; Chen, Y.; Marcus, J. S.; Scherer, A.; Quake, S. R.; Taylor, C. R.; Weiner, L. P. *Lab Chip* **2008**, *8*, 68-74.

(58)   Marcy, Y.; Ouverney, C.; Bik, E. M.; Losekann, T.; Ivanova, N.; Martin, H. G.; Szeto, E.; Platt, D.; Hugenholtz, P.; Relman, D. A.; Quake, S. R. *Proc. Natl. Acad. Sci. U. S. A.* **2007**, *104*, 11889-11894.

(59)   Huang, B.; Wu, H. K.; Bhaya, D.; Grossman, A.; Granier, S.; Kobilka, B. K.; Zare, R. N. *Science* **2007**, *315*, 81-84.

(60)   Kartalov, E. P.; Quake, S. R. *Nucleic Acids Res.* **2004**, *32*, 2873-2879.

(61)   Ottesen, E. A.; Hong, J. W.; Quake, S. R.; Leadbetter, J. R. *Science* **2006**, *314*, 1464-1467.

(62)   Hansen, C. L.; Skordalakes, E.; Berger, J. M.; Quake, S. R. *Proc. Natl. Acad. Sci. U. S. A.* **2002**, *99*, 16531-16536.

(63)   Balagadde, F. K.; You, L. C.; Hansen, C. L.; Arnold, F. H.; Quake, S. R. *Science* **2005**, *309*, 137-140.

(64)   Hong, J. W.; Studer, V.; Hang, G.; Anderson, W. F.; Quake, S. R. *Nat. Biotechnol.* **2004**, *22*, 435-439.

(65)   Gomez-Sjoberg, R.; Leyrat, A. A.; Pirone, D. M.; Chen, C. S.; Quake, S. R. *Anal. Chem.* **2007**, *79*, 8557-8563.

(66)   Ng, J. M. K.; Gitlin, I.; Stroock, A. D.; Whitesides, G. M. *Electrophoresis* **2002**, *23*, 3461-3473.

(67)   McDonald, J. C.; Whitesides, G. M. *Acc. Chem. Res.* **2002**, *35*, 491-499.

(68)   Ziaie, B.; Baldi, A.; Lei, M.; Gu, Y. D.; Siegel, R. A. *Adv. Drug Delivery Rev.* **2004**, *56*, 145-172.

(69)   McDonald, J. C.; Duffy, D. C.; Anderson, J. R.; Chiu, D. T.; Wu, H. K.; Schueller, O. J. A.; Whitesides, G. M. *Electrophoresis* **2000**, *21*, 27-40.

(70)   Zhao, X. M.; Xia, Y. N.; Whitesides, G. M. *J. Mater. Chem.* **1997**, *7*, 1069-1074.

(71)   Xia, Y. N.; Whitesides, G. M. *Annu. Rev. Mater. Sci.* **1998**, *28*, 153-184.

(72)   Quake, S. R.; Scherer, A. *Science* **2000**, *290*, 1536-1540.

(73)   Eddings, M. A.; Johnson, M. A.; Gale, B. K. *J. Micromech. Microeng.* **2008**, *18*.

(74)   Lee, J. N.; Park, C.; Whitesides, G. M. *Anal. Chem. Symp. Ser.* **2003**, *75*, 6544-6554.

(75)   Toepke, M. W.; Beebe, D. J. *Lab Chip* **2006**, *6*, 1484-1486.

(76)   Liu, J. K.; Lee, M. L. *Electrophoresis* **2006**, *27*, 3533-3546.

(77)   Dolnik, V. *Electrophoresis* **2004**, *25*, 3589-3601.

(78)   Makamba, H.; Kim, J. H.; Lim, K.; Park, N.; Hahn, J. H. *Electrophoresis* **2003**, *24*, 3607-3619.

(79)   Ocvirk, G.; Munroe, M.; Tang, T.; Oleschuk, R.; Westra, K.; Harrison, D. J. *Electrophoresis* **2000**, *21*, 107-115.

(80)   Dodge, A.; Brunet, E.; Chen, S. L.; Goulpeau, J.; Labas, V.; Vinh, J.; Tabeling, P. *Analyst* **2006**, *131*, 1122-1128.

(81)   Huang, B.; Wu, H. K.; Kim, S.; Zare, R. N. *Lab Chip* **2005**, *5*, 1005-1007.

(82)   Huang, B.; Kim, S.; Wu, H.; Zare, R. N. *Anal. Chem.* **2007**, *79*, 9145-9149.

(83)   Cui, H. C.; Horiuchi, K.; Dutta, P.; Ivory, C. F. *Anal. Chem.* **2005**, *77*, 1303-1309.

(84)   Xu, Y. H.; Jiang, H.; Wang, E. K. *Electrophoresis* **2007**, *28*, 4597-4605.

(85)   Dou, Y. H.; Bao, N.; Xu, J. J.; Meng, F.; Chen, H. Y. *Electrophoresis* **2004**, *25*, 3024-3031.

(86)   Lindberg, P.; Dahlin, A. P.; Bergstrom, S. K.; Thorslund, S.; Andren, P. E.; Nikolajeff, F.; Bergquist, J. *Electrophoresis* **2006**, *27*, 2075-2082.

(87)   Hu, S. W.; Ren, X. Q.; Bachman, M.; Sims, C. E.; Li, G. P.; Allbritton, N. *Electrophoresis* **2003**, *24*, 3679-3688.

(88)   Hu, S. W.; Ren, X. Q.; Bachman, M.; Sims, C. E.; Li, G. P.; Allbritton, N. L. *Anal. Chem.* **2004**, *76*, 1865-1870.

(89)   Hu, S. W.; Brittain, W. J. *Macromolecules* **2005**, *38*, 6592-6597.

(90)   Xiao, D. Q.; Zhang, H.; Wirth, M. *Langmuir* **2002**, *18*, 9971-9976.

(91)   Xiao, D. Q.; Van Le, T.; Wirth, M. J. *Anal. Chem.* **2004**, *76*, 2055-2061.

(92)   Roman, G. T.; Hlaus, T.; Bass, K. J.; Seelhammer, T. G.; Culbertson, C. T. *Anal. Chem.* **2005**, *77*, 1414-1422.

(93)   Abate, A. R.; Lee, D.; Do, T.; Holtze, C.; Weitz, D. A. *Lab Chip* **2008**, *8*, 516-518.

(94)   Papra, A.; Bernard, A.; Juncker, D.; Larsen, N. B.; Michel, B.; Delamarche, E. *Langmuir* **2001**, *17*, 4090-4095.

(95)   Wu, D. P.; Zhao, B. X.; Dai, Z. P.; Qin, J. H.; Lin, B. C. *Lab Chip* **2006**, *6*, 942-947.

(96)   Wang, A. J.; Xu, J. J.; Chen, H. Y. *J. Chromatogr. A* **2007**, *1147*, 120-126.

(97)   Muck, A.; Svatos, A. *Talanta* **2007**, *74*, 333-341.

(98)   Hu, S. W.; Ren, X. Q.; Bachman, M.; Sims, C. E.; Li, G. P.; Allbritton, N. L. *Langmuir* **2004**, *20*, 5569-5574.

(99)   Hu, S. W.; Ren, X. Q.; Bachman, M.; Sims, C. E.; Li, G. P.; Allbritton, N. *Anal. Chem.* **2002**, *74*, 4117-4123.

(100)   Wu, D. P.; Qin, J. H.; Lin, B. C. *Lab Chip* **2007**, *7*, 1490-1496.

(101)   Rolland, J. P.; Van Dam, R. M.; Schorzman, D. A.; Quake, S. R.; DeSimone, J. M. *J. Am. Chem. Soc.* **2004**, *126*, 2322-2323.

(102)   Rolland, J.; van Dam, R. M.; Hagberg, E. C.; Carter, K. R.; Quake, S. R.; DeSimone, J. *Abstracts Of Papers Of The American Chemical Society* **2004**, *228*, U386-U386.

(103)   Hung, L. H.; Lin, R.; Lee, A. P. *Lab Chip* **2008**, *8*, 983-987.

(104)   Sung, W. C.; Makamba, H.; Chen, S. H. *Electrophoresis* **2005**, *26*, 1783-1791.

(105)   Koster, S.; Verpoorte, E. *Lab Chip* **2007**, *7*, 1394-1412.

(106)   Foret, F.; Kusy, P. *Electrophoresis* **2006**, *27*, 4877-4887.

(107)   Chen, X.; Cui, D. F. *Microsystem Technologies-Micro-And Nanosystems-Information Storage And Processing Systems* **2009**, *15*, 667-676.

(108)   Ekstrom, S.; Malmstrom, J.; Wallman, L.; Lofgren, M.; Nilsson, J.; Laurell, T.; Marko-Varga, G. *Proteomics* **2002**, *2*, 413-421.

(109)   Bergkvist, J.; Ekstrom, S.; Wallman, L.; Lofgren, M.; Marko-Varga, G.; Nilsson, J.; Laurell, T. *Proteomics* **2002**, *2*, 422-429.

(110)   Ramsey, J. D.; Collins, G. E. *Anal. Chem.* **2005**, *77*, 6664-6670.

(111)   Oleschuk, R. D.; Shultz-Lockyear, L. L.; Ning, Y. B.; Harrison, D. J. *Anal. Chem.* **2000**, *72*, 585-590.

(112)   Jemere, A. B.; Oleschuk, R. D.; Ouchen, F.; Fajuyigbe, F.; Harrison, D. J. *Electrophoresis* **2002**, *23*, 3537-3544.

(113) Yu, C.; Davey, M. H.; Svec, F.; Frechet, J. M. J. *Anal. Chem.* **2001**, *73*, 5088-5096.

(114) Liu, J. K.; Chen, C. F.; Tsao, C. W.; Chang, C. C.; Chu, C. C.; Devoe, D. L. *Anal. Chem.* **2009**, *81*, 2545-2554.

(115) Lee, E. Z.; Huh, Y. S.; Jun, Y. S.; Won, H. J.; Hong, Y. K.; Park, T. J.; Lee, S. Y.; Hong, W. H. *J. Chromatogr. A* **2008**, *1187*, 11-17.

(116) Tan, A. M.; Benetton, S.; Henion, J. D. *Anal. Chem.* **2003**, *75*, 5504-5511.

(117) Lion, N.; Gellon, J. O.; Jensen, H.; Girault, H. H. *J. Chromatogr. A* **2003**, *1003*, 11-19.

(118) Lion, N.; Gobry, V.; Jensen, H.; Rossier, J. S.; Girault, H. *Electrophoresis* **2002**, *23*, 3583-3588.

(119) Mao, X. L.; Luo, Y.; Dai, Z. P.; Wang, K. Y.; Du, Y. G.; Lin, B. C. *Anal. Chem.* **2004**, *76*, 6941-6947.

(120) Harrison, D. J.; Manz, A.; Fan, Z. H.; Ludi, H.; Widmer, H. M. *Anal. Chem.* **1992**, *64*, 1926-1932.

(121) Harrison, D. J.; Fluri, K.; Seiler, K.; Fan, Z. H.; Effenhauser, C. S.; Manz, A. *Science* **1993**, *261*, 895-897.

(122) Dolnik, V.; Liu, S. R. *J. Sep. Sci.* **2005**, *28*, 1994-2009.

(123) Peng, Y. Y.; Pallandre, A.; Tran, N. T.; Taverna, M. *Electrophoresis* **2008**, *29*, 157-178.

(124) Wu, D. P.; Qin, J. H.; Lin, B. C. *J. Chromatogr. A* **2008**, *1184*, 542-559.

(125) Zhang, B.; Liu, H.; Karger, B. L.; Foret, F. *Anal. Chem.* **1999**, *71*, 3258-3264.

(126) Lazar, I. M.; Ramsey, R. S.; Sundberg, S.; Ramsey, J. M. *Anal. Chem.* **1999**, *71*, 3627-3631.

(127) Li, J. J.; Wang, C.; Kelly, J. F.; Harrison, D. J.; Thibault, P. *Electrophoresis* **2000**, *21*, 198-210.

(128) Mao, X. L.; Chu, I. K.; Lin, B. C. *Electrophoresis* **2006**, *27*, 5059-5067.

(129) Thorslund, S.; Lindberg, P.; Andren, P. E.; Nikolajeff, F.; Bergquist, J. *Electrophoresis* **2005**, *26*, 4674-4683.

(130) Dahlin, A. P.; Wetterhall, M.; Liljegren, G.; Bergstrom, S. K.; Andren, P.; Nyholm, L.; Markides, K. E.; Bergquist, J. *Analyst* **2005**, *130*, 193-199.

(131) Abad-Villar, E. M.; Kuban, P.; Hauser, P. C. *Electrophoresis* **2005**, *26*, 3609-3614.

(132) Shadpour, H.; Hupert, M. L.; Patterson, D.; Liu, C. G.; Galloway, M.; Stryjewski, W.; Goettert, J.; Soper, S. A. *Anal. Chem.* **2007**, *79*, 870-878.

(133) Fruetel, J. A.; Renzi, R. F.; VanderNoot, V. A.; Stamps, J.; Horn, B. A.; West, J. A. A.; Ferko, S.; Crocker, R.; Bailey, C. G.; Arnold, D.; Wiedenman, B.; Choi, W. Y.; Yee, D.; Shokair, I.; Hasselbrink, E.; Paul, P.; Rakestraw, D.; Padgen, D. *Electrophoresis* **2005**, *26*, 1144-1154.

(134) Lacher, N. A.; de Rooij, N. F.; Verpoorte, E.; Lunte, S. M. *J. Chromatogr. A* **2003**, *1004*, 225-235.

(135) Hofmann, O.; Che, D. P.; Cruickshank, K. A.; Muller, U. R. *Anal. Chem.* **1999**, *71*, 678-686.

(136) Sommer, G. J.; Hatch, A. V. *Electrophoresis* **2009**, *30*, 742-757.

(137) Shimura, K. *Electrophoresis* **2009**, *30*, 11-28.

(138) Cui, H. C.; Horiuchi, K.; Dutta, P.; Ivory, C. F. *Anal. Chem.* **2005**, *77*, 7878-7886.

(139) Han, J.; Singh, A. K. *J. Chromatogr. A* **2004**, *1049*, 205-209.

(140) Li, Y.; DeVoe, D. L.; Lee, C. S. *Electrophoresis* **2003**, *24*, 193-199.

(141) Wen, J.; Lin, Y. H.; Xiang, F.; Matson, D. W.; Udseth, H. R.; Smith, R. D. *Electrophoresis* **2000**, *21*, 191-197.

(142) Kohlheyer, D.; Eijkel, J. C. T.; van den Berg, A.; Schasfoort, R. B. M. *Electrophoresis* **2008**, *29*, 977-993.

(143) Spesny, M.; Foret, F. *Electrophoresis* **2003**, *24*, 3745-3747.

(144) Zalewski, D. R.; Schlautmann, S.; Gardeniers, H. *Electrophoresis* **2008**, *29*, 4887-4893.

(145) Zalewski, D. R.; Schlautmann, S.; Schasfoort, R. B. M.; Gardeniers, H. *Lab Chip* **2008**, *8*, 801-809.

(146) Wang, Z. Ph.D. theses, University of Alberta (Canada), Edmonton, 2007.

Chapter 2

Punch-Pack-Plug (3P) Technique Combined with Weir Traps in Two-Layer Polydimethylsiloxane (PDMS) Devices with Microvalves for Multiple Bead Packing[*]

2.1 Introduction

Polydimethylsiloxane (PDMS) microfluidic devices have been widely explored for applications since Quake *et al.* expanded soft lithography to multilayer soft lithography for fabrication of functional multilayered PDMS devices.[1] Such PDMS devices are capable of integrating multiple simple components, mixers, pumps, valves, multiplexers and other functional analytical components in a complex way on a single chip to perform multiple functions. The valve-based multilayer PDMS platform has shown its power in analyses which need high throughput, operation automation and large-scale integration.[2-5] For biological applications, integration of chromatographic columns or reactions beds is necessary, either for separation,[6, 7] selective sample trapping,[8-10] chemical reactions[11-13] or other surface-based bioanalysis.[14-16] Packing beads is the most straightforward and popular way to introduce solid phases into microfluidic

---

devices. Beads can provide large surface to volume ratios and various surface chemistries for analytical operations. However, fabrication and packing of multiple beds for multiple channel analysis is a big challenge in complicated valve-based PDMS devices.

The first strategy for on-chip bead-based chemistry is to flow and pack the packing material into the microchannels. A number of different immobilization methods have been explored to retain beads in specific locations within devices, such as physical barriers, surface immobilization, magnetic fields and so on.[14, 17,] [18] The fabrication of physical barriers has been particularly popular. An elegant weir design in glass devices was initially developed by Harrison's group,[6] where 10-μm-deep channels were obstructed by 9 μm high weirs to leave a 1 μm gap to trap beads within a bed, while allowing for reagent delivery and transport. The same principle was used to trap beads for electrochromatography,[6, 9] highly sensitive solid phase extraction (SPE),[9] and on-chip protein digestion by trypsin beads.[11] Such weir-style design was applied in silicon chips in Laurell's group, with reverse phase bead packing for purification and enrichment of peptide mixtures containing urea.[19] Another kind of in-situ/flexible weir was developed in multilayered PDMS devices for bead trapping,[10, 13, 20] by using column valves or sieving valves. A slightly opened PDMS valve on a fluidic channel with a rounded profile, called a column valve, can trap beads while allowing fluidic flow. A sieve valve is a valve intentionally designed to create a leak, using a flow channel with a rectangular profile instead of a rounded profile. Column valves can be replaced by sieve valves to minimize the escape of beads through the valve. It

39

is very sensible to use valves for the formation of an in-situ weir, as the beads can be easily washed away when the valve is opened and a new bed regenerated, even though the packing quality may be affected by the distorted bed shape at the valve interface. Another clever approach to barrier formation is to fabricate pillars/grids as filters to retain particles in a channel, while allowing solution flow, as has been fabricated in silicon by deep reactive ion etching to constrain beads.[21] A grid structure was fabricated on a silicon chip to retain beads for on-line proteomic sample preparation.[8] Similar structures were also realized in PDMS devices,[16, 22-24] where the post design was limited by the aspect ratio of PDMS, but details were not discussed. There are other techniques, such as packing with the help of a magnet,[25] where only magnetic beads can be used; packing by the use of a "keystone effect";[26] using larger beads to trap smaller beads;[24] packing by forming frits with polymer reactions/nanoglues/sol-gel techniques;[27, 28] or other methods.[14, 18] Each method may have drawbacks in fabrication or application. Overall, the weir-design is relatively straightforward and convenient for application in a PDMS device, whereas the formation of polymers within devices to create beds is strictly limited due to swelling, reactions of PDMS, or oxygen transport within PDMS.

Side channels or main channels are used to introduce beads into beds, while allowing a particle-free channel for sample and reagent delivery. When filling a bed from the main channel only a single frit or weir can be used to trap the particles. This approach can cause problems with bed stability, density and uniformity. In designs with side channels connected to the beds, the side channels

40

are either permanently blocked by forming solid plugs, or temporarily blocked using valves in PDMS devices. These techniques are acceptable for less complicated devices, but are not convenient or efficient for application in more complex devices. For example, with sieving valves for bead trapping and valves for side channel blocking, a four-bed PDMS device resulted in complex design,[13] clearly leading to large challenges when trying to make 8, 16 or more beds.

Here we report a fabrication and packing method for loading multiple beds in PDMS devices that is compatible with multiplexed valve-based devices. A stable weir structure made in PDMS for bead packing, compatible with multi-layered valve devices, is reported here. In addition, new bead introduction techniques were explored, which eliminate bead introduction channels in the design. Such a combination provides a convenient, efficient and effective method for multiple bed preparation in a complex design. The packed beds were tested for SPE, in-situ protein digestion, as well as chromatographic effects for peptides, using electrospray ionization mass spectrometry (ESIMS) detection.

2.2 Experimental

2.2.1 Chemicals and Reagents

Cytochrome c (horse heart), trypsin (bovine pancreas), ammonium bicarbonate, ammonium hydroxide were obtained from Sigma-Aldrich (Oakville, ON, Canada). The elution buffer solution was made of formic acid (Fluka, Buchs, SG, Switzerland) and LC-MS grade methanol (Riedel-de Haen, Seelze, Germany). All aqueous solutions were prepared in deionized water (Millipore Canada,

Mississauga, ON) and filtered through 0.2 μm filters (Nalgene, Rochester, NY, USA) prior to use.

On-chip protein digestion was performed by injecting protein solution into the SPE bed, washing with water, loading trypsin buffer solution (pH 8.6) into the bed region and incubating at room temperature for 30 min, washing with water, and, finally, eluting the digests to ESIMS (elution buffer 50% methanol containing 0.1 M formic acid). Off-chip protein digestion was done with immobilized TPCK-trypsin beads (Pierce, Rockford, IL, USA) at 37 ℃ in the digestion buffer (pH 8.0), according to the manufacturer's procedure.

2.2.2 Chip Design and Fabrication

Si Substrate

AZ P4620

Litho Pattern

Bake for thermal reflow and full hardening at 190 °C for > 3 h (100 μm wide, 12 μm high)

SU8 2050 on a leveled station overnight (500 μm wide, 105±1 μm or 76±0.5 μm high)

Litho Pattern

Then mold is hardened at 150 °C for 30 min; then treated by trichloro-(1,1,2,2-perfluorooctyl) silane
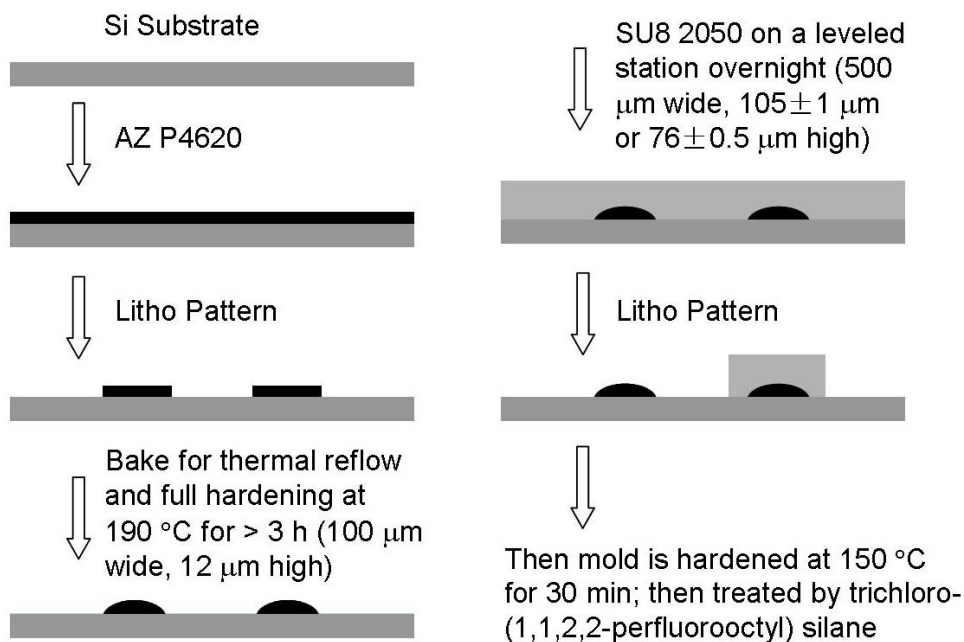
Figure 2.1 The mold fabrication flow for the two-layered device with beds.

A detailed fabrication process for the mold is shown in Figure 2.1. First, a thin layer of AZ P4620 was spin-coated onto a silicon wafer (ϕ 4", Virgin Test, Silicon Valley Microelectronics, Inc., San Jose, CA, USA). After UV exposure and development, the photoresist edges were rounded by reflow at 150 ℃ for 30 min, then further baked at 190 ℃ > 3 h for full hardening. The structure was very stable during later photolithographic processing. During the next step, thick SU8 2050 (105 μm or 76 μm) was used on the same wafer to form the second layer pattern for the thick beds. SU8 was spin-coated on the wafer and left on a leveled platform overnight, which relaxes the film stress and releases any bubble inside. After the photolithographic process, a square-profiled pattern was obtained for the beds, giving uniform bed thicknesses of 105 ± 1 μm and 76 ± 0.5 μm for two individual wafers. Finally, the mold was silanized by exposure to trichloro(1,1,2,2-perfluorooctyl) silane (Sigma-Aldrich, Oakville, ON, Canada) vapor overnight to prevent the adhesion of silicone rubber. The shapes and dimensions of the pattern were measured on the profilometer (Alphastep 200, Tencor, Milpitas, CA, USA).

A two-layered PDMS device with microvalve integration was obtained using a routine shaping procedure on a mold. Briefly, well-mixed PDMS pre-polymer mixture (Sylgard® 184 silicone elastomer kit, A and B in 10 to 1 ratio, Dow Corning, Midland, MI, USA) was poured onto the mold and cured for 4 h in a 70 ℃ oven. Then the PDMS layer was peeled off and bonded to another piece of PDMS layer after plasma oxidation (MicroEtch RIE, PlasmaLab, Oxfordshire, OX, UK). Finally, the whole device was bonded to a piece of glass. The pattern

with the fluidic channel and beds is on one PDMS layer, while the pattern with pneumatic control lines is on another PDMS layer. Details can be found in Chapter 1, Figure 1.5 for multilayer soft lithography fabrication flow.

2.2.3 Bead Introduction Techniques

For the direct needle injection loading of a bed, a needle (30G × 1/2in., regular wall, regular bevel, Becton Dickinson, Oakville, ON, Canada) was inserted through the soft wall of PDMS, as shown in Figure 2.3A. The needle tip touched the bed bottom with the tip mouth opened to the bed. Bead suspension was loaded into the needle which was then connected to a solution reservoir and pressure tank by nut fittings (Figure 2.3B). Pressure (20-30 psi) was applied to push the bead suspension into the bed for packing. After the packing was completed, drops of uncured PDMS mixture were used to seal the injection point, then cured at room temperature overnight followed by about 30 min at 70 ℃.

The punch-pack-plug (3P) technique consists of three main steps, to punch a hole, to pack the beads and to plug the hole, as shown in Figure 2.4. First, the holes were punched through soft PDMS material into the bed region with home-made metal punchers (specially sharpened at the tip, made by the machine shop, University of Alberta). Bead suspension was introduced with a pipette tip inserted via the hole into the bed, where beads were trapped by weirs, by applying vacuum to the exit reservoir. Finally, the punched piece was plugged back into the hole and uncured PDMS was delivered on top for further sealing. PDMS was cured at room temperature overnight followed by about 30 min at 70 ℃.

Plug sealing was examined using a pressure tolerance test. A syringe pump (Harvard Apparatus, PHD2000 Infuse/Withdraw) was used as the pressure source. A gas-tight syringe (1mL, Model 1001, Hamilton) was connected to the sealed PDMS device via a 1/16" tygon microbore tubing (Cole-Parmer). A home-made pressure gauge with pressure transducer (NPC-1210-100-D-3L, Lucas, Fremont, CA) connected by a glued flangeless nut (Upchurch) was located before the device to monitor pressure in the system relative to atmosphere. The electrical transducer signal was recorded by Labview, and calibrated against an accurate test gauge (Matheson, 0-220 psi). A plasma-bonded PDMS device was tested both with and without a packed column, a 1/16" tubing access hole, with a hole punched into the channel and resealed by the 3P technique. Prior to the tests, all channels and reservoirs were filled with water.

The interface between plugs and holes were imaged by optical microscope, as well as Leo 1430 scanning electron microscope (SEM) with a gun voltage of 10 kV. Prior to SEM imaging, devices were sputter coated with Au, with base pressure 100 mT and deposition time 120 s, giving a thickness of about 15 nm.

2.2.4 Instrumentation and Connection to ESIMS

MS analysis was performed using a single quadrupole Sciex API 150EX (Applied Biosystems / MDS Sciex, Foster City, CA, USA). Positive electrospray ionization with electrospray voltages in the range $3 - 3.6$ kV was used. The mass spectrometer was scanned at 0.5 amu per step with a dwell time of 1 ms.

Electrospray was accomplished through a shaped capillary tip. The capillary was bought from Polymicro Technologies Inc. (OD 360 μm, ID 50 μm, Phoenix, AZ, USA), then pulled by capillary puller (Model P-2000, Sutter Instrument Co., tip OD ~72 μm, ID ~10 μm) and metal-coated for conduction, as described previously in detail.[29] A small opening (ϕ ~300 μm) was punched into the exit channel and the ESI tip was directly inserted into the outlet. The capillary was guided to the MS with the help of a curved metal tube, into which the capillary was inserted.

Cytochrome c peptides were identified by database search of the MS-Digest by Protein Prospector (http://prospector.ucsf.edu). A tolerance of ± 0.5 Da/z was set for peptide molecular mass. Search parameters were selected as follows: trypsin digest, 3 missed cleavages (MC), peptide N-terminus = hydrogen, peptide C-terminus = free acid, modifications considered = oxidation of methionine and protein N-terminus acetylated, cysteine unmodified. Trypsin autodigestion peaks are indentified by data searching using the user protein by pasting the sequence obtained from the Swiss-Prot accession number for bovine trypsinogen [precursor], P00760 with first 20 residues removed.

2.3 Results and Discussion

2.3.1 Soft Lithography Fabrication of Rounded Channel and Bed with Double Weirs

A two-layer mask was designed to fabricate the mold to realize the weir concept for bead trapping. Two kinds of photoresist were used to fabricate regions

with different depths on the mold, creating a fluidic channel (shallow) and a bed (deep). A round-shaped fluidic channel is essential for microvalve integration. However, usually the photoresist (e.g., AZ photoresist) used to form the rounded fluidic channel cannot withstand the fabrication process for the thick photoresist (e.g., SU8 photoresist). A full hardening step turned out to be required to combine the shallow AZ P4620 (Clariant Co., Charlotte, NC, USA) and thick SU8 2050 (MicroChem Co., Newton, MA, USA) in mold fabrication, which makes the device compatible with microvalve integration.

Fabrication parameters were optimized as shown in Figure 2.2 (A1 – A4). The mold was made from AZ P4620, a positive photoresist with a glass transition temperature in the 105 – 110 ℃ range. Without postbake, the channel was trapezoidal-shaped. Postbaking below 110 ℃ distorted the channel with a depression in the middle. With an appropriate postbake above 110 ℃ (tested range 110 – 190 ℃, bake time 30 min), a rounded channel can be fabricated; Figure 2.2A1 shows a mold shaped at 150 ℃ for 1 h. A mold with this kind of mild postbake (at 150 ℃ for 1 or 2 h) cannot withstand the SU8 fabrication process, as shown in Figure 2.2 (A2 or A3), because the photoresist dissolves in the developer. A mold reflowed at 150 ℃ for 30 min was further baked for a full hardening at 190 ℃ for 3 h, which evaporates the solvent and completely crosslinks the polymer. The channel on the mold can withstand the SU8 fabrication process and becomes inert to light exposure, as can be seen from Figure 2.2A4. In addition, such a treatment still gives well rounded shape of the

photoresist channel, which is essential for proper microvalve performance. Device

fabricated using reflowing at 150 ℃ for 30 min, then at 190 ℃ for > 3 h for full

hardening exhibited good valve performance (data shown in Chapter 3). We also
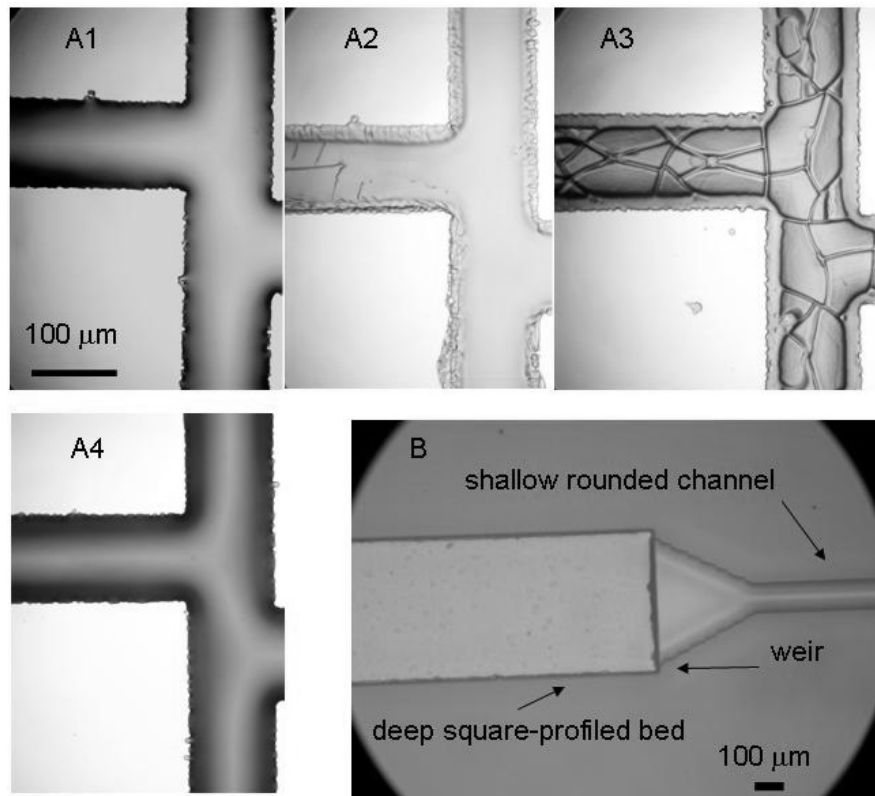
Figure 2.2 The exploration of the fabrication parameters (A1 – A4) and image of the device with rounded fluidic channel and square-profiled bed (B) (A1, AZ P4620 after shaping at 150 °C 1 h; A2, shaped mold (at 150 °C 1 h) after putting in SU8 developer for 30 min; A3, shaped mold (at 150 °C 2 h) after putting in SU8 developer for 30 min; A4, fully hardened mold (at 190 °C 3 h) after putting in SU8 developer for 30 min and futher through the whole SU8 fabrication process. There were fuzzy edges in A1 and A4 because an old low resolution transparency mask was used for this test).

found that a single postbake at 190 ℃ for > 3 h may be used for fabrication, since

such a bake gives both the right shape and sufficient hardening.

Optimized temperature bake parameters were successfully used to fabricate the prototype with a rounded channel and a bed with double weirs. Figure 2.2B gives an image of the device, showing the deep bed pattern aligned to the shallow fluidic channel. The weirs were formed at the interface of the two channel region, the shallow channel acting as the weir. Such a weir, with a channel depth of around 12 μm, was successfully used to trap the beads (30 μm or 20 μm, small leakage observed for 7 μm beads) under vacuum. Under pressure above 30 psi, the front edge of the packed beads may be pushed into the large triangle region of the weir interface, since PDMS is very soft and easily shaped. Such a drawback may be reduced by fabricating some posts in the triangle region, since post structures can be realized in PDMS devices for bead packing.[16, 22-24] Stable packing through clamp-effects and anchor-effects, as discussed in detail in the literature,[24, 28] can occur in PDMS, without needing a trapping restriction.

2.3.2 Bead Introduction Techniques Characterization

Bead introduction channels (mostly as side channels to the beds) are routinely included in designs, which significantly complicate the channel patterns and experimental operation. Two techniques were developed for bead introduction, using a 3-dimensional approach to eliminate the need for bead introduction channels. Direct injection of beads into the bed through the wall of the PDMS device by syringe was evaluated. An alternative, termed the punch-pack-plug (3P) technique, involved punching a small hole (200 to 420 μm) into the bed region for direct bead loading. Such techniques are based on the unique property of the

49

PDMS material, softness, which makes injection through the wall or small size perforation possible.

2.3.2.1 Direct Injection Method

Direct injection method was explored and characterized, involving the insertion of a needle into the bed, followed by bead loading. The basic concept is shown in Figure 2.3A; A needle is inserted right through the soft wall of PDMS, onto the targeted bed, with tip mouth open to the bed, to let beads flow into the bed. There are several operational parameters. First, the needle needs to be strong enough to insert through 4 – 6 mm thick PDMS layer, while aiming at a spot on a bed with a dimension of 500 μm width and 3 mm length. The soft PDMS clamps and holds the syringe needle tightly, avoiding leaks through the insertion path within a certain pressure range. Second, the needle tip size needs to match the bed depth, since the tip needs to touch the bed bottom with the tip mouth open to the bed. In addition, the inner diameter needs to well exceed the bead size, in order to avoid difficulty in flowing the beads through. Furthermore, the needle needs to be sharp enough to smoothly puncture the PDMS.

Based on the above considerations, an injection system was set up with a regular-beveled needle with a dimension of 305 μm OD., 140 μm ID. and 1.27 cm length. This is the optimal choice available commercially. As shown in Figure 2.3B, a needle is inserted, loaded with bead suspension and connected to a source of solution and pressure. Such a needle works for the direct injection of beads into a 105 μm deep bed. At a bed depth of 76 μm bead injection becomes difficult or

beads easily leak through the injection path. The needle was further machined

(machine shop, University of Alberta) to give a short bevel and short length for
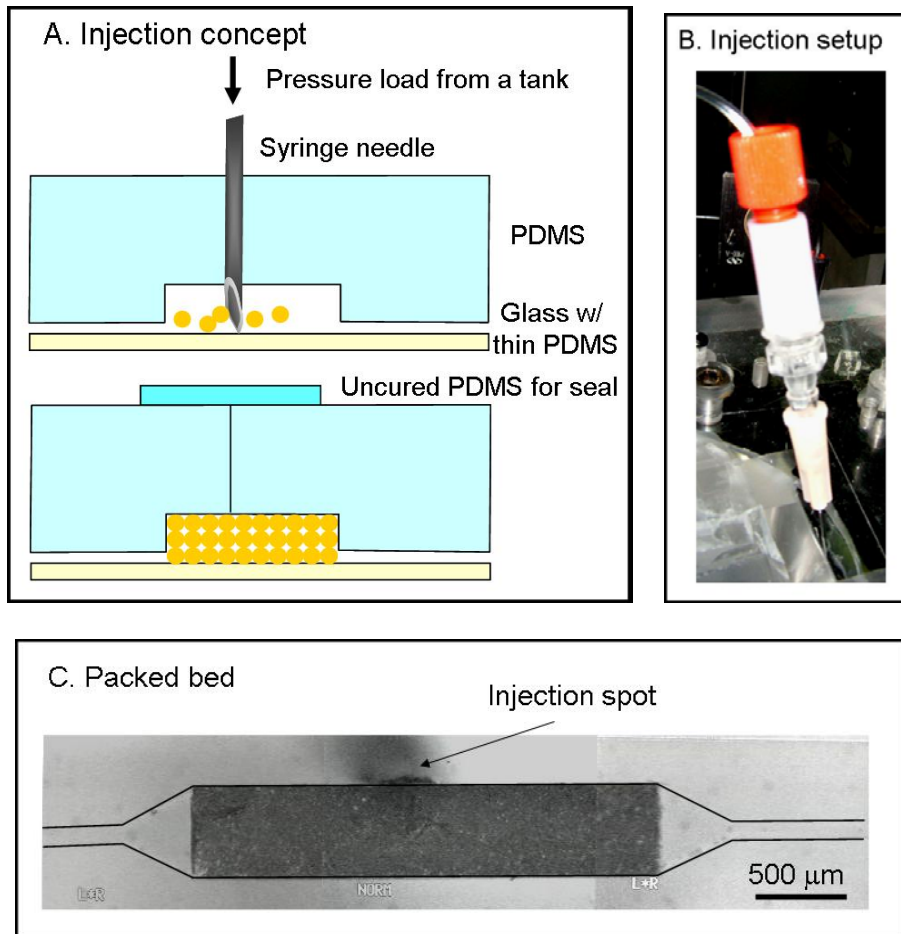
Figure 2.3 Characterization of direct injection method: (A) schematic side-view drawing of the direct injection concept; (B) experimental setup for direct injection of beads; (C) image of one packed device (beads introduced via direct needle injection into the bed; bed 500 μm wide, 3 mm long, 105 μm deep; YMC-Gel liquid chromatography 20 μm C18 beads).

bead injection into a shallower bed; however, successful injections were very hard

to achieve.

An image of successful packing by the direct injection technique is shown in Figure 2.3C. By using the setup in Figure 2.3B, 20 μm beads are injected into a bed with dimension of 500 μm width, 3 mm length and 105 μm depth, and packed to a 3 mm column without leaking through the injection path. The injection point is close to the middle of the column, indicated by the arrow and shadow in the image.

The injection technique seems very attractive, but it is hard to control manually. A 30 G needle is a little bit flexible for insertion through thick PDMS (4 − 6 mm), thus it sometimes fails to insert into the bed region. The regular beveled tip is sharp enough to give a smooth injection, yet the angled tip mouth does not easily access a deep bed. A translation stage controlled operation with a specially optimized needle, may be required for future development of this technique.

2.3.2.2 Punch-Pack-Plug Technique
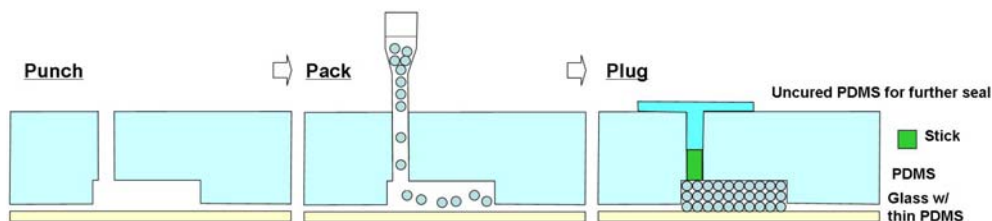
Figure 2.4 Schematic side-view drawing of the 3P technique processes.

The punch-pack-plug (3P) technique involves three simple steps, as shown in Figure 2.4. Compared to the direct injection method, the 3P technique was more controllable and convenient, especially when multiple bed packing is needed. A

series of experiments were performed to characterize the 3P technique, including

perforation limitations, leak testing, and plug interface examination.
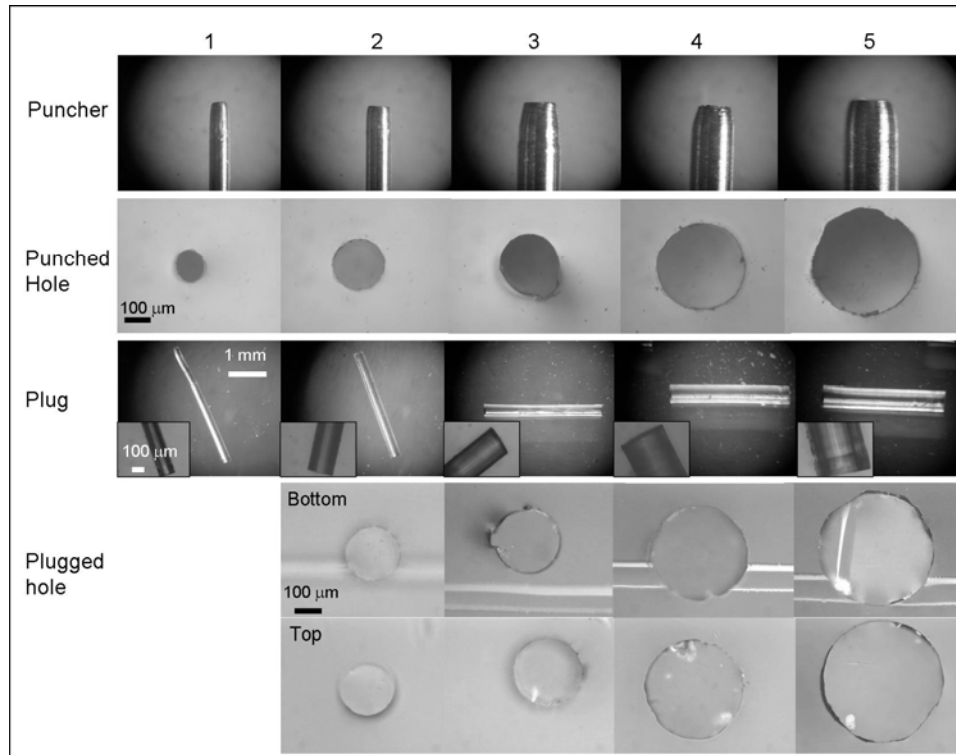
	1	2	3	4	5
Puncher (OD × ID) / μm	330 × 178	406 × 305	711 × 406	711 × 508	889 × 660
Plug / μm	126	207	252	369	427
Punched Hole / μm	120	200	250	350	420
Plugged hole /μm	—	194	234	349	419

Figure 2.5 Summary on the dimension of the 3P technique involved punch: images and corresponding dimensions of the puncher, punched hole, PDMS plug and plugged hole.

A series of holes (with diameters of 420, 350, 250, 200, 120 μm) were punched. The details are summarized in Figure 2.5. The hole can be punched as small as 120 μm, using a metal puncher with a dimension of 330 μm OD. and 178 μm ID. This punch was large enough that it did not challenge any machining limits. We did not try a smaller puncher, since bed widths are typically larger than 200 μm. Punched PDMS pieces were successfully plugged back into holes of 200 – 420 μm diameter, in 3 or 4 mm thick PDMS devices. For 120 μm holes, the punched PDMS was too soft to be plugged back in again. Stiff materials such as dimension-matchable metal wire or filled capillary might be tested as the plug for such small hole, but this was not investigated.

Leak tests show no leakage from plug boundaries up to 115 psi. The highest tested pressure was limited by failure of the tubing connections to the chip. Figure 2.6 illustrates typical leak test curves, where curve a is for the device with a channel and 420 μm plugged hole, b is for one with a channel and a 200 μm plugged hole. Tests were performed at a syringe pump rate of 10 μL/min. With increasing pumping time, the pressure in the device increases, any gas present is compressed and driven out through the gas-permeable PDMS, and the flexible PDMS expands. At some pressure, failure occurs. Frequently the inlet connection tubing detaches (as shown for the 420 μm plug), or water leaks at the tubing/chip interface and accumulates (as shown for the 200 μm plug). In both cases, the break point can be easily seen. The step-like curves obtained here may be related to the syringe pump mechanism and the elasticity (dP/dV or dP/dt) of the system. If the time difference between the two runs shown in Figure 2.6 had come from a
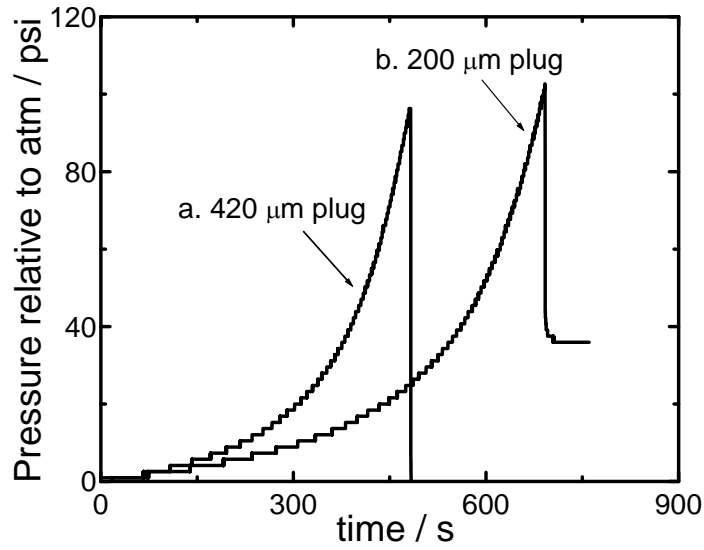
Figure 2.6 The typical leak test curves for 3P fabricated method for two plug sizes, flow rate 10 μL/min. 420 μm plug catastrophically failed at the tubing/chip connection; 200 μm plug tubing/chip connection started to visibly leak.
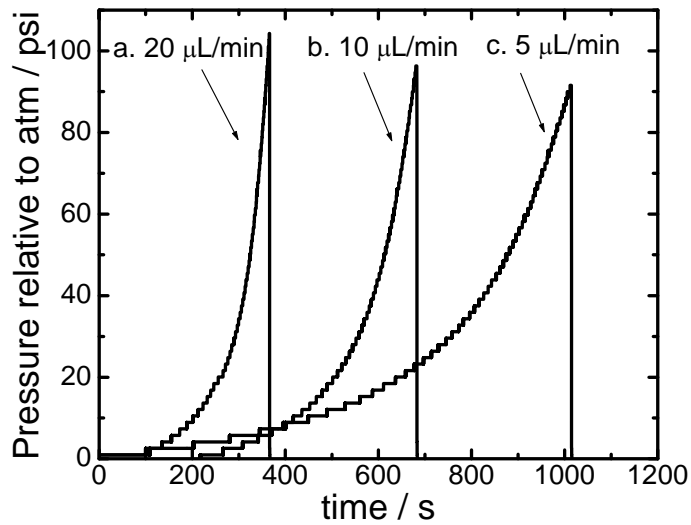
Figure 2.7 Leak tests for the same PDMS device with a channel and a 420 μm plugged hole at different flow rates.

tiny leak, that would mean the volume leaked was around 35 μL, which would be obviously seen. We conclude that variations in time responses between runs can occur due to differences in the air in the system, reproducibility of the tubing insertion, different lengths of the tygon tubing (5 to 10 mm cut prior to insertion), refilling and reconnection of the syringe, etc. These variations will result in a system with different elasticity.

Since the connection failure does not cause serious damage to the connection, the device can be repeatedly connected and tested. As shown in Figure 2.7, the same device was tested three times at different syringe pump rates and similar break pressures were obtained. Figure 2.8 shows results for devices plugged in a variety of ways. The break pressure ranged from 80 − 120 psi, indicating quite similar performance independent of the fabrication method. The range of plug formation methods tested covered the following: device with complete plug insertion without curing a drop of PDMS on top of the plug, with incomplete plug insertion with curing of a drop of PDMS, complete plug insertion with curing of a drop of PDMS, complete plug insertion after dipping the plug in uncured PDMS, followed by curing of a drop of PDMS, a bead packed device with incomplete plug insertion with curing of a drop of PDMS, devices with holes of either 420 μm or 200 μm. The relative standard deviation (RSD) of the slopes for the break points (Figure 2.6, dP/dt, n = 8, slopes based on data fitting from (t − 40 s) to the break point t) was 7.6%. At the break points, differences in induction periods between runs can be neglected, and we observe that the pressure in the system is
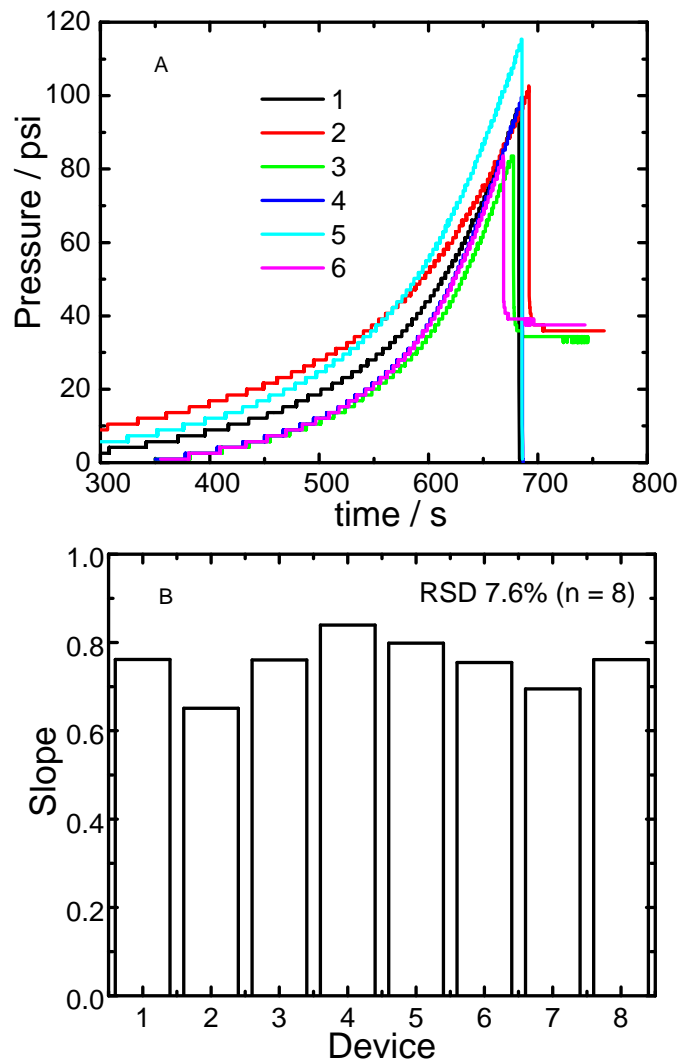
Figure 2.8 (A) Leak tests for PDMS devices plugged in a variety of ways with different fabrication details and (B) the slopes obtained based on the fitting of the data starting from t-40s to the break point t (1 – incomplete plug insertion with curing of a drop of PDMS, 420 μm hole; 2 – incomplete plug insertion with curing of a drop of PDMS, 200 μm hole; 3 – complete plug insertion with curing of a drop of PDMS, 420 μm hole; 4 – complete plug insertion after dipping the plug in uncured PDMS, followed by curing of a drop of PDMS, 420 μm hole; 5 – complete plug insertion without curing a drop of PDMS on top of the plug, 200 μm hole; 6 – a bead packed device with incomplete plug insertion with curing of a drop of PDMS, 420 μm hole; 7, 8 – device without holes; RSD of the break slopes (n = 8) 7.6%; time scale was adjusted to let all the break points sit close).

linearly increasing with pumping time. The slopes are similar in this region.

There are two major effects creating a good seal at the plug. One is a clamping effect between the plug and the wall of the opening. The punched PDMS piece is slightly (several microns) larger than the hole, due to polymer relaxation. The difference can be increased after further curing of the punched devices for bonding, which shrinks the hole. Since the plug is larger than the hole, the press jet this creates enhances the seal along the walls. If uncured PDMS is added on top of the plug and then cured the seal should be further enhanced. Because both seals are stronger than the tubing/chip connection we do not observe the failure point of the plugs. As a result, we can not distinguish the bonding procedures, but can say they withstand ~ 100 psi or more.

From the leak test, we can conclude that the 3P approach works, even though images show that the interface of the plugged hole may be not perfect. As shown by SEM (Figure 2.9), the 200 μm hole is well punched and there are no obvious cracks at the boundaries of the plugged hole. Some gaps of 1 − 2 μm caused by PDMS irregularities or particulates at the interfaces are seen for some devices (Figure 2.10). It is unlikely that these gaps extended the length of the plug. In any event, we usually dripped uncured PDMS on top of the plug overnight (more than 15 hrs) to patch the top part of the plug. The home-made puncher may have some distortions, so that a perfectly round punch, operated in a clean room environment could create a better plug interface. Dipping the plug in PDMS prepolymer
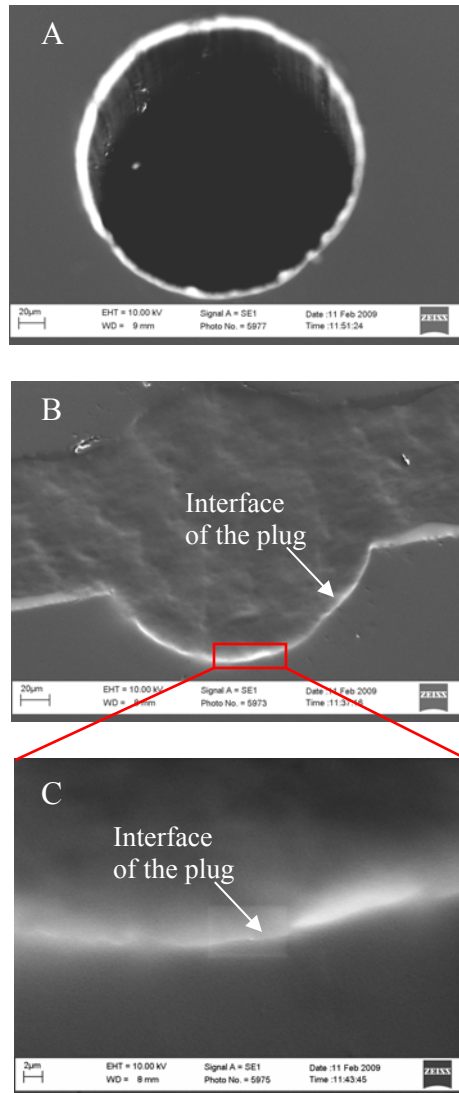
Figure 2.9 SEM of the PDMS devices (A. a punched hole with a diameter of 212.7 μm; a punched and plugged hole into the channel with a diameter of 190.5 μm at lower resolution (B) and higher resolution (C); all viewed at 90°, imaging the underneath of the interface of the plugged hole).

mixtures before sealing may also help, though there may still be some defects at

the boundaries (Figure 2.11).
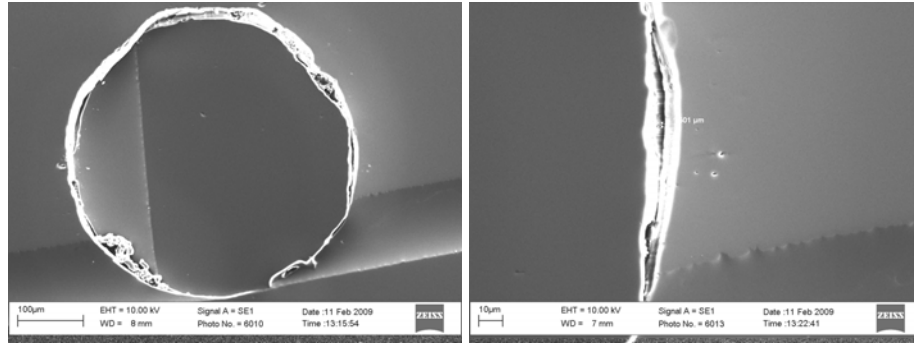
Figure 2.10 SEM of the PDMS device with a punched and plugged hole at lower resolution (left) and higher resolution (right), showing some dirt and gaps at the interface; all viewed at 90°, imaging the underneath of the interface of the plugged hole.
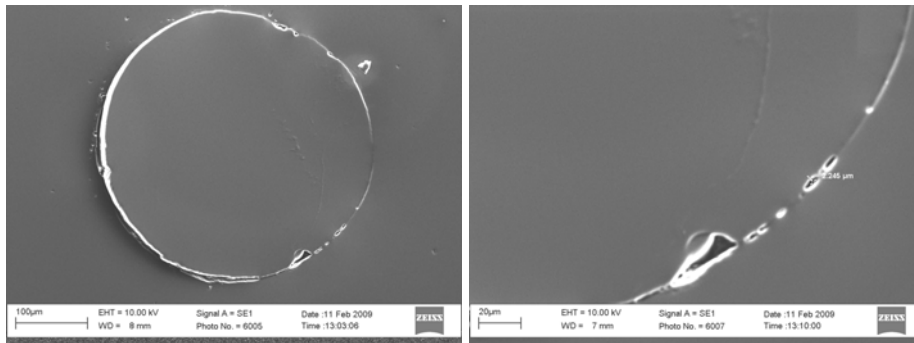
Figure 2.11 SEM of the PDMS device with a punched hole plugged by uncured-PDMS-dipped stick at lower resolution (left) and higher resolution (right), showing some defects at the interface; all viewed at 90°, imaging the underneath of the interface of the plugged hole.

2.3.3 The 3P Technique Packed Multiple Beds and Some Application Tests

2.3.3.1 Multiple Packing by 3P Technique

Packed beds formed by delivering beads through holes with diameters of 420 or 200 μm are illustrated in Figure 2.12. Figure 2.12A shows packing with
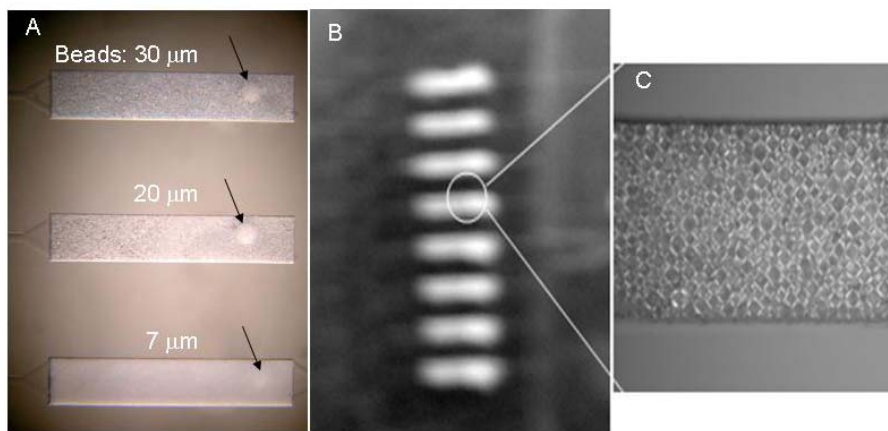
Figure 2.12 Images of multiple packed beds (bed 500 μm wide, 3 mm long): (A) three sizes of bead packing via 200μm holes (30 μm Oasis® HLB beads, 20 μm YMC-Gel liquid chromatography C18 beads, 7 μm Nucleosil ® 500-7 C8-Silica beads, arrow indicating the inlet positions); (B) eight beds with 30 μm Oasis® HLB beads packed via 420 μm holes; (C) one of the eight packed bed imaged at higher resolution.

different particle sizes (30, 20 and 7 μm) via 200 μm holes. Denser/lighter spots indicate the inlet positions, indicated by arrows in Figure 2.12A. The weir can successfully trap 30 or 20 μm beads. The 7 μm beads were trapped by the 10 μm-weir due to the keystone-effect,[26] although some leakage of beads can be observed during packing. Figure 2.12B shows an image of eight packed beds with 30 μm particles, packed by bead introduction through 420 μm holes, with an

image at higher resolution for one of the beds shown in Figure 2.12C. It is very convenient to introduce multiple beds in a device, using the 3P method.

2.3.3.2 SPE

SPE has become a very popular technique on chip for sample cleanup and enrichment, being used to overcome detection-limit problems or to eliminate interferences. Bead packing is an amenable and straightforward way to introduce well characterized SPE stationary phase on chip. The 30 μm Oasis® HLB beads showed good solid phase extraction ability for proteins and peptides.

The solid phase extraction behavior of a bed with a 0.116 μL free volume (500 μm width × 3 mm length × 76 μm depth) was tested, as shown in Figure 2.13. About 8 μL of 5 μg/μL of 30 μm diam. Oasis® HLB bead suspension was loaded into the bed, resulting in a bead packing density of 0.35 μg/nL. Different amounts of cytochrome c were individually loaded onto the bed: 0.05 μg (5 μL 0.01 mg/mL), 0.1 μg (10 μL 0.01 mg/mL), 0.125 μg (2.5 μL 0.05 mg/mL), 0.25 μg (5 μL 0.05 mg/mL), 0.5 μg (2.5 μL 0.2 mg/mL), 0.744 μg (3.72 μL 0.2 mg/mL), 0.8 μg (4 μL 0.2 mg/mL). After each loading, the bed was rinsed with water, and cytochrome c was eluted to the MS with 50% MeOH / 0.1 M formic acid. Figure 2.13A shows the elution traces for three measurements, as indicated; the plot of peak area versus protein load (Figure 2.13B) tells us that saturation occurred at 0.5 μg cytochrome c. According to the observed peak shape, the mass detector was not saturated at this mass load or concentration. Up to 1.2 μg cytochrome c load was tested using the same mass spectrometer at similar driven flow rate

62

without saturation of the mass detector.[29] We conclude the bed loading capacity is 0.5 µg cytochrome c per 0.04 mg of beads. In our beds we measured a capacity of 12.5 µg protein/mg beads. Previous work by C. Wang in this group[30] using 60 µm diam. Oasis® HLB beads showed the beads had a capacity of 36 µg protein digest/mg beads. This capacity is obtained off-chip by vortexing mixtures of digest and beads, leading to better adsorption efficiency than when adsorption is tested on-chip using a flowing stream. Thus the bed fabricated in this study with 30 µm diam. beads has a lower loading capacity than predicted by C. Wang's results for 60 µm beads. Such a difference may come from the difference in the testing method, especially on-chip adsorption by flowing through for ~ 10 min versus off-chip adsorption with vortexing. The difference in diameter might also have some effect. To design a bed, one consideration is the needed capacity.[31] If 10 µg of protein (an overestimate[32]) is loaded via capillary isoelectric focusing (cIEF) and fractionated into 20 channels, it will result in 0.5 µg of protein for each channel, assuming an even distribution. Another consideration is packing stability and activity, where the bed volume is limited by the packing material (bead size 30 µm diam.). Thus a bed with dimensions of 500 µm width × 3 mm length × 76 µm depth was used, giving a predicted loading capacity of 1.44 µg of protein digest with relatively efficient packing quality in the fractionation device (Chapter 4). The lower loading capacity of 0.5µg we obtained from measurements of the chip is still sufficient for a multiplexed fractionation design (Chapter 1, Figure 1.3).
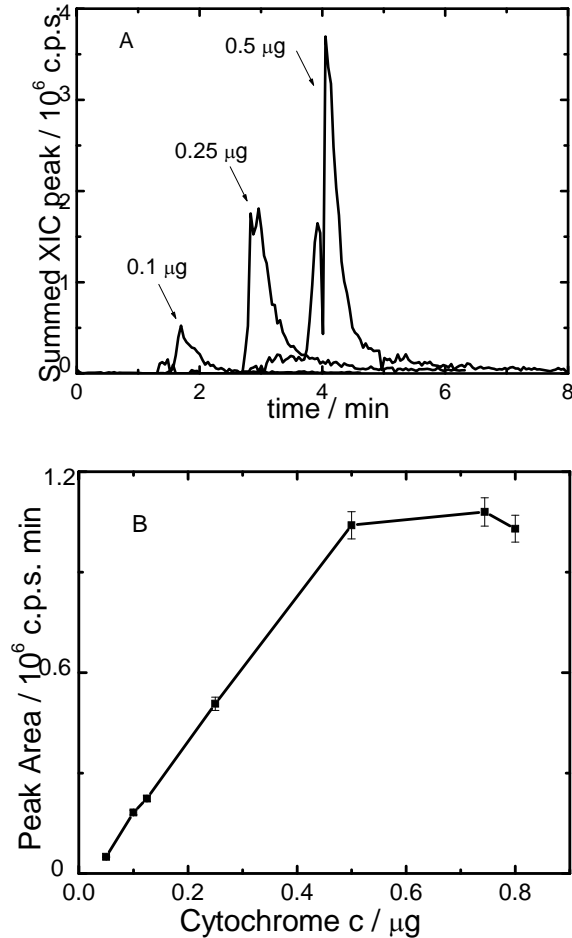
Figure 2.13 Cytochrome c load: (A) summed extracted ion count (XIC) peak for three different cytochrome c loads as indicated; (B) Peak area versus cytochrome c load for different loads.

The sensitivity of a single SPE-ESIMS manifold was tested. Figure 2.14 gives the analyzed results for digested cytochrome c peptides; extracted ion counts and the corresponding mass spectrum are shown. The insets are plots of peak area under the XIC curve versus different digest loads for three low amounts, 16, 80 and 160 fmol, generated by loading 2 μL of 0.0001, 0.0005, and 0.001 mg/mL digest solutions individually, then eluting with 50% MeOH, 0.1 M formic acid.
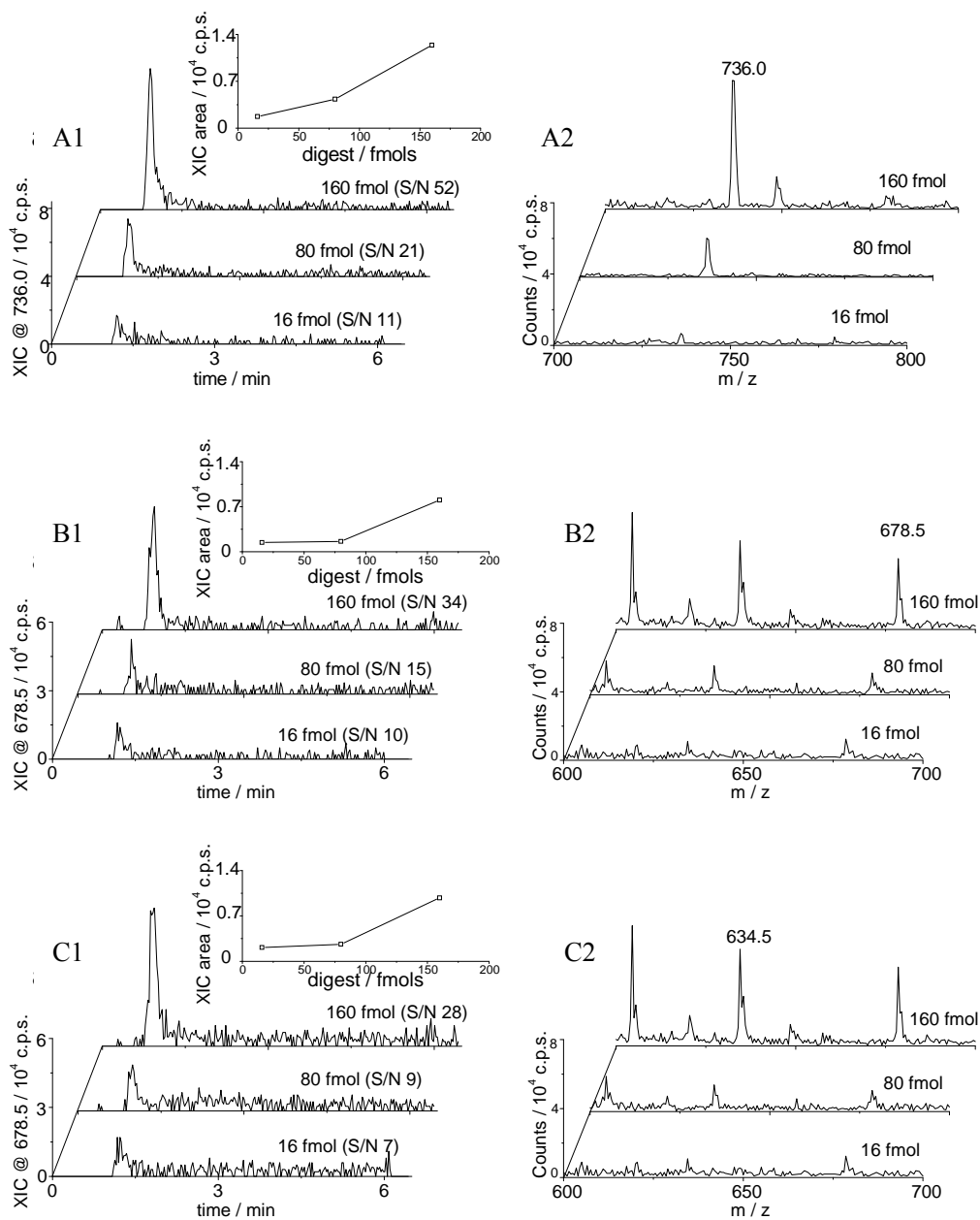
Figure 2.14 Detection sensitivity in single SPE-ESIMS system obtained from three peptides with m/z of 736.0 (top), 678.5 (middle) and 634.5 (bottom); XIC graph (left), MS (right), and integrated XIC area dependent on amount (inset).

Table 2.1 Volume calculations on column and post column connections

1. column		post column connections to MS					
		2. bed to channel exit		3. interfacing between channel exit and capillary inlet		4. capillary	
width / μm	500	width / μm	100	diameter / μm	300	diameter / μm	50
length / mm	3	length / mm	3	height / μm	5 - 20	length / cm	5
depth / μm	76	depth / μm	12	volume / nL	0.4 -1.4	volume / nL	98
volume / nL	114	volume / nL	3.6				
column porosity / nL	45.6						

The analysis of cytochrome c digests (in Figure 2.14) shows that a 16 fmol load was measurable (S/N 11), and 80 fmol was high enough to give a reliable spectrum (S/N 21) for a peptide with m/z of 736.0. The amount is calculated according to the amount of digested protein, and may actually be lower than the calculated values. In addition, sensitivity may be increased by further optimization of the spray, such as elution velocity. The sensitivity response is sample dependent, and also differs between peptides, as seen with m/z 678.5, m/z 634.5 fragments. This effect is mainly ascribed to ionization efficiency differences, though the sample concentration may vary to some extent too. The detection sensitivity observed is comparable to the data reported in a regular SPE-ESIMS system by pressure driven flow of several μL/min.[33-35] A detailed comparison is shown in Chapter 5, Table 5.1. For example, Oleschuk[33] reported a S/N of 21 and 115 for 23 and 696 fmol, respectively, of leucine enkephalin with microsphere entrapped emitters used for sample preconcentration and ESIMS (API 3000 triple-Q MS, 3 μm SPE beads, 0.8 μL/min). The total volume from column porosity and post column connections is ~ 150 nL, as shown in Table 2.1. A higher sensitivity may be obtained with a decrease in the transport volume to the MS, using a more compact bed with an integrated in-line emitter.

Reproducibility of the packed beds was measured by quantitative loading of cytochrome c into the beds (about half of the saturation amount) and detection by elution to ESIMS, as shown in Figure 2.15 and 2.16. All the beds were packed with 30 μm beads loaded via 420 μm punched holes. Figure 2.15 shows results obtained within the same bed for four sequential loadings of cytochrome c on the
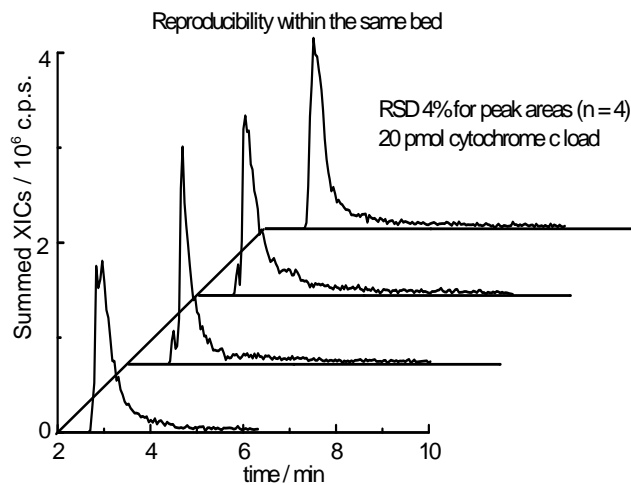
Figure 2.15 Reproducibility within the same bed (packing stability in the same bed) the summed XIC peaks from four times of cytochrome load to SPE bed.
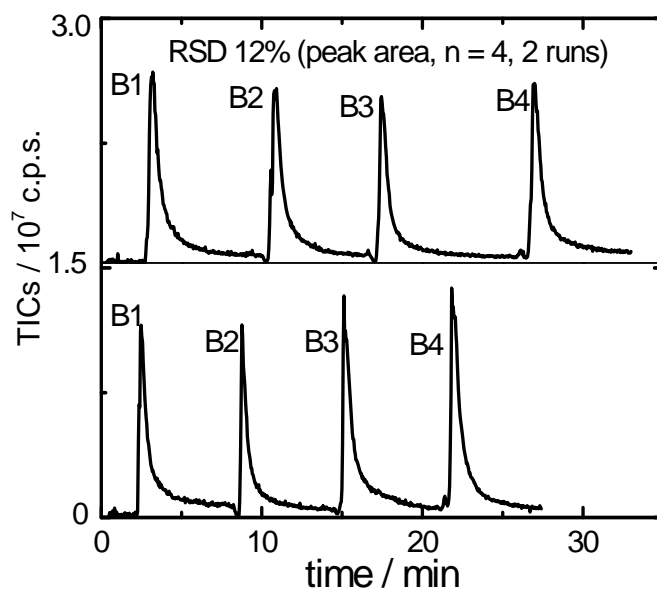
Figure 2.16 Bed-to-bed reproducibility: two runs of 20 pmol cytochrome c load to and eluted from four different beds in sequence; the switch rates from bed to bed were manually controlled and different for the two runs.

SPE bed. Figure 2.16 shows two runs of cytochrome c on four different beds eluted in sequence; where the switch rates from bed to bed were manually controlled and differed for the two runs. The relative standard deviation is 4% (n = 4, peak area) for measurements within the same bed and 12% (n = 4, peak area) for measurements between multiple beds. According to the reproducibility measurements, packing was relatively consistent and efficient for the multiple channels. The repeatability for multiple beds is reasonable considering the large bead size (ϕ30 μm) and small bed (76 μm depth × 500 μm width × 3mm length, 114 nL), which means packing of the bed was relatively loose. Further optimization of bed dimensions may increase the reproducibility, in particular the use of a higher particle diameter to bed depth ratio.

2.3.3.3 Protein Digestion

Protein digestion is a very important step for integrating protein processing on a chip. The common method is to integrate immobilized tryspin reactors on chip, which can provide faster digestion, fewer trypsin autolysis products and potentially higher enzyme stability.[11] Another method is to preconcentrate the proteins directly, then digest the proteins "in situ" on the beads by introducing trypsin.[30, 36, 37] This method increases protein concentration prior to digestion and removes contaminants from the sample in a single step, which facilitates on chip integration and automation.

The in-situ digestion of extracted protein was tested on 30 μm bead packed columns in PDMS using cytochrome c at a loading of 4 pmol. The results show

the method works well. As shown in Figure 2.17, twenty peaks were identified as cytochrome c fragments, while seven peaks were trypsin autodigestion peaks. The sequence coverage for cytochrome c was 87%. Identified cytochrome c peptides and trypsin autodigestion peptides in Figure 2.17 were listed in Table 2.2 and Table 2.3. It is well known that the main parameters affecting the digestion are buffer pH, digestion temperature, digestion time, and enzyme to protein ratio. The buffer used here was NH_4HCO_3 at pH 8.6, which is a favorable digestion buffer for trypsin, but the digestion was carried out at room temperature, not at the
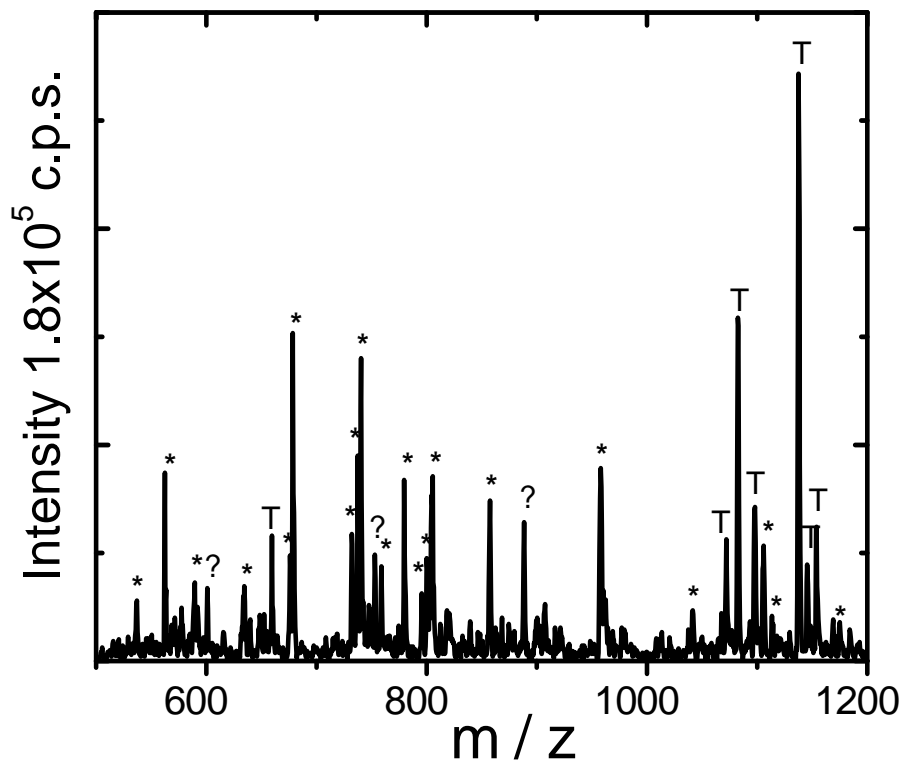
Figure 2.17 The mass spectrum of cytochrome c digest with an SPE bed (* - cytochrome c peptides, T - trypsin autodigestion peaks, ? – unidentified peaks; sequence coverage is 87%; elution buffer 50% methanol/0.1 M formic acid).

Table 2.2 Identified cytochrome c tryptic peptides in Figure 2.17

m/z	MC	modifi-cations	position	sequence
536.5^{+3}	3		87 – 99; 88 - 100	KKTEREDLIAYLK; KTEREDLIAYLKK
562.5	1		100 - 104	KATNE
589.5	0	AcetN	1 - 5	GDVEK
634.5	0		9 - 13	IFVQK
676^{+2}	1		89 - 99	TEREDLIAYLK
678.5	0		74 - 79	YIPGTK
736.0^{+2}	0		40 - 53	TGQAPGFTYTDANK
737.0^{+3}	2		56 - 73	GITWKEETLMEYLENPKK
740.0^{+2}	2		88 – 99; 89 - 100	TEREDLIAYLKK; KTEREDLIAYLK
759.6^{+2}	3	AcetN	1 - 13	GDVEKGKKIFVQK
779.5	0		80 - 86	MIFAGIK
795.5	0	1Met-ox	80 - 86	MIFAGIK
800.0^{+2}	1		39 - 53	KTGQAPGFTYTDANK
806.5	1		73 - 79	KYIPGTK
857.5^{+2}	1		40 - 55	TGQAPGFTYTDANKNK
957.5^{+3}	3		56 - 79	GITWKEETLMEYLENPKKYI PGTK
1041.5^{+2}	1		56 - 72	GITWKEETLMEYLENPK
1105.5^{+2}	2		56 - 73	GITWKEETLMEYLENPKK
1113.5^{+2}	2	1Met-ox	56 - 73	GITWKEETLMEYLENPKK
1168.5	0		28 - 38	TGPNLHGLFGR

Table 2.3 Identified trypsin autodigestion peptides in Figure 2.17

m/z	MC	modifi-cations	position	sequence
660.0	0		44 - 49	SGIQVR
1071.0^{+3}	1	1Met-ox	140 - 170	APILSDSSCKSAYPGQITSNM FCAGYLEGGK
1082.3^{+2}	0		50 - 69	LGEDNINVVEGNEQFISASK
1098.0^{+2}	0		150 - 170	SAYPGQITSNMFCAGYLEGG K
1137.8^{+2}	0		70 - 89	SIVHPSYNSNTLNNDIMLIK
1145.2^{+2}	0	1Met-ox	70 - 89	SIVHPSYNSNTLNNDIMLIK
1154.0	0		126 - 136	SSGTSYPDVLK

optimal temperature of 37 ℃. Digestion was done by loading trypsin buffer solution (pH 8.6) into the bed region and incubating for 30 min, at room temperature. Then the bed was rinsed with water, and digests were eluted to ESIMS in the elution buffer of 50% methanol containing 0.1 M formic acid. Appropriate concentrations of trypsin (tested range 0.05 mg/mL to 0.3 mg/mL) were tested, for a loading of 4 pmol of cytochrome c on the SPE bed (10% saturation of the bed). The optimal trypsin concentration was about 0.1-0.2 mg/mL. A lower trypsin concentration led to lower extent of protein digestion with more missed cleavages, while higher concentration increased the intensity of autodigestion peaks.

2.3.3.4 Chromatographic Effects

Another application of the packed beds is chromatographic separation. The 3 mm column shows an acceptable chromatographic effect, as shown in Figure 2.18. Two peptides from the cytochochrome c digest were partially separated while being eluted from the SPE column. The first peak, with an m/z of 648.5^{2+}, identified as NH_2-TGPNLHGLFGRK-COOH, has a pI close to 11.00 (ExPASy, http://ca.expasy.org/tools/pi_tool.html). The second peak with m/z 678.5^{+1}, identified as NH_2-YIPGIK-COOH, has a pI of around 8.59. Based on calculation with the Peptide Property Calculator (GenScript, https://www.genscript.com/ssl-bin/site2/peptide_calculation.cgi), peptide NH_2-TGPNLHGLFGRK-COOH has 25% of hydrophilic residues, 25% of hydrophobic residues and 50% of others, while NH_2-YIPGIK-COOH has 17% of hydrophilic residues, 33% of
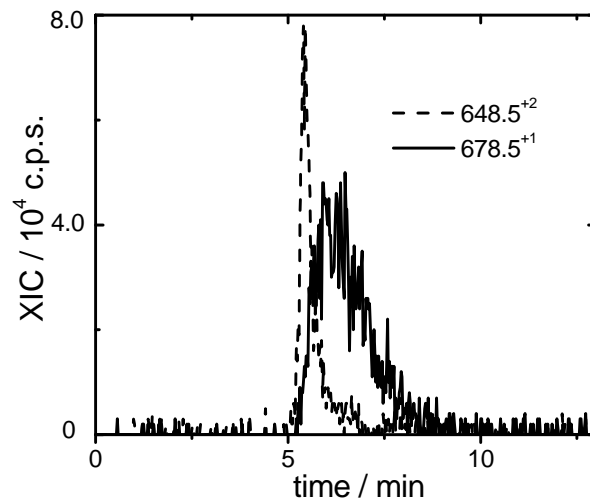
Figure 2.18 Chromatographic effects for peptides (the two peaks corresponding to two cytochrome c digest peaks, with m/z 648.5 and 678.5 respectively; Elution buffer 50% methanol + 0.1 M formic acid).

hydrophobic residues and 50% of others. Since the SPE column has different affinity to peptides with different hydrophobicity, the two peptides can be partially separated based on their hydrophobic properties. Thus, the column shows some chromatographic effects, however, for an effective chromatographic separation, noticeably smaller beads (less than 10 μm) and a longer column need to be used.

2.4 Conclusion

A convenient technique has been developed in order to fabricate and pack multiple beds in PDMS device compatible for microvalve integration. A soft lithography process was optimized to fabricate the device with double weirs for bead trapping and rounded channel for microvalve integration. The 3P technique

developed eliminates bead introduction channels in the fluidic pattern, providing

more space for complex designs. It is a very convenient and controllable method

for multiple packing. While the technique was realized in a PDMS device, but is

not limited to the PDMS elastomer, should work with other polymer materials.

2.5 References

(1)   Unger, M. A.; Chou, H. P.; Thorsen, T.; Scherer, A.; Quake, S. R. *Science* **2000**, *288*, 113-116.

(2)   Whitesides, G. M. *Nature* **2006**, *442*, 368-373.

(3)   Melin, J.; Quake, S. R. *Annu. Rev. Biophys. Biomol. Struct.* **2007**, *36*, 213-231.

(4)   Haeberle, S.; Zengerle, R. *Lab Chip* **2007**, *7*, 1094-1110.

(5)   Maerkl, S. J. *Integrative Biology* **2009**, *1*, 19-29.

(6)   Oleschuk, R. D.; Shultz-Lockyear, L. L.; Ning, Y. B.; Harrison, D. J. *Anal. Chem.* **2000**, *72*, 585-590.

(7)   Yin, N. F.; Killeen, K.; Brennen, R.; Sobek, D.; Werlich, M.; van de Goor, T. V. *Anal. Chem.* **2005**, *77*, 527-533.

(8)   Bergkvist, J.; Ekstrom, S.; Wallman, L.; Lofgren, M.; Marko-Varga, G.; Nilsson, J.; Laurell, T. *Proteomics* **2002**, *2*, 422-429.

(9)   Jemere, A. B.; Oleschuk, R. D.; Ouchen, F.; Fajuyigbe, F.; Harrison, D. J. *Electrophoresis* **2002**, *23*, 3537-3544.

(10)   Lee, C. C.; Sui, G. D.; Elizarov, A.; Shu, C. Y. J.; Shin, Y. S.; Dooley, A. N.; Huang, J.; Daridon, A.; Wyatt, P.; Stout, D.; Kolb, H. C.; Witte, O. N.; Satyamurthy, N.; Heath, J. R.; Phelps, M. E.; Quake, S. R.; Tseng, H. R. *Science* **2005**, *310*, 1793-1796.

(11)   Wang, C.; Oleschuk, R.; Ouchen, F.; Li, J. J.; Thibault, P.; Harrison, D. J. *Rapid Commun. Mass Spectrom.* **2000**, *14*, 1377-1383.

(12)   Huang, Y. Y.; Castrataro, P.; Lee, C. C.; Quake, S. R. *Lab Chip* **2007**, *7*, 24-26.

(13)   Marcus, J. S.; Anderson, W. F.; Quake, S. R. *Anal. Chem.* **2006**, *78*, 3084-3089.

(14)   Verpoorte, E. *Lab Chip* **2003**, *3*, 60N-68N.

(15)   Sivagnanam, V.; Song, B.; Vandevyver, C.; Gijs, M. A. M. *Anal. Chem.* **2009**, *81*, 6509-6515.

(16)   Kim, D. N.; Lee, Y.; Koh, W. G. *Sens. Actuators B* **2009**, *137*, 305-312.

(17)   Gijs, M. A. M. *Microfluidics And Nanofluidics* **2004**, *1*, 22-40.

(18)   Peterson, D. S. *Lab Chip* **2005**, *5*, 132-139.

(19)   Ekstrom, S.; Malmstrom, J.; Wallman, L.; Lofgren, M.; Nilsson, J.; Laurell, T.; Marko-Varga, G. *Proteomics* **2002**, *2*, 413-421.

(20)   Hong, J. W.; Studer, V.; Hang, G.; Anderson, W. F.; Quake, S. R. *Nat. Biotechnol.* **2004**, *22*, 435-439.

(21)   Andersson, H.; van der Wijngaart, W.; Enoksson, P.; Stemme, G. *Sens. Actuators B* **2000**, *67*, 203-208.

(22)   Buranda, T.; Huang, J. M.; Perez-Luna, V. H.; Schreyer, B.; Sklar, L. A.; Lopez, G. P. *Anal. Chem.* **2002**, *74*, 1149-1156.

(23)   Yang, Y.; Nam, S. W.; Lee, N. Y.; Kim, Y. S.; Park, S. *Ultramicroscopy* **2008**, *108*, 1384-1389.

(24)   Flemming, J. H.; Baca, H. K.; Werner-Washburne, M.; Brozik, S. M.; Lopez, G. P. *Sens. Actuators B* **2006**, *113*, 376-381.

(25)   Jiang, G. F.; Harrison, D. J. *Analyst* **2000**, *125*, 2176-2179.

(26)   Ceriotti, L.; de Rooij, N. F.; Verpoorte, E. *Anal. Chem.* **2002**, *74*, 639-647.

(27)   Li, W.; Fries, D. P.; Malik, A. *J. Chromatogr. A* **2004**, *1044*, 23-52.

(28)   Gaspar, A.; Piyasena, M. E.; Gomez, F. A. *Anal. Chem.* **2007**, *79*, 7906-7909.

(29)   Martinez, D. Ph.D. theses, University of Alberta (Canada), Edmonton.

(30)   Wang, C. Ph.D. theses University of Alberta (Canada), Edmonton, 2001.

(31)   Taylor, J. PhD theses, University of Alberta (Canada), Edmonton, 2004.

(32)   Shen, Y. F., Smith, R.D. *Electrophoresis* **2002**, *23*, 3106-3124.

(33)   Koerner, T.; Xie, R. X.; Sheng, F.; Oleschuk, R. *Anal. Chem.* **2007**, *79*, 3312-3319.

(34)   Bonneil, E.; Li, J. J.; Tremblay, T. L.; Bergeron, J. J.; Thibault, P. *Electrophoresis* **2002**, *23*, 3589-3598.

(35)   Lindberg, P.; Dahlin, A. P.; Bergstrom, S. K.; Thorslund, S.; Andren, P. E.; Nikolajeff, F.; Bergquist, J. *Electrophoresis* **2006**, *27*, 2075-2082.

(36)   Craft, D.; Li, L. *Anal. Chem.* **2005**, *77*, 2649-2655.

(37)   Aguilar, M. I.; Clayton, D. J.; Holt, P.; Kronina, V.; Boysen, R. I.; Purcell, A. W.; Hearn, M. T. W. *Anal. Chem.* **1998**, *70*, 5010-5018.

Chapter 3

Application of Polydimethylsiloxane (PDMS) Microvalves as Electric Switches[*]

3.1 Introduction

Pressure-actuated in-channel polydimethylsiloxane (PDMS) microvalves based on multilayer soft lithography (MSL) method have been used as a powerful control system for many biological or chemical processing systems in microfluidic devices.[1-6] Applications include single cell analysis, protein crystallization, nuclei acid extraction, cell culture, and drug discovery. Several layers of PDMS can be irreversibly bonded to each other using the MSL technique, resulting in a monolithic, three-dimensionally patterned structure using crossed architecture and rounded flow channels to define in-channel microvalves.[1] PDMS microvalves have very attractive advantages, such as easy actuation, multiplexed operation, relatively easy and inexpensive manufacturing, small dimensions, and low to zero dead volume. This technology has provided a prominent and inspiring microfluidic platform offering a large scale integration platform, due to the ability to integrate extremely high-density mechanical microvalves on a single chip.[3]

Although PDMS microvalves were developed originally to control pressure-driven fluidic flow, designers may be forced to use microvalves

---

[*] A version of this chapter has been prepared for submission to *Electrophoresis.*

combined with electrokinetic flow control in highly integrated devices. PDMS microvalves designed with a push-down valve scheme[7] were claimed to be suitable for electrically isolating fluidic compartments on chip reversibly, with a typical impedance of 5 GΩ in the closed state and 10 MΩ in the open state.[8, 9] The electromechanical properties of the valve were studied to specify the ideal operating conditions for future high throughput drug discovery applications using parallel planar patch clamp devices.[9] Microchip capillary electrophoresis (μCE) separation has become a prevalent tool for integrated analysis on chip, since the first adaption of CE on chip by Harrison *et al.*[10] PDMS microvalves were used as switches in a two-dimensional μCE separation system to isolate sample and buffers, with a closed-valve resistance of about 1 GΩ.[11] Independent 2-D separation of proteins, isoelectric focusing (IEF) and capillary gel electrophoresis (CGE) was obtained using microvalve isolation. It appears inevitable that valves will be used with high electric fields in complicated integrated devices,[12-14] PDMS microfluidic platforms for proteomic analysis,[12, 14] or for counting low-copy number proteins in a single cell.[13] However, detailed studies (eg. design parameters and performance) of such microvalves in the presence of strong electric fields have not been reported.

Here, pressure-actuated in-channel microvalves used in a push-up valve scheme are described. The valves show a high closed-valve resistance (100 – 1000 GΩ), and high enough flow resistance to stop pressure-driven flow. The phenomenon of current breakthrough and electrical damage to the valves (under certain applied voltage and valve dimensions) is reported. The breakthrough

mechanism was studied, and the key parameters for control of the performance of the valves in strong fields are discussed, specifically membrane thickness, valve dimensions and surface roughness.

3.2 Experimental

3.2.1 Fabrication of PDMS Valves

PDMS valves were fabricated using a multilayer soft lithography method. The fluidic master pattern was formed with a 10 μm layer of AZ P4620 on a silicon wafer, rounded by reflowing at 150 ℃ for 30 min, then baked at 190 ℃ for > 3 h for full hardening. The round, stable form was patterned with SU8 2050 to create a second, thicker structure (referring to Chapter 2 for details). The control channel master layer was fabricated using spin-coated SU8 2050 to make a 30 μm deep pattern on a silicon wafer. Both masters were silanized by exposure to trichloro(1,1,2,2-perfluorooctyl) silane (Sigma-Aldrich, Oakville, ON, Canada) vapor to prevent the adhesion of PDMS.

PDMS pre-polymer (Sylgard® 184 silicone elastomer kit, A and B in 10 to 1 ratio, Dow Corning, Midland, MI, USA) was used to duplicate the pattern on the masters, by spin-coating a thin layer on the control master, and pouring a thick layer on the fluidic master. The PDMS was cured on a leveled station for 1 h at room temperature, and then for at least 4 h in a 70 ℃ oven. The thin membrane thickness was measured by a stylus profilometer (Alpha Step 200 Profilometer, Tencor Instruments). The target membrane thickness was about 45 μm. In the regions of the pneumatic control lines the membrane was thinned to about 15 μm

by the photolithographic patterning. The thickness is dependent on the thin PDMS membrane thickness (45 μm) and the control channel pattern mold depth (30 μm).

After plasma oxidation (MicroEtch RIE, PlasmaLab, Oxfordshire, OX, UK) for about 10 s at an O_2 pressure of 200 mTorr, the two PDMS layers were bonded together with the control layer on the bottom, forming microvalves for a push-up valve scheme. The membrane thickness between fluidic and control channels (as shown in Figure 3.1c, indicated as a valve membrane) was about 15 μm, when a 45 μm thick membrane layer and 30 μm deep control channel are used. Bonding was further enhanced by heating in an oven at 70 ℃, resulting in a total bake time of about 72 h. After complete bonding, the assembled layers were bonded to a glass substrate (the same plasma treatment was repeated). As shown in Figure 1.5 and 3.1, microvalves are formed at the intersections between fluidic and control channels. The flow channel is normally open, closing when sufficient pressure is applied in the control channel to deform the thin membrane and pinch off the flow in the fluidic channel. The flow channel is rounded to enable complete valve closing. Figure 1.5 in Chapter 1 provides an outline of the multilayer soft lithography fabrication flow.

3.2.2 Threshold Voltage Measurement

Threshold breakdown voltage was measured to determine the electrical durability of PDMS microvalves, i.e., the voltage causing current breakthrough in closed microvalves. For threshold breakdown voltage measurements, a 1 MΩ resistor was connected in series with the fluidic channel (4 cm long) and a high

voltage power source. The voltage drop across the resistor was measured with a multimeter (Fluke, 87 III), with a resolution of 0.1 mV and internal resistance of 10 MΩ. A breakthrough voltage was determined by increasing the applied high voltage until a significant voltage change was observed on the multimeter, i.e., a steep voltage rise corresponding to a current flow. The current and microvalve resistance are calculated based on the circuit employed, correcting for 9% loading by the meter. The fluidic channel and the control channel were filled with buffer (Tris-H_3BO_3 buffer, 100 mM-20 mM, pH 9) and deionized water, respectively. The microvalves are actuated by applying air pressure to the water-filled control channels (referring to Chapter 4 for connection details). The breakthrough electric fields were obtained by normalizing the voltage by the corresponding valve contact length.

Damage experiments (breakdown of the PDMS membrane) were carried out to evaluate the intrinsic properties of the PDMS material. For the breakdown voltage measurements of PDMS, both fluidic and control channels were filled with buffer. The voltage was applied in between the two types of channel manifolds. The breakdown electric fields were obtained by normalizing the voltage with the 15 μm membrane thickness.

3.2.3 Length of Contact Surfaces from Micrographs

When enough pressure was applied in the control channel, the thin membrane between control channel and fluidic channel was deflected up to block the flow in the fluidic channel. Two visible edges were formed, which indicated the length of

the contact surfaces of the valve, as shown in Figure 3.1b. The lengths were obtained from optical micrographs.

3.2.4 Surface Roughness Measurement by AFM

PDMS roughness was determined by Asylum AFM (MFP-3D-CF™) measurements, using Al-coated tip (OMCL - AC240TS, resonant frequency 70 kHz, spring constant 1.8 N/m) operating in the tapping mode, at a drive frequency of about 70 kHz. Roughness was calculated for 5×5 μm^2 surface and corresponds to the root mean square (rms) value of the surface heights.

3.3 Results and Discussion

3.3.1 PDMS Microvalve Actuation

A PDMS microvalve is formed by a crossed architecture and actuated in a push-up scheme, as shown by images taken by microscope, and the schematic side view in Figure 3.1. The valve sits at the intersection between fluidic and control channels. The flow channel is normally open, and closed when actuated by sufficient external pressure. When actuated, the valve membrane is deflected into the fluidic channel, contacting the opposite wall and forming two visible edges. The control channel is filled with water instead of air to eliminate the introduction of air bubbles into the fluidic channel during actuation.

PDMS microvalve actuation was characterized as shown in Figure 3.2. Minimum actuation pressures required to close the push-up PDMS valves are shown as a function of valve dimensions (valve membrane thickness 15 μm;

fluidic channel width from 50 to 200 μm; control channel width from 30 to 400

μm). The closing of the valves in Figure 3.2 was judged by visual inspection
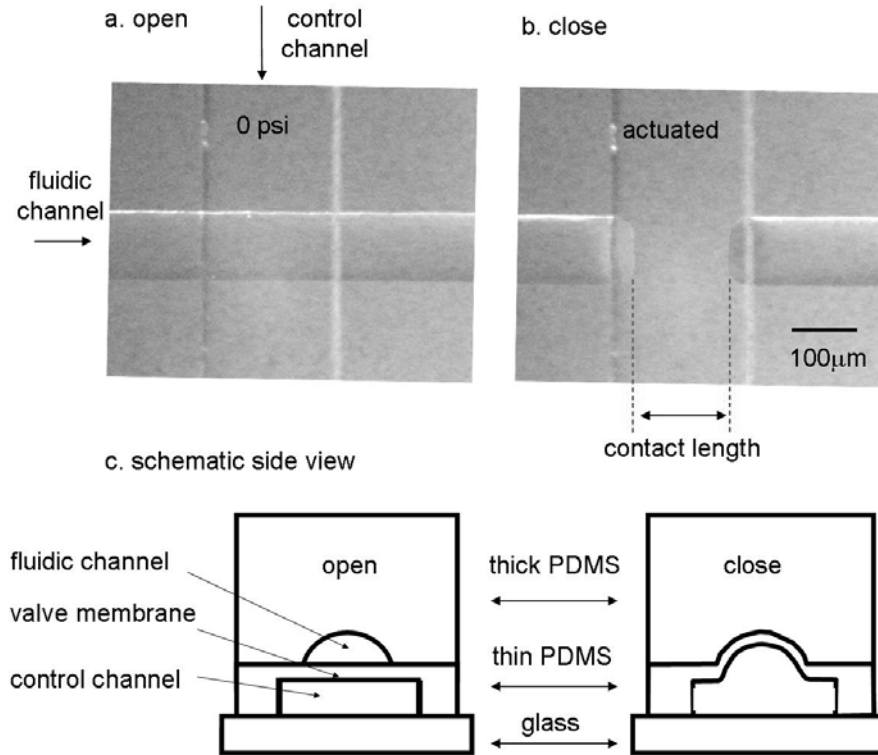
Figure 3.1 Bottom-viewed images of push-up microvalve when opened (a) and closed (b), and the corresponding schematic side view (c); contact length obtained from two visible contact edges when microvalve closed; valve membrane indicated in the side view.

under a microscope; when the fluidic channel is pinched off by the membrane

deflection two edges in the fluidic channel are visible.

The valve actuation was further evaluated by leak testing with fluorescence

detection in/downstream the valve region. Leaks were evaluated by closing the

valve and then applying pressure to the fluid channel to cause breakthrough of the

fluorescent dye. A typical leak test curve with downstream fluorescence detection

is shown in Figure 3.3. The fluidic channel was filled with fluorescence dye, and
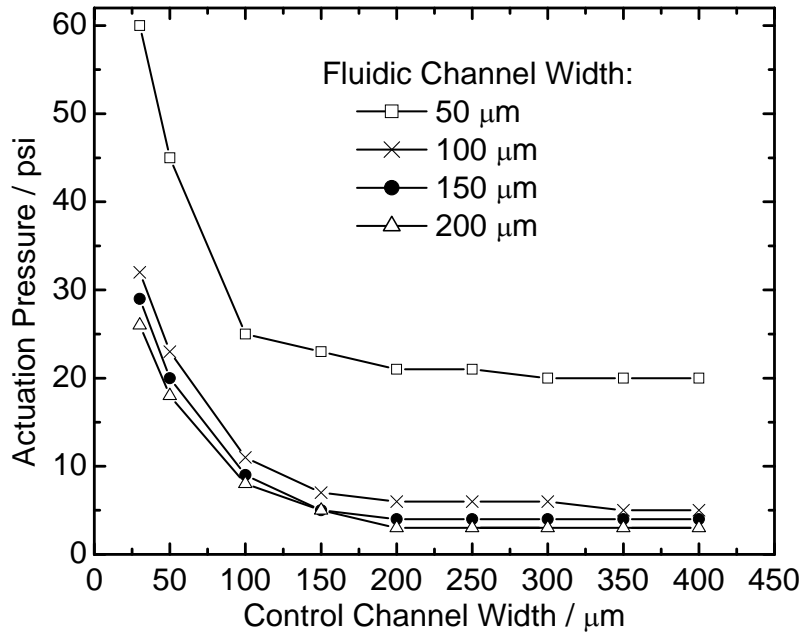
Figure 3.2 Minimum pressures to actuate push-up PDMS microvalves as a function of valve dimensions (valve membrane thickness 15 μm).
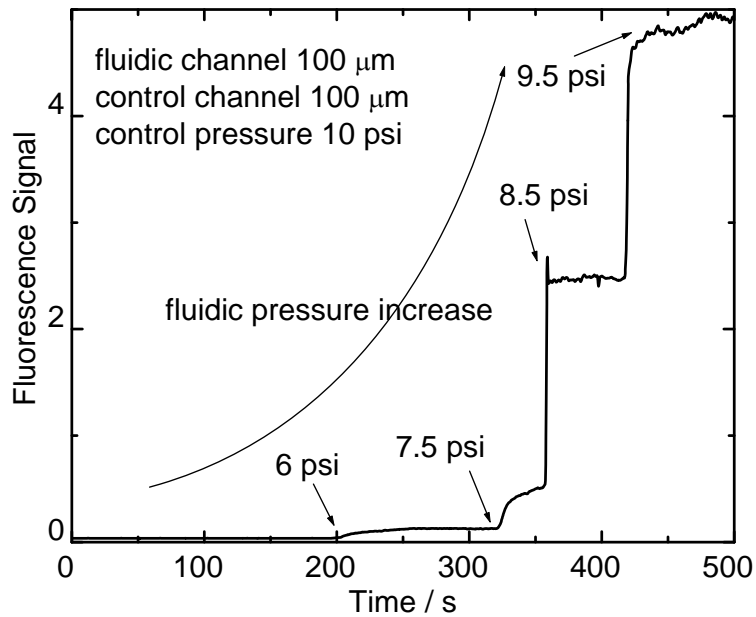
Figure 3.3 A typical leak test curve with a valve (fluidic channel 100 μm, control channel 100 μm, control pressure 10 psi), showing the fluidic leak through the valve at a fluidic pressure of 6 psi under an actuation pressure of 10 psi.

then the valve was closed while the segment of the fluidic channel downstream of the valve was rinsed with water. The valve (fluidic channel width 100 μm, control channel width 100 μm) was closed at 10 psi, according to visual inspection. Fluorescence is detected when the pressure in the fluidic channel is increased to 6 psi, indicating fluid leak through the valve. Once the PDMS valve is closed, it can stand some pressure in fluidic channel (about 6 psi in this case versus 10 psi actuation), because of the surface forces arising from PDMS-PDMS sticking.[7]

3.3.2 PDMS Microvalve Breakdown Phenomenon

Three different electrical breakdown scenarios were evaluated; breakdown within the fluidic channel across a single valve and across two valves, while the third case was breakdown across the valve membrane between the fluidic channel and the pneumatic control channel. Table 3.1 gives the measured values for breakdown threshold voltage (V) and the corresponding electric field (E) across the valve, for all three test scenarios. All three geometries are shown in the first column of the table as a top view drawing of the device, with denotation of the voltage applied. Control channels (horizontal) and fluidic channels (perpendicular) were overlapped at the location of the microvalve. Most of the data are for brand-new valves. Two valves were partially damaged at high voltages and measured for subsequent breakdown voltages. The fluidic channel widths (FCW) vary from 50 to 200 μm, and control channel widths (CCW) vary from 30 to 250 μm. The control pressure (CP) was 20 or 35 psi, which is sufficient to fully close the valves. Electric fields across the valves were obtained by normalizing

threshold voltages to the observed valve contact length in order to give E_A. The breakdown voltage across the membrane, measured in the third configuration of Table 3.1, was normalized by the membrane thickness to give E_B.

Figure 3.4 gives an example of the breakthrough curve measurement in terms of current (square) and resistance (star) of the channel vs. applied voltage. With a closed valve, the resistance was very high (around $10^{11} - 10^{12}$ Ω) and only nAmp range current was observed. However, once a high enough voltage was applied the valve failed, as evidenced by a drop in resistance and a current increase. Threshold voltages for single-valve breakdown show a linear dependence on the valve dimensions under fixed control pressures, as shown in Figure 3.5 (solid curves), increasing with control channel width (100 – 250 μm). As shown in Figure 3.6, the contact length of the valve increases linearly with increasing control channel width when other parameters remain the same, demonstrating that the threshold breakdown voltage depends linearly on valve contact length. As shown in Figure 3.7, increasing the control pressure obviously causes an increase of the contact length, within a certain range. The threshold occurs at a constant electric field strength of 39 ± 4 V/μm (n = 7, in Figure 3.5, dashed curve), as is seen when the threshold voltages are normalized to the corresponding contact length.

The measured breakdown E_B of a 15 μm thick PDMS valve membrane is about 280 V/μm (280 ± 96 V/μm, *n* = 7) as shown in Table 3.1, significantly higher than the manufacturer-stated value of 21 V/μm. Similar results were reported previously, where a membrane breakdown E_B was much higher for thin

membrane and varied with membrane thickness.[15-18] Better crosslinking may occur with thin membranes,[19] leading to the higher breakdown field. The actual breakdown value likely depends on several influential factors. When the valve is closed, the thin membrane is deflected, stressed, and becomes thinner, which may cause a lower electric field breakdown. In addition, any defects in the membrane may also cause large variations in the breakdown field. These factors likely account for the large standard deviation observed in the breakdown field results.

Frequently a voltage difference may occur across two valves in series. In the tests reported here, when two valves in the same fluidic channel are closed the threshold voltage is 8 kV. Results are shown in Table 3.1 for a 150 μm wide fluidic channel with two closed valves operated at 20 psi, separated by 4 mm along the channel. One valve length was 100 μm, while the other was 150 μm. The breakdown field E_A is 44 V/μm, when normalized to the summed length of the contact surfaces of the two valves. This is similar to the value (39 ± 4 V/μm, $n = 7$) obtained in a channel with a single valve, indicating the breakdown resistance of the two valves is simply additive.

We observed that breakthrough of the valve under threshold voltage causes some damage to the valve. The damage is indicated by a lower threshold E on subsequent tests, and is dependent on the degree of damage in the previous test. Representative results are shown in Table 3.1 with "a" superscripts.

Table 3.1 Comparison of threshold voltages and electric fields
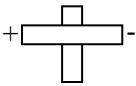
Top view	FCW / μm	CCW / μm	CP / psi	V / kV	E_A / (V/μm)	E_B / (V/μm)
1. First scenario	50	100; 150; 200; 250	35	1.2; 3.2; 4.3; 5.2	35; 43; 34; 36	40; 107; 143; 173
	100	100; 150; 250	20	2.3; 4.0; 7.7	42; 40; 41	77; 133; 257
	100	150	20	1.4	11[a] (Broken valve)	47
2. Second scenario	150	100 and 150	20	8.0	44	133
	50	150 and 250	35	4.0	19[a] (Broken valve)	67
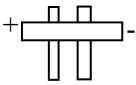
Continued

88

Continued **Table 3.1**

Top view	FCW / μm	CCW / μm	CP / psi	V / kV	E_A / (V/μm)	E_B / (V/μm)
3. Third scenario	100; 150; 200	30		3.3; 6.7; 3.2		220; 447; 213
	50; 100; 150; 200	50		3.5; 3.3; 5.8; 3.5		233; 220; 387; 233
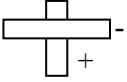
(FCW — fluidic channel width; CCW — control channel width; CP — control pressure; E_A — electric field by normalizing voltage to contact length; E_B — electric field by normalizing voltage to membrane thickness; a —valves after high voltage breakthrough, all others except a are brand-new valves; three different breakdown scenarios shown in the first column: 1. breakthrough in channel closed with single valve; 2. breakthrough in channel closed with double valves with a distance of 4 mm; 3. breakdown of thin PDMS membrane in between the fluidic channel and control channel. The drawing showed the top view of the device with control channels horizontal and fluidic channels perpendicular. ±, the positions of the voltage applied).
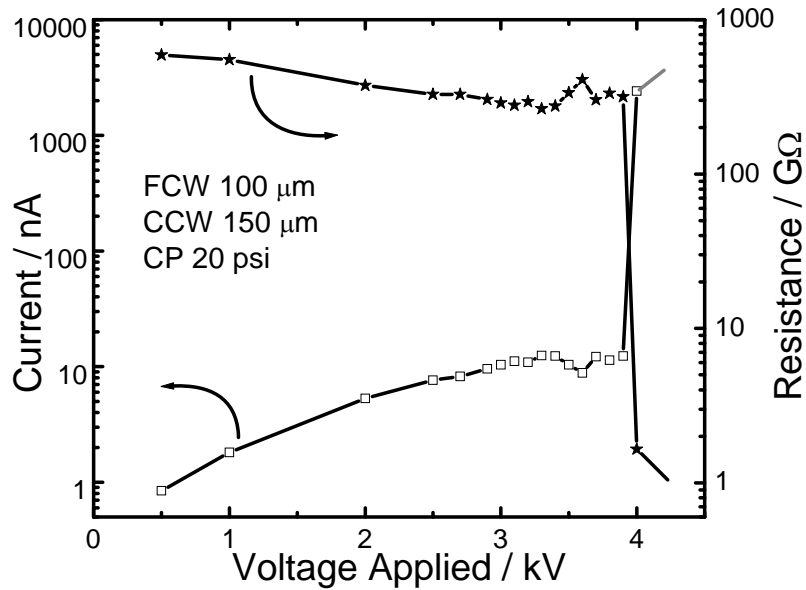
Figure 3.4 One example of the breakthrough curve in terms of current (square) and resistance (star) of the channel *vs.* applied voltage (FCW 100 μm, CCW 150 μm, CP 20 psi).
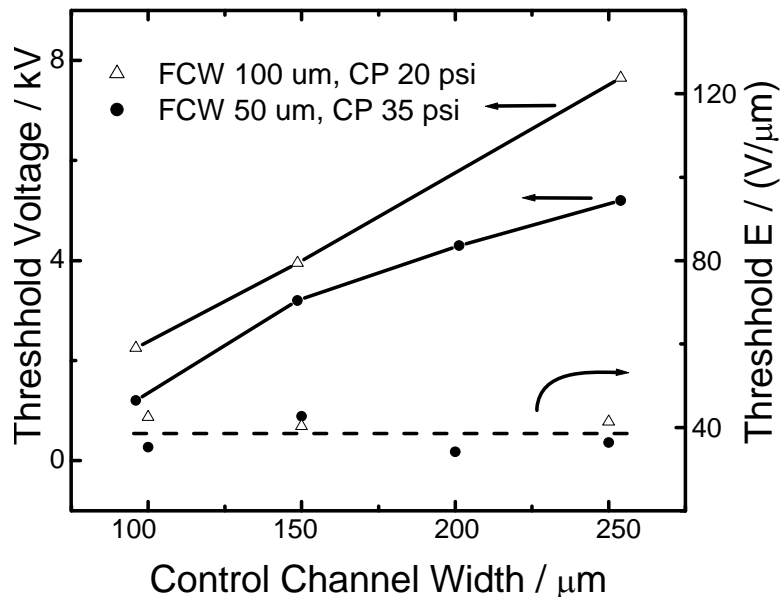
Figure 3.5 The threshhold voltage (solid) and normalized threshhold electric field (dashed) as a function of the control channel width under two control pressures; the normalized threshhold *E* was 39 ± 4 V/μm (n = 7).
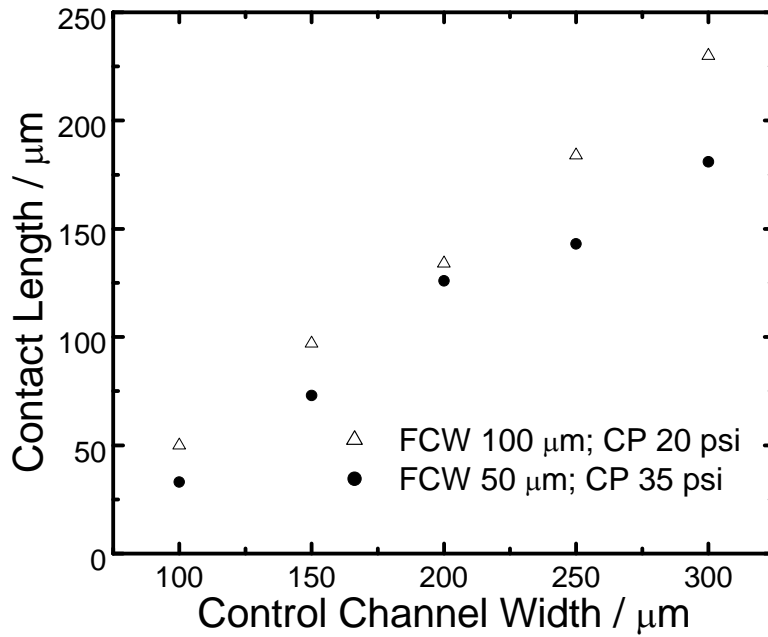
Figure 3.6 The length of contact surfaces as a function of control channel width under fixed fluidic channel width and control pressure.
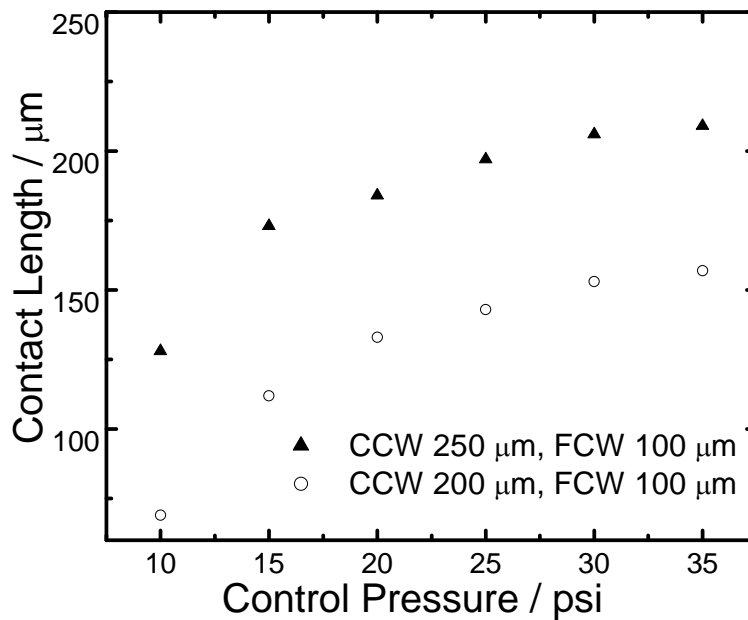
Figure 3.7 The contact length as a function of control pressures under fixed valve dimensions.

3.3.3 PDMS Microvalve Breakdown Mechanism

There are two possible pathways for breakthrough at the interface of the valve: surface breakthrough via the PDMS surfaces making contact along the fluidic channel walls (curved line, path A in Figure 3.8A), or PDMS material breakdown via the thin PDMS membrane and the water in the control channel (as shown in Figure 3.8A, smooth line, path B). The observed threshold E (in terms
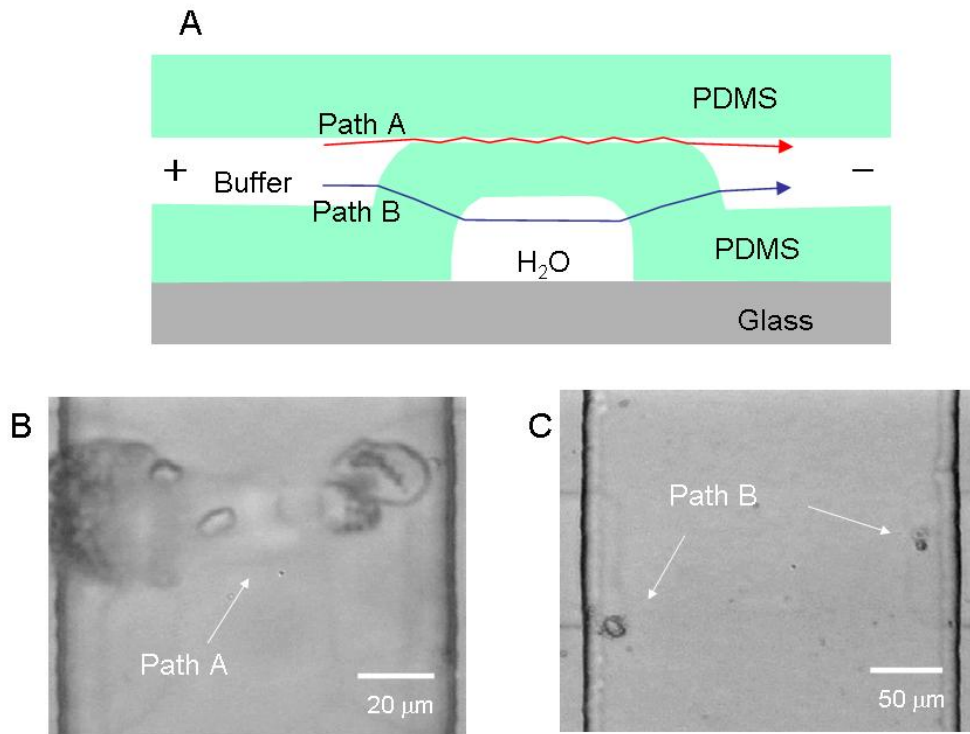
Figure 3.8 (A) The schematic side view of the valve (curved line — path A, surface breakthrough; smooth line — path B, membrane material breakdown; $\pm$ — voltage applied in the fluidic channel); (B) Micrograph of a representative path A breakthrough (CCW 100 μm, FCW 100 μm, CP 20 psi, V 2.3 kV); (C) Micrograph of a representative path B breakthrough (CCW 250 μm, FCW 100 μm, CP 20 psi, V 7.7 kV).

of valve contact length) was about 39 V/μm for path A (E_A) and 280 V/μm (in terms of membrane thickness) for path B (E_B). For each valve design we can estimate the field across each pathway as E_A' and E_B', in order to determine which path will be more likely. The values of E_A' and E_B' at the observed breakdown voltages are shown in Table 3.1. When E_A' is about 39 V/μm while E_B' is much smaller than 280 V/μm, path A will be taken for breakthrough. This condition holds for almost all designs tested (as shown in Table 3.1), so that the most common breakdown path is along the surface of the PDMS that forms the valve walls. For some valve geometries both E_A' and E_B' are close to the breakdown values at the observed threshold voltages, and either pathway may fail. This is the case for the valve with FCW of 100 μm and CCW of 250 μm, for which E_A' is 41 V/μm and E_B' is 257 V/μm. Obviously, when E_A' is much smaller than 39 V/μm while E_B' is close to 280 V/μm, path B will be taken for breakthrough. None of the valves we designed follow this scenario.

Movies taken under the microscope provide further evidence for the mechanism of the breakthrough, as shown in the two representative snapshots in Figure 3.8B and 3.8C, and a series of snapshots in Figure 3.9. The images show the microvalve region, with the fluidic channel located horizontally, the control channel located vertically, and voltage applied to the fluidic channel. The edges of the channels and the valve membrane contact regions are visible. For the breakdown measurement with the valve shown in Figure 3.8B (CCW 100 μm, FCW 100 μm, CP 20 psi, V 2.3 kV), the calculated breakdown fields along each pathway, E_A' and E_B', are 42 and 77 V/μm, respectively. We can conclude that

A. CCW 100 μm, FCW 100 μm,
CP 20 psi, V 2.3 kV

B. CCW 250 μm, FCW 100 μm,
CP 20 psi, V 7.7 kV

time / s

4.00

4.07

6.60

6.67

6.73

6.80

7.70

time / s

4.67

4.73

4.80

4.87

4.93

5.00

6.13
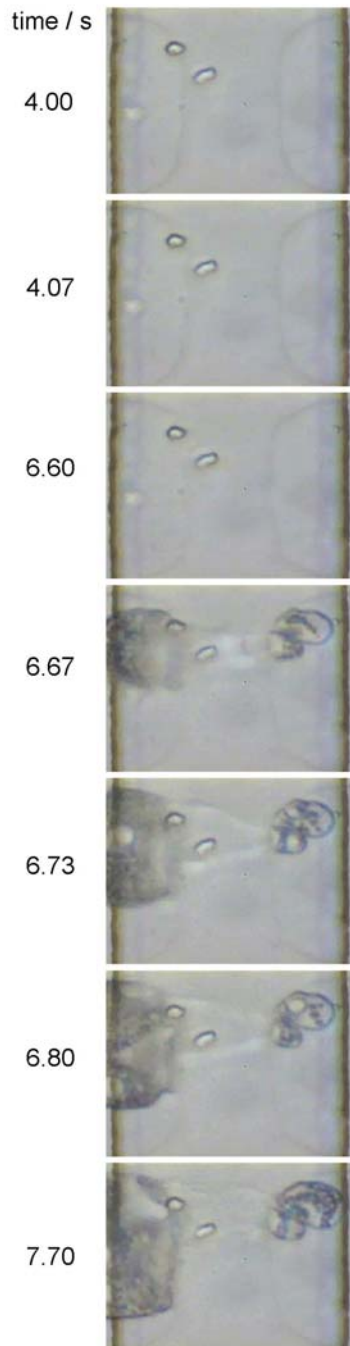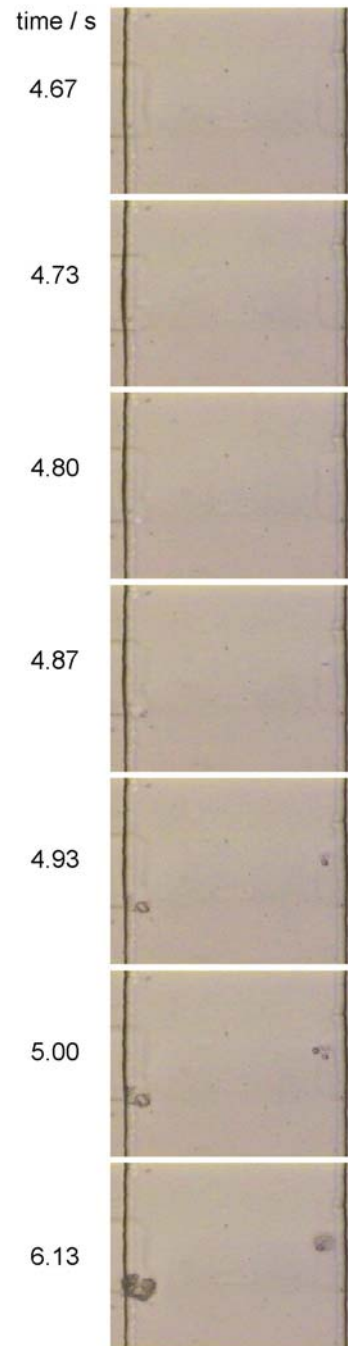
Figure 3.9 Images at different recording time taken from the movies.

path A is taken in this case, and this is supported by the movie and image shown in Figure 3.8B and 3.9A. A moving shadow of the buffer within the valve region is observed, indicating solution transport along the surface of the PDMS that forms the fluidic channel walls. Some yellowish debris forms at the interface, which is easily cleaned by operating the valves. For the breakdown measurement with the valve shown in Figure 3.8C (CCW 250 µm, FCW 100 µm, CP 20 psi, V 7.7 kV), the calculated breakdown fields of E_A' and E_B' for each pathway are 41 and 257 V/µm, respectively. We cannot estimate which path will be taken. The movie and image in Figure 3.8C and 3.9B show that path B is taken for this example. Two small holes were observed in the membrane and the debris formed was not easily removed. During breakdown, one hole forms first and the two holes created do not form the shortest path through the control channel and back into the fluidic channel, indicating the weakest membrane spot is where breakthrough most likely occurs.

Breakthrough path A may arise from surface conduction or nanochannel conduction,[20-25] originating from the double layer property of a charged surface in solution. Similar breakdown at the interface of reversibly and irreversibly bonded PDMS/glass has been observed,[26, 27] where leakage at the former is assigned to nanochannel effects and leakage at the latter has been proposed to arise from dielectric breakdown of the material. The conclusions that these authors reached were partially based on the manufacture-stated breakdown value of 21 V/µm. In the first case, an electric field of 5 – 10 V/µm was used to break a 20 µm thick, reversibly bonded, PDMS/glass gap between two channels and the leakage was

assigned to nanochannel effects.[26] Such a breakdown was used for protein concentration and caused no obvious material damage. In the second case, an electric field of 25 V/μm was used to break a 40 μm membrane gap between two channels in an irreversibly bonded PDMS/glass device,[27] and the breakdown was assigned to material damage rather than nanochannel effects. However, the PDMS layer was irreversibly bonded to glass after plasma oxidation, so that surface roughness could have contributed a role for nanochannels.

It is sensible that the leakage observed in reference 26 is due to surface breakdown, since the breakdown electric field is lower than the material breakdown strength and the weak, reversibly bonded PDMS/glass interface facilitates the formation of nanochannels. However, it is not clear that the breakdown in reference 25 is correctly assigned to material breakdown, as the leakage may still arise from surface nanochannel conduction. Those authors made an assignment based on the manufacture-stated material breakdown value of 21 V/μm, concluding that a breakdown number of 25 V/μm must mean that material breakdown occurred. We and others observed much higher membrane breakdown values for thin PDMS membranes.[15-18] So the breakdown field strength is significantly variable, and has a dependence on film thickness. Therefore, their observed breakdown field doesn't ensure a material breakdown pathway. In addition, they used plasma treatment which makes a very rough surface that is more prone to channel formation. The breakdown fields they see of 25 V/μm is very similar to the surface breakdown value of 5 - 10 V/μm that was reported in reference 24. Surface breakdown still causes damage, so the damage they saw is

still consistent with surface breakdown. The discrepancy in the breakthrough electric fields between the above reported values and ours (39 V/µm) may arise from several differences, such as the interface difference (PDMS/glass *vs.* PDMS/PDMS), operation of the valves with/without pressure involved, surface roughness differences, PDMS curing differences and design differences.

Surface roughness was measured to characterize the surface properties in our case, as roughness may play a role in surface/nanochannel conduction. As shown in Figure 3.10, three sets of PDMS surfaces were characterized by AFM before and after plasma etching. The fluidic channel walls are comprised of a PDMS surface formed on the photoresist pattern on a silicon fluidic mold to form the side walls, and a top surface that was open to atmosphere during curing, referring to 3.2.1, Figure 1.5, and Figure 3.1. These two kinds of surfaces are characterized, as shown in Figure 3.10 b and c. The PDMS surface formed on the silicon surface on a silicon fluidic mold is also characterized for comparison, as shown in Figure 3.10a. For the PDMS surfaces formed on the silicon surface, the surface roughness changes from 1.6 nm to 5.1 nm after plasma etching. For the PDMS surfaces formed on the photoresist pattern, the roughness changes from 1.3 nm to 6.0 nm after etching. No etching effect is observed for the top air-facing surface of thin PDMS, since the roughness stays < 0.5 nm. Therefore, the roughness for the membrane comprising the fluidic channel in the device is 6.0 nm for one side, and < 0.5 nm for the other side. This roughness (6.0 nm) comes from oxygen plasma etching, which is also observed by others to be in the range of tens of nm.[28, 29] An optimization of the process to decrease the surface roughness may
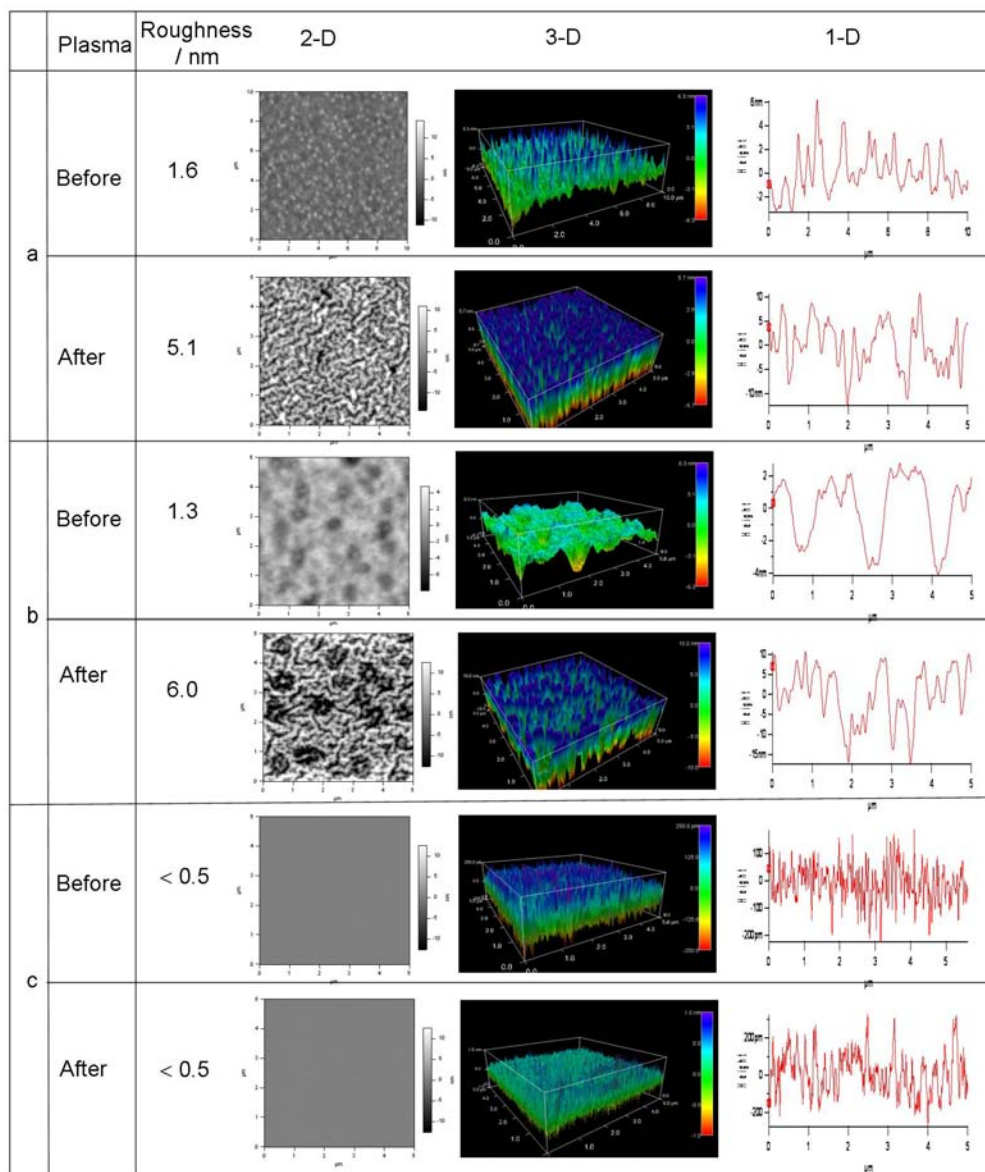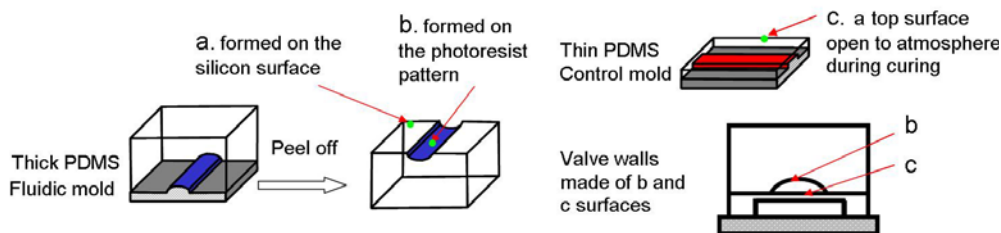
Figure 3.10 Comparison of the surface roughness of PDMS before and after plasma etching, measured by AFM (three sets of PDMS surfaces studied: a, PDMS surface formed on the silicon surface on fluidic mold; b, formed on the photoresist pattern on fluidic mold; c, surface exposed to atmosphere during curing; fluidic channel in PDMS device comprised of surfaces from b and c, with roughness of 6.0 nm and < 0.5 nm, respectively).

help to increase the valve resistance to breakdown at high voltage, since roughness will induce nanochannels.

Based on the above results and discussion, in order to design an in-channel microvalve in an electrified device, both the threshold electric fields normalized by valve contact length ($E_A < 39$ V/μm) and valve membrane thickness ($E_B < 280$ V/μm) should be taken into account. The required contact length and valve membrane thickness can be easily determined for the given target voltage. If the required contact length is large, a single large valve will result in a slow valve response. Multiple smaller valves instead can be placed in series on the same fluidic channel to increase the contact length. If the required valve membrane is thick, the actuation pressure will become high. Multiple thinner valves in series on the same fluidic channel can increase the breakthrough membrane thickness by summation of each membrane thickness, for the case where the control channels for these valves are not connected by a conductive path such as the control channels. An optimized bonding technique with minimum PDMS surface roughness may also help. Currently five major techniques have been developed for irreversible PDMS bonding;[30] surface oxidation by oxygen plasma, surface oxidation by corona discharge, partial curing, varying curing ratio, and the use of uncured PDMS adhesive/UV glue. It is possible that these different bonding methods may exhibit different surface and membrane breakdown voltage.

3.4 Conclusion

Design parameters and the performance of PDMS microvalves in the

presence of high electric fields were studied in detail. Even though the valve's high impedance when closed makes the valves useful, the high field breakdown regime must be considered in the overall design of the device. The measured threshold voltages depend on the valve dimensions, and control pressures. For devices prepared using the methods described, the field along the length of the valve should be less than 39 V/µm, while the valve membrane thickness should give a field strength that is less than 280 V/µm. For most valve designs, the lower field breakdown path will be along the surface of the PDMS. In all cases, the damage is not fully reversible.

3.5 References

(1)   Unger, M. A.; Chou, H. P.; Thorsen, T.; Scherer, A.; Quake, S. R. *Science* **2000**, *288*, 113-116.

(2)   Melin, J.; Quake, S. R. *Annu. Rev. Biophys. Biomol. Struct.* **2007**, *36*, 213-231.

(3)   Haeberle, S.; Zengerle, R. *Lab Chip* **2007**, *7*, 1094-1110.

(4)   Whitesides, G. M. *Nature* **2006**, *442*, 368-373.

(5)   Maerkl, S. J. *Integrative Biology* **2009**, *1*, 19-29.

(6)   Hong, J. W.; Quake, S. R. *Nat. Biotechnol.* **2003**, *21*, 1179-1183.

(7)   Studer, V.; Hang, G.; Pandolfi, A.; Ortiz, M.; Anderson, W. F.; Quake, S. R. *J. Appl. Phys.* **2004**, *95*, 393-398.

(8)   Hao Chen, J.-C. D. M. *Biophysical Society 49th Annual Meeting, Long Beach, California, USA,* **2005 February 12-16** 853-Pos.

(9)   Chen, H.; Gu, W.; Cellar, N.; Kennedy, R.; Takayama, S.; Meiners, J. C. *Anal. Chem.* **2008**, *80*, 6110-6113.

(10)   Harrison, D. J.; Manz, A.; Fan, Z. H.; Ludi, H.; Widmer, H. M. *Anal. Chem.* **1992**, *64*, 1926-1932.

(11)   Wang, Y. C.; Choi, M. N.; Han, J. Y. *Anal. Chem.* **2004**, *76*, 4426-4431.

(12)   Dodge, A.; Brunet, E.; Chen, S. L.; Goulpeau, J.; Labas, V.; Vinh, J.; Tabeling, P. *Analyst* **2006**, *131*, 1122-1128.

(13)   Huang, B.; Wu, H. K.; Bhaya, D.; Grossman, A.; Granier, S.; Kobilka, B. K.; Zare, R. N. *Science* **2007**, *315*, 81-84.

(14)   Lu, Q., Bao, J.-B., Harrison, D.J.   *Eleventh International Conference on Miniaturized Systems for Chemistry and Life Sciences* Paris, FRANCE 2007,   October 7 - 11; 44-46.

(15)   Pelrine, R.; Kornbluh, R.; Joseph, J.; Heydt, R.; Pei, Q. B.; Chiba, S. *Materials Science & Engineering C-Biomimetic And Supramolecular Systems* **2000**, *11*, 89-100.

(16)   Dubois, P.; Rosset, S.; Koster, S.; Stauffer, J.; Mikhailov, S.; Dadras, M.; de Rooij, N. F.; Shea, H. *Sens. Actuators A* **2006**, *130*, 147-154.

(17)   Kim, H. K.; Shi, F. G. *IEEE Trns. Dielectr. Electr. Insul.* **2001**, *8*, 248-252.

(18)   Lee, J. H.; Ji, W. Y. In *Proceedings of the 7th International Conference on Properties and Applications of Dielectric Materials, Vols 1-3*; Ieee: New York, 2003, pp 591-594.

(19)   Liu, M.; Sun, J. R.; Sun, Y.; Bock, C.; Chen, Q. F. *J. Micromech. Microeng.* **2009**, *19*, 035028.

(20)   Masliyah, J. H., and Bhattacharjee, Subir, *Electrokinetic and colloid transport phenomena*; JohnWiley & Sons, Inc, 2006.

(21)   Qiao, R.; Aluru, N. R. *Nano Lett.* **2003**, *3*, 1013-1017.

(22)   Schoch, R. B.; van Lintel, H.; Renaud, P. *Phys. Fluids* **2005**, *17*.

(23)   Stein, D.; Kruithof, M.; Dekker, C. *Phys. Rev. Lett.* **2004**, *93*.

(24)   Karnik, R.; Castelino, K.; Fan, R.; Yang, P.; Majumdar, A. *Nano Lett.* **2005**, *5*, 1638-1642.

(25)   Schoch, R. B.; Han, J. Y.; Renaud, P. *Rev. Mod. Phys.* **2008**, *80*, 839-883.

(26)   Kim, S. M.; Burns, M. A.; Hasselbrink, E. F. *Anal. Chem.* **2006**, *78*, 4779-4785.

(27)   Lee, J. H.; Chung, S.; Kim, S. J.; Han, J. Y. *Anal. Chem.* **2007**, *79*, 6868-6873.

(28)   Tserepi, A.; Cordoyiannis, G.; Patsis, G. P.; Constantoudis, V.; Gogolides,

E.; Valamontes, E. S.; Eon, D.; Peignon, M. C.; Cartry, G.; Cardinaud, C.; Turban, G. *J. Vac. Sci. Technol. B* **2003**, *21*, 174-182.

(29)   Tsougeni, K.; Tserepi, A.; Boulousis, G.; Constantoudis, V.; Gogolides, E. *Japanese Journal Of Applied Physics Part 1-Regular Papers Brief Communications & Review Papers* **2007**, *46*, 744-750.

(30)   Eddings, M. A.; Johnson, M. A.; Gale, B. K. *J. Micromech. Microeng.* **2008**, *18*.

Chapter 4

Coupled CE-Fractionation-SPE-ESIMS Peptide Analysis on Valve-Based Microchip[*]

4.1 Introduction

Proteomics involves identifying all proteins (their functionality, abundance, modification state, and subcellular location) expressed within healthy and stressed or diseased biological samples. It is an overwhelming challenge, considering the complexity of proteins: ~20,000 different proteins in mammalian samples, a wide range of pI, polarity, solubility and abundance, existence of post-translational modifications, nonspecific adsorption onto many surfaces, and so on. The techniques to solve this problem require high throughput and multiplexed capabilities. Mass spectrometry (MS) is the most powerful method to date for protein identification. The most commonly used method for proteome profiling is based on two-dimensional (slab) gel electrophoresis (2DGE) separation of proteins samples, followed by chemical processing and MS identification.[1] The throughput of the 2D-PAGE based method is low since the individual extraction,

---

[*] A version of this chapter has been prepared for submission to *Lab Chip*.

A portion of this chapter has been presented as, Lu, Q.Y., Bao, J.-B., Harrison, D.J. *Eleventh International Conference on Miniaturized Systems for Chemistry and Life Sciences*, Paris, FRANCE, October 7 – 11, 2007, 44-46.

A portion of this chapter has been presented as, Lu, Q.Y., Bao, J.-B., Harrison, D.J. *the Edmonton Regional Meeting of the Canadian Proteome Society*, Edmonton, Canada, February 21 – 22, 2008.

A portion of this chapter has been presented as, Lu, Q.Y., Bao, J.-B., Harrison, D.J. *the 91st Canadian Chemistry Conference*, Edmonton, Canada, May 24–28, 2008.

digestion, and analysis of each spot from 2D-PAGE is tedious and time-consuming. The system is also biased, since proteins exhibiting more extreme characteristics (i.e. high or low pI, high MW, low abundance, low solubility such as membrane proteins) are often not seen. An alternative method, "shotgun proteomics", uses multiple-dimensional liquid chromatography to separate fully digested samples of protein mixtures for MS analysis.[2] It is relatively unbiased, relatively faster, more sensitive and more amendable to automation. However, the peptides need to be analyzed using a combination of tandem MS sequencing and very complex data analysis (SEQUEST), leading to a limitation of the system throughput.

Microfluidic platforms are regarded as an alternative for sample preparation for MS analysis, due to advantages such as rapid separation (e.g., capillary electrophoresis, CE), favorable reaction kinetics, high capacity to integrate multiple steps, relatively easy automation with less robotics, and low sample consumption. The coupling of electrospray ionization (ESI) as a continuous flow source is particularly suitable for microfluidic devices.[3] Impressive work has been done developing protein processing on chip for MS; chemical processes such as digestion, concentration and cleanup of the sample, multi-dimensional separations, and interfacing with MS[4] [5] have been demonstrated. Most work has focused on devising high peak capacity methods with high speed for protein or peptide separation, in order to replace slab-gel-based 2DGE or shotgun-based 2D column chromatography (2DCC). A few researchers succeeded in integrating several functions in a single chip, with either column chromatography[6-9] or CE based[10-12]

104

separations. Harrison's group[12] developed the first fully integrated miniaturized platform for proteomic analysis, by integrating a solid phase extraction (SPE) bed for sample pretreatment, a narrow channel for CE separation and a low-dead-volume nanospray emitter for ESIMS coupling. The chip was interfaced via a transfer line to an autosampler. The system was able to analyze tryptic digests at a rate of 12 samples per hour with a detection limit of 5 nM (25 fmol on chip), and was used for identification of 72 proteins of human prostate cancer LNCap cells obtained from 2DGE spots. The same group[11] demonstrated integrating immobilized trypsin bead beds for on-line protein digestion, CE separation of digests, and an electrospray mass spectrometry interface for automated sample processing. Rapid digestion, separation and identification of proteins were shown. Regnier's group[9] developed a multicolumn polydimethylsiloxane (PDMS) chip, incorporating a trypsin-derivatized bead-packed column for trypsin digestion, an immobilized metal affinity capture bead-packed column for selection of histidine-containing tryptic peptides, and a microfabricated collocated monolithic support structure for reversed-phase column (RPC) for capillary electrochromatography (CEC) of trapped peptides. The device was demonstrated by running fluorescently-labeled BSA samples, so its compatibility with MS detection remains unknown. Xie *et al.* developed a chip made of a combination of parylene, silicon and PDMS; integrating gradient pumps, an injector, mixer, reversed-phase separation column, electrodes and ESI nozzle.[8] The system performance is close to that of a commercial nanoflow LC system, when comparing the analysis of digested BSA samples. Agilent Technologies developed a compact,

commercialized polyimide microdevice composed of a sample enrichment loop, bead-based liquid chromatography column and laser-ablated in-line nanoflow ESI emitter.[7] This system performance was demonstrated by analysis of BSA digest and comparable to standard state-of-the-art nano-LC-MS. The device was further developed for 2-Dimensional LC separation of tryptic digests and plasma samples.[6] Ramsey's group developed an integrated device for digestion, separation and postcolumn labeling of proteins and peptides.[13] Recently, they reported an integrated compact glass chip, including CE separation and an in-line direct ESI spray from the corner of a rectangular device.[10] The CE-MS analysis of peptides and proteins showed efficiencies of over 10^6 plates/m.

A fully integrated, multiplexed, automated microfluidic platform for protein processing interfaced to an MS has not been reported, even though multiplexing of microfluidic systems for protein analysis provides a powerful route to more rapid, less costly proteomics research.[14] Our group has been working on the integration of several protein processes together in one microchip before ESI mass spectrometry detection, to make it compact and multifunctional. A single channel device developed by C. Wang *et al.* was further developed into a two-bed system with one bed of trypsin digestion beads, a second bed of reverse-phase beads for solid phase extraction (SPE) of the eluted peptides, and then CE-ESIMS detection for peptides elution.[15] J. Taylor then tried to further develop the two-bed system into a multiplexed platform with 20 channels via delay line control, each containing the trypsin and SPE beds.[16] However, due to poor bead packing reproducibility and the associated variability in flow rates, elution to the mass

106

spectrometer from each channel occurred at rates that could not be predetermined. Taylor's design required predictable delivery rates from each channel. The challenge of making many channels with SPE or chromatographic beds identical in terms of flow resistance has encouraged us to explore mechanical valve-based systems, in which each channel can be eluted totally independently. Pneumatically actuated valves, introduced by VerLee[17] and developed into complex systems by Quake[18] provide a powerful alternative actuation system in addition to electroosmotic flow (EOF). The valve design of Quake's was chosen because it has zero dead volume[19, 20] which is good for separation integration. In addition, the polydimethylsiloxane (PDMS) chip was thought to be a compatible material for ESI-MS[21, 22] and a viable choice for demonstrating complicated integration idea.

We describe here the design and operation of a system that performs electrokinetic separation, followed by fractionation into multiple channels, SPE extraction and sample cleanup on packed reaction beds, using a multiplexed, hydraulically valved system, with subsequent MS analysis. This coupled multiple channel CE-Fractionation-SPE-ESIMS platform on a valve-based microchip was successfully applied to peptide analysis.

4.2 Chip Design

Individual components or single channel designs reported in the literature[4, 6, 11] are of scientific interest and increase the size of the microfluidics toolbox, but have very limited real applications. Our goal is to develop a fully integrated,

multiplexed microfluidic system with potential applications in proteomics. Such a system needs to comprise protein separation, fractionation, solid phase extraction, an MS analysis interface, and other components. The first challenge is to manipulate all these components individually and understand their performance. Of two reported designs for microfluidic valves, Mathies' valve allows protein samples to be stored or transported in glass channels with very limited exposure to PDMS.[23] This could be an advantage because of extensive knowledge we have gained on protein adsorption on glass materials. Unfortunately, Mathies' design has a significant valve chamber volume (usually hundreds of nL), making it incompatible with the resolution of any on-chip CE-based separation method. The valve developed by Quake offers zero dead volume[19, 20] and hence becomes our option in this work. To use Quake's valve, we need to operate samples in channels and reservoirs made of PDMS. Various coating methods have been reported to reduce protein adsorption on PDMS surfaces.[24-27] However, our preliminary trials on CE separation of proteins show very poor quality, whereas our tests on peptide samples exhibit much better results. Therefore, the "shot-gun" method becomes our preferred option, because it allows us to analyze peptides instead of protein samples on a PDMS chip. After evaluation of various methods for peptide separation, CZE was selected due to its simplicity and compatibility with subsequent steps, in particular with mass analysis.

A proteome chip was developed based on the above considerations; It consists of two PDMS layers on a glass substrate, one as control layer (red), the other as fluidic layer (blue), as shown in Figure 4.1 (upper). The fluidic design can be

divided into four different sections, solution inputs, separation and fractionation, SPE, and MS interfacing, labeled as A to D. The system was designed to perform CE separation (B), followed by an in-line fractionation (B) into multiple channels, SPE enrichment and desalting on packed bead beds (C), and subsequent multiplex elution of the samples in each channel to ESIMS. A multiplexed, hydraulically valved system was developed to control each step, and isolate each channel in the manifold from all the others. The fluidic layer includes a double-T CE separation channel (B), eight branch channels with SPE beds used for the collection of fractions, where each fractionation section is 1.5 mm long separated by fractionation valves (B and C), three solution input channels (A), and two exit channels either to waste or to ESIMS (D), as shown in Figure 4.1. The CE separation section includes four reservoirs, indicated as buffer, buffer waste, sample, and sample waste. The injector for sample loading is designed to be 200 μm long. The starting and ending points of the in-line fractionator in the separation channel are indicated in the graph; starting at 2.55 cm away from the injector. The valves in the control layer are divided into five groups in terms of the control purpose, marked as group 1 to group 5 valves. Group 1 includes three control channels, and three valves individually sitting on each solution input channel. Different solutions can be placed in input reservoirs and introduced into the chip by switching the group 1 valves on and off. Group 2 includes six control channels, and twenty – four valves sitting on the eight different fluidic channels, and, with a multiplexer used to minimize the external control points. The multiplexer is a binary tree design, using $2\log_2 N$ horizontal valve control channels

to control N vertical flow channels with $Nlog_2N$ valves.[28] Using these valves, the opening/closing of eight fluidic channels are controlled. Group 3 includes one control channel, and nine valves to fractionate separated samples into eight sections. Group 4 includes one control channel, eight valves to close the side eight channels during separation step. Group 5 includes two control channels, and two valves for the switch between waste and ESIMS. The valves are designed to be 200 μm wide, and the bridges where the control channels cross over the fluidic channels are 30 μm wide. The details of the device layout and dimensions are shown in Figure 4.2.

Device operation includes four steps, as shown in Figure 4.1 (below). The first is a CE separation step, where all the valves are closed except the fractionation valves (group 3), depicted in Figure 4.1 (below (1)). Voltage is applied in the four reservoirs. Sample is loaded into the double-T intersection, then separated in the separation channel. The second step is in-line fractionation and collection, where fractionation valves are closed simultaneously to trap the separated samples, and buffer is delivered to flush the fractions into individual SPE beds by operating group valves 1, 2, 4 and 5, as indicated in Figure 4.1 (below (2)). The third step is desalting and enrichment in the SPE beds (Figure 4.1 (below (3)). Water is delivered for rinsing and exit channel is connected to waste. The final step is multiplexed elution to the MS, where samples in each bed are sequentially eluted to the MS for detection by operating the multiplexer valves of group 2 (Figure 4.1 (below (4)). Elution buffer is delivered and the exit channel is connected to MS.
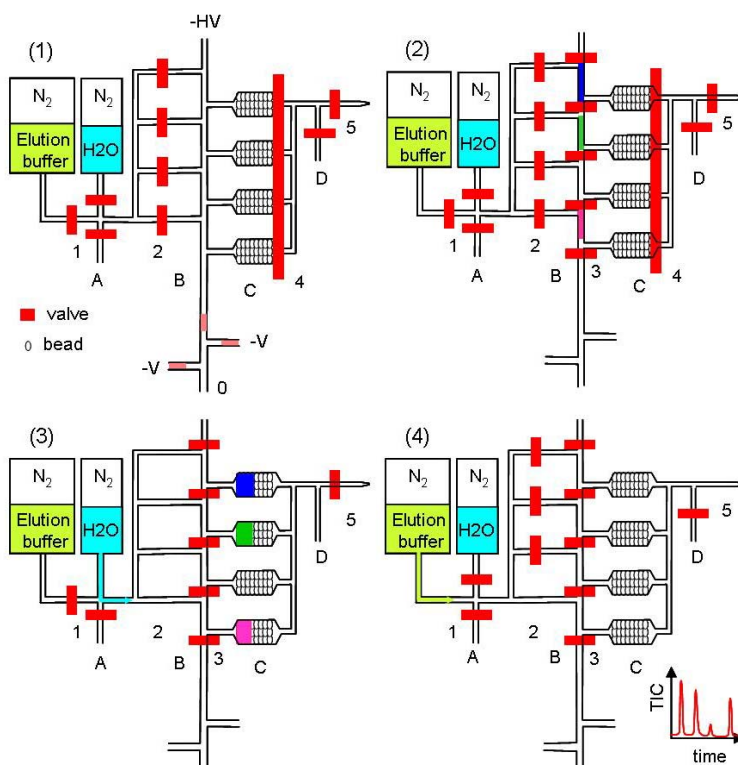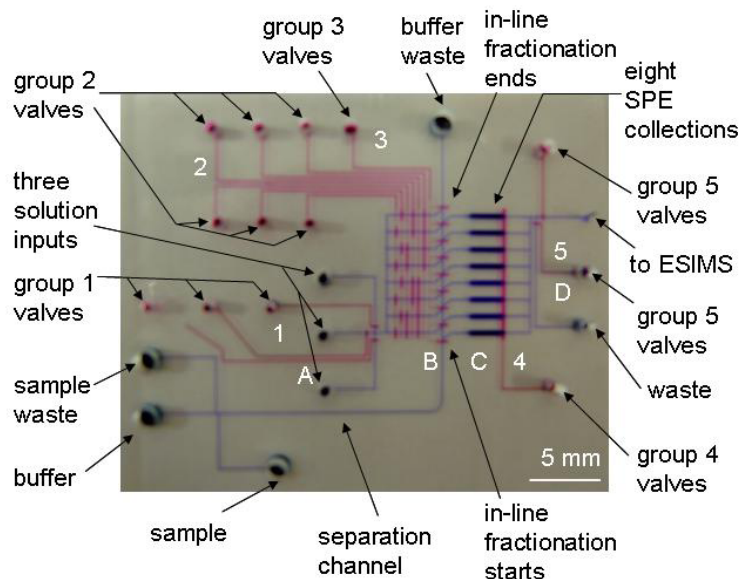
Figure 4.1 The optical micrograph of a PDMS proteomic analysis system without external pressure lines (upper) and the demonstration of the chip operation with four collection channels (below) (A – D, indicating different sections of the fluidic layer design; A – solution inputs; B – separation and fractionation; C – SPE; D – MS interfacing. 1 – 5, indicating different groups of the valves; Major chip operation steps: (1) CE separation; (2) in-line fractionation and collection into multiple SPE beds; (3) sample desalting and enrichment in the SPE beds; (4) multiplexed elution to the MS).

A. Device	B. Separation Channel
PDMS Fluidic layer (4 – 6 mm thick)	0.5 cm, 1 cm
PDMS control layer (45 μm thick)	1 cm
Glass support	Double T injector 200 μm long
Bonded together	In-line fractionator shown in C
Final device	4.5 cm

C. Image of 8-section In-line Fractionator

2.55 cm away from injector

each section 1.5 mm

separation channel

side sample collection channels   fractionation valves

D. **Main design dimensions**						
fluidic channel	CE separation		fractionator		column	
	injector length	200 μm	each section length	1.5 mm	length	3 mm
	width	100 μm	width	100 μm	width	500 μm
	depth	12 μm	depth	12 μm	depth	76 μm
control channel	valve width	200 μm	bridge width	30 μm	depth	30 μm

Figure 4.2 Details of the device layout and dimensions: (A) Device comprised of three layers, PDMS fluidic layer with fluidic channel pattern (4 – 6 mm thick), PDMS control layer with valve control channel pattern (about 45 μm thick) , and glass as support; (B) Separation channel layout; (C) Image of the eight-section in-line fractiontor, which is 2.55 cm away from CE injector; each fractionation section is 1.5 mm long; horizontal line is the main separation channel; one vertical side channels for solution inputs, another for sample collections; fractionation realized by patterning of in-line valves; (D) List of the main design dimensions, column design and post column connections referring to chapter 2, Table 2.1, column to exit channel ranged from 7 mm to 18 mm.

4.3 Experimental

4.3.1 Chemicals and Reagents

The following chemicals were from Sigma-Aldrich (Oakville, ON, Canada): cytochrome c (horse heart), Trizma$^®$ Base, fluorescein isothiocyanate isomer I (FITC), ammonium bicarbonate, ammonium hydroxide, HPLC grade acetone and acetic acid. Boric acid was from BDH Chemicals. The elution buffer solution was comprised of 0.1 M formic acid (Fluka, Buchs, Switzerland) and LC-MS grade methanol (Riedel-de Haen, Seelze, Germany). All aqueous solutions were made in ultrapure water (Millipore Canada, Mississauga, ON) and filtered through 0.2 μm filters (Nalgene, Rochester, NY, USA) prior to use. Chemicals n-dodecyl-β-D-maltoside (DDM) (Acros organics, New Jersey, USA), sodium dodecyl sulfate (SDS) (Sigma, St. Louis, MO), methyl cellulose (MC, approximate viscosity at 2%, 25℃, 400cPs) (Sigma, St. Louis, MO) were tested for dynamic coating of PDMS. Ampholyte Bio-lyte (pH 3-10) was obtained from (Bio-RAD, CA). Green fluorescent protein (GFP) was a gift from Huiwang Ai in Dr. Campell's group in Department of Chemistry, University of Alberta. Bovine serum albumin (BSA, 66 kDa) and trypsin inhibitor (soybean, 20.1 kDa) were bought from Sigma (St. Louis, MO), and labeled using an Alexa Fluor 488 Microscale Protein Labeling kit (Invitrogen, Carlsbad, CA).

Cytochrome c was digested off-chip on immobilized TPCK-trypsin beads (Pierce, Rockford, IL, USA). Washed, centrifuged trypsin-immobilized beads were suspended in 200 μL of digestion buffer, added to 1 mg of cytochrome c in 0.5 mL digestion buffer (0.005 M NH$_4$HCO$_3$, pH 8.0), and shaken at 37 ℃ for 16

113

h. Beads and digest were separated by centrifugation. The sample was concentrated by SpeedVac as needed. The digest was labeled with FITC by adding 16 μL of FITC in acetone (1 mM) to 100 μL of the 0.16 mM digest solution, and reacting for 20 h at 4 ℃ in the dark.[29]

.

4.3.2 Chip Fabrication

Chips were fabricated using multilayer soft lithography, employing master fabrication, PDMS molding and shaping, and multilayer bonding. Two different masters, fluidic and control level masters, were produced lithographically, using both AZ P4620 (Clariant Co., Charlotte, NC, USA) and SU8 2050 photoresists (MicroChem Co., Newton, MA, USA). The fluidic master used a two-step process to form channels with different depths. First, a thin layer (10 μm) of AZ P4620 was spin-coated onto a silicon wafer (ϕ 4", Virgin Test, Silicon Valley Microelectronics, Inc., San Jose, CA, USA). After UV exposure and development, the photoresist edges were rounded by reflow at 150 ℃ for 30 min, then further baked at 190 ℃ (> 3 h) for full hardening. The structure was very stable during later photolithographic processes. A 76 μm thick SU8 2050 layer was used on the same wafer to form the second layer pattern for the thick SPE beds. A square-profiled pattern was obtained for the beds. Details are given in Chapter 2. The control master was fabricated using spin-coated SU8 2050 to form a 30 μm deep pattern on a silicon wafer. Finally both masters were silanized with trichloro(1,1,2,2-perfluorooctyl) silane (Sigma-Aldrich, Oakville, ON, Canada) vapor overnight.

The PDMS pre-polymer (Sylgard® 184 silicone elastomer kit, A and B in 10 to 1 ratio, Dow Corning, Midland, MI, USA) was well mixed and degassed in a desiccator under vacuum. A portion was spun onto the control master (500 rpm, 30 s, and 1200 rpm, 60 s) to obtain a control layer ~ 45 μm thick. Another portion was poured onto the fluidic master to give a 4-6 mm thick fluidic layer. After sitting on a leveled station for 1 h, the two layers were cured for at least 4 h in a 70 ℃ oven on a leveled platform.

After curing, the thick layer was peeled off the mold and holes were punched for solution port access. The layer was protected by thin PDMS layers in a sandwich mode to avoid contamination. The thin layer, still mounted on a mold, and the trimmed, thick layer, were treated with oxygen plasma (MicroEtch RIE, PlasmaLab, Oxfordshire, OX, UK) for 10 s at a vacuum pressure of 200 mTorr. Then the two layers were aligned under a mask aligner (ABM Inc., SanJose, CA, USA) and contacted to each other within 6 min. Bonding was further enhanced by heating the layers in an oven at 70 ℃. After complete bonding, the device was peeled off the mold and another set of holes were punched for access to the control channels. The assembled layers and glass substrate were then treated with oxygen plasma, bonded together, and heated at 70 ℃. The total bake time was adjusted to 72 h, which gives the lowest background for MS.[30] To obtain the best alignment of the two PDMS layers, the control layer design was scaled (98.9%) to compensate for the experimentally determined shrinkage of the fluidic layer when it is cured. The incubation temperature was adjusted around a range of 70 ℃. The thick layer will shrink when peeled off the mold at room temperature, while the

thin layer on the mold doesn't shrink as it is still held by the mold. This will cause an alignment problem for the two layers. To relieve the shrinkage problem, one way is to scale one layer pattern in the design to compensate for the experimentally determined shrinkage. Another way is to cure the PDMS at room temperature, which is not a good choice as the room temperature is not the optimal curing conditions and also takes time for curing. The shrinkage is temperature dependent, and after selecting a 1.1% mask scale difference it was necessary to adjust the curing temperature to get a good alignment between layers. Several pieces of chip were made by curing the PDMS layers at temperature between 65 and 75 ℃. The temperature at which the PDMS layers cured and best aligned, was chosen as the right temperature for making the device, and this was 70 ℃. Plasma oxidation bonding was chosen since the off-ratio PDMS bonding method has higher detrimental background in MS.[22] Refer to Chapter 1, Figure 1.5 for multilayer soft lithography fabrication flow.

4.3.3 Multiple SPE Bed Packing

SPE beads were packed in bed regions (76 μm deep) defined by weirs (12 μm deep). Two techniques were developed for bead introduction, to eliminate the need for bead introduction channels. One method was to directly inject beads into the bed through the wall of the PDMS device by syringe. Another, termed the punch-pack-plug (3P) technique, involved punching a small hole (200 to 420 μm) into the bed region for direct bead loading. The latter method turned out to be more robust and convenient for multiple bed packing. A small hole was punched

into the bed region for direct bead loading under vacuum. SPE beads were removed from a cartridge (Oasis® HLB Plus, 30 μm, a free gift from Waters Canada, Lachine, QC, Canada), washed three times with MeOH, three times with water and suspended in 50% MeOH. Then the bead channel was washed with MeOH, and the bead suspension from a freshly sonicated suspension was loaded into each bed. Bead suspension was introduced with a pipette tip inserted via the hole into the bed, and packed by vacuum. The punched PDMS pieces were inserted back into the punched holes and uncured PDMS was placed on top for further sealing. The sealing of the plug was affirmed by pressure tolerance tests. A more compact packing was obtained prior to use by further flushing the packed beds at about 20 psi. Further details are given in Chapter 2.

4.3.4 Continuous Pressure Control Interfacing and Connection to ESIMS

Figure 4.3 gives the schematic drawing of the pressure control system and some images of the connections and controls. A constant pressure control system was built for the control of valve operation and liquid delivery on chip, as shown in Figure 4.3A. Each regulated pressure line was connected to a gas reservoir and then to a solution reservoir. Details about the off-chip operation system for solution loading and pressure control are given in Appendix A.1.

The control channels were connected to the common ports of an array of solenoid valves (LHDA1223111H C HDI Face Mount - 12VDC - 30 psid, Lee Company, Westbrook, CT, USA), which were face-mounted on the eight-channel manifolds (LFMX0510538B E Manifold 8 place HDI FM-NC/NO, Lee company).

The Lee valves were pin-connected, powered and controlled by an in-house built set of switches. Regulated external pressure was provided to the normally closed port, allowing the control channel to be pressurized or vented to atmosphere by switching the miniature valve. Because PDMS is gas permeable, the control channels were filled with water prior to use in order to prevent air bubble formation in the fluidic channels under high-pressure operation of the valves. The control channels were connected to the corresponding channels on the manifolds using Tygon microbore tubing. The connection lines were filled with water and connected to a reservoir, which was pressurized by a regulated external pressure. Water was added individually into each control channel reservoir, tubing filled with water was then inserted into the reservoir. Finally pressure (about 10 psi) was applied to drive the water into the control channel. The air inside was compressed, and, presumably, slowly escaped through the PDMS layers.

The fluidic channels were connected to individual solution reservoirs via Teflon PFA tubing (Tub PFA Nat 1514 1/16'' OD, Upchurch, Oak Harbor, WA, USA). Two kinds of solutions were used, the washing buffer and MeOH/H_2O MS buffer.

The connection to ESIMS was achieved by a shaped capillary tip. The capillary was purchased from Polymicro Technologies Inc. (OD 360 μm, ID 50 μm, Phoenix, AZ, USA). An ESI tip was pulled by capillary puller (Model P-2000, Sutter Instrument Co., tip OD ~72 μm, ID ~10 μm) and metal-coated for conduction, as described previously in detail.[31] A small hole (ϕ ~300 μm) was punched into the exit channel and an ESI capillary tip was directly inserted into
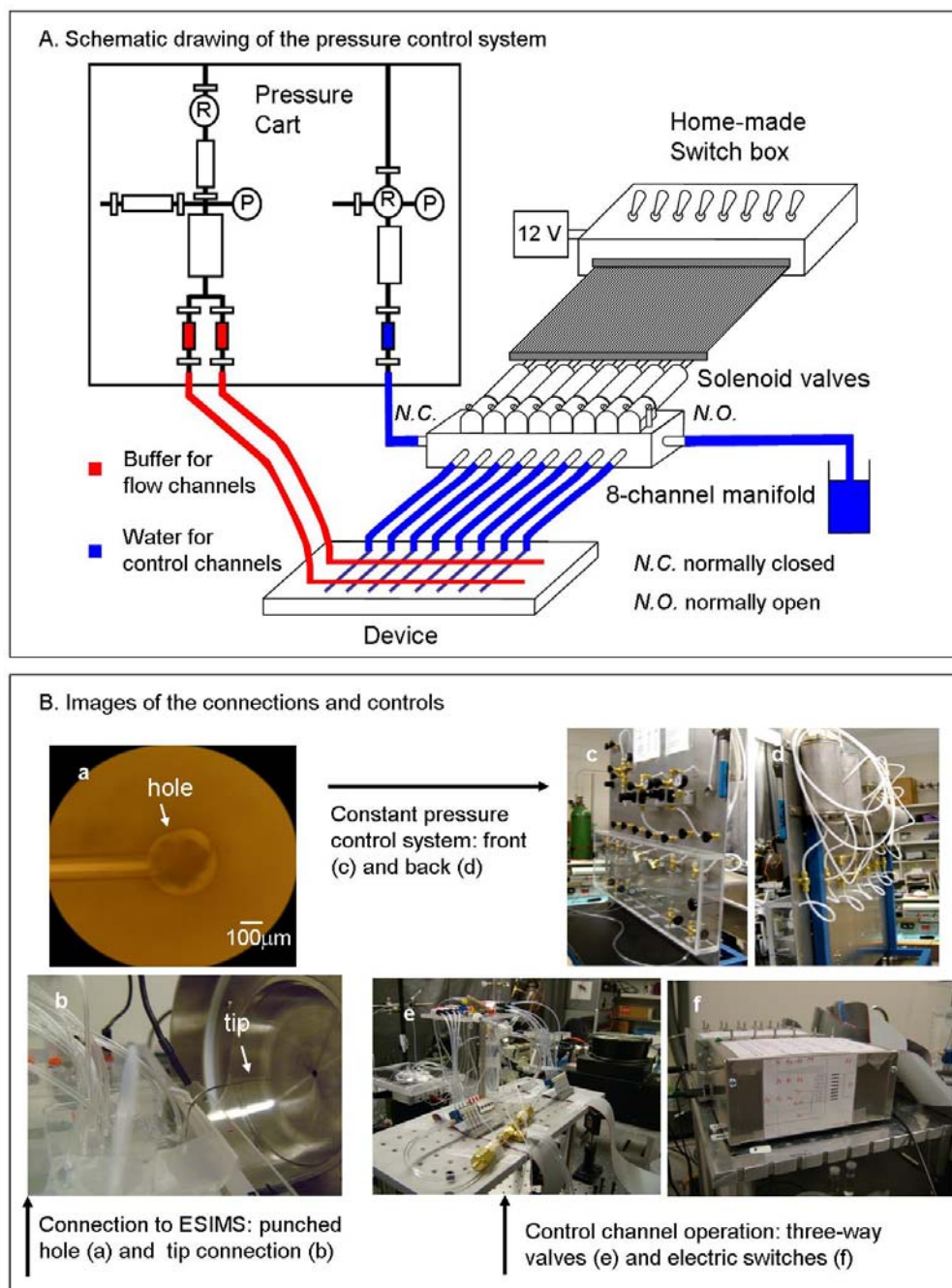
Figure 4.3 The schematic drawing of the pressure control system (A), and images of the connections and controls (B) (punched hole (a) and rounded capillary tip connection (b) to ESIMS; front (c) and back (d) of constant pressure control system; three-way valves (e) and electric switches (f) for control channel operation).

the hole. There is ~ 1.4 nL connection chamber volume between the channel exit and capillary inlet, assuming the capillary inlet is 5 - 20 μm away from the bottom of the channel (20 μm used for calculation). Further details about post column connections are given in Chapter 2, Table 2.1. The capillary was guided to the MS with the help of a curved metal tube. An optical micrograph of a PDMS device connected to the ESIMS interface is shown in Figure 4.3B (a and b).

4.3.5 Instrumentation

Laser-induced fluorescence detection utilized a custom-built inverted, confocal, epiluminescent microscope with an air cooled argon ion laser (488nm, Uniphase 2214-10SL, San Jose, CA).[32] A photomultiplier tube (PMT, Hamamatsu, Japan) was mounted on the microscope tube for signal detection. Electrophoregrams were recorded with a program written in LabView (National Instruments, Austin, TX, USA) at a sampling rate of 100 Hz. To take images, a CCD camera was connected to the microscope, coupled with a $5 \times$ objective and an expander for low-magnification imaging. Images were analyzed using ImageJ (NIH, Bethesda, MD, http://rsb.info.nih.gov/ij/).

The high voltage control system used two high voltage power supplies and five relays, which were controlled by LabView. Drawings about the voltage control are shown in Appendix A.6. To inject sample, a negative potential was applied at the sample waste reservoir with the other three reservoirs grounded. The separation was run with a voltage of - 4.5 kV between the buffer and the

buffer waste reservoirs. A voltage of - 0.48 kV was applied to the sample and sample waste reservoirs in order to prevent leakage.

MS analysis was done using a single quadrupole Sciex API 150EX (Applied Biosystems / MDS Sciex, Foster City, CA, USA). All experiments were done using positive electrospray ionization with electrospray voltages in the range 3 – 3.6 kV applied close to the ESI capillary tip. The peptide fragments were assigned on the basis of MS-Digest database at http://prospector.ucsf.edu.

4.4 Results and Discussion

The experimental results on the multiplex device will be analyzed and discussed in the following three sections: multiple SPE bed packing, CE separation with fluorescence detection, and coupled CE-fractionation-SPE-ESIMS. Protein separations in single channel PDMS devices, evaluated to determine the direction of future work will be discussed in the last section.

4.4.1 Multiple SPE Bed Packing

A soft lithography technique was developed to fabricate stable weirs in PDMS devices along with integrated PDMS-based valves. A 12 μm gap was employed to efficiently trap large beads (Oasis® HLB Plus, 30 μm) in a bed. Waters Inc. claimed that there is a ≤ 1.0 % fine content (the percent of total particle volume in particles with diameters smaller than 10 μm) in the supplied beads. During initial stages of packing, particles were observed to cross the weir, but once particles started to build up at the weir no further leakage of fine content was observed.

Trapping of particles smaller than the weir may be attributed to keystone, clamp or anchor effects that arise in part from the flexibility of PDMS, as has been very recently discussed in the literature.[33, 34]

In order to simplify the device design and experimental operation, we explored methods to eliminate introduction channels for the beads. The approach of using bead introduction channels becomes too complex when there are a large number of integrated packed beds. We developed a technique to punch the chip, pack the bed, and then plug the access port, which we refer to as the 3P technique which is described in Chapter 2. Figure 4.4 shows an image of eight packed beds
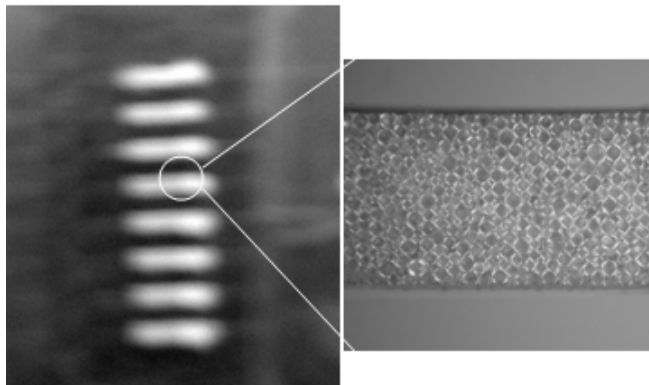
Figure 4.4 Optical micrograph of eight packed beds (bed 500 μm wide, 3 mm long, 76 μm deep; Oasis® HLB beads, 30 μm). Refer to Chapter 2, Figure 2.12 for details.

formed using the 3P technique. A series of leak tests were done in plasma-bonded PDMS devices. The system was comprised of a channel with or without a packed column, 1/16" access tubing to the channel, a hole punched into the channel and resealed by the 3P technique, and a syringe pump rate of 10 μL/min. The system outlet was sealed after filling with water, and the syringe pump was used to build

up pressure. No leaking was observed from the plug used to reseal the beds at pressures up to 115 psi. Leaking was observed to happen at the 1/16" tubing port, as evidenced by water accumulating at the connection. For a given device, the failure pressure and location at the fitting were reproducible. The results show the 3P method is robust and does not introduce leakage. The 3P technique provides a very convenient method for packing multiple beds in a complex design.

The reproducibility of SPE beds formed by the 3P method was measured by quantitatively loading cytochrome c onto the beds and eluting the extracts to ESIMS for detection. The relative standard deviation for measurements within the same bed was 4% (n = 4). The relative standard deviation for measurements between multiple beds was 12% (n = 4). The reproducibility of the multiple beds is reasonable considering that the bead size is large (ϕ 30 μm) and the bed is small (76 μm depth × 500 μm width × 3 mm length), which leads to relatively loose packing of the bed. Because each bed is individually addressable by the integrated valving system the difference between beds is acceptable, and can be accounted for by calibration. Further details are given in Chapter 2.

4.4.2 CE Separation with Fluorescence Detection

CE separation of FITC-labeled cytochrome c digest in Tris-H_3BO_3 buffer (100 mM-20 mM, pH 9) is shown in Figure 4.5. The injection to detection distance (L_d) was 2.55 cm. Five peptide peaks were detected and are labeled with numbers in the electrophoregram. A free FITC peak was also identified using FITC as a control.
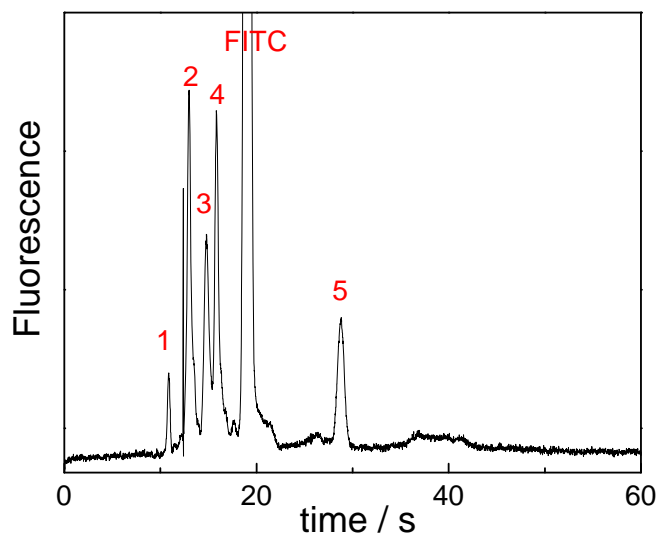
Figure 4.5 CE separation of FITC-labeled cytochrome c digest (0.1 mg/mL; Tris-H_3BO_3 buffer, 100 mM-20 mM, pH 9); a voltage of - 4.5 kV applied between the buffer reservoir and the buffer waste reservoir, with an anti-leakage voltage of - 0.48 kV applied to the sample and sample waste reservoirs; injection to detection distance 2.55 cm; 1 – 5, indicating the peptide peaks).

Table 4.1 Migration times t_m, Peak width W, Efficiencies N for the electrophoregram given in Figure 4.5

Peak	t_m / s	W_A / s	W_B / mm	W_C / mm	Plates N / 10^5/ m
1	10.87	0.33	2.0	2.4	2.4
2	12.98	0.43	2.0	2.4	2.0
3	14.79	0.63	2.8	3.3	1.2
4	15.85	0.44	1.8	2.1	2.8
5	28.80	0.85	2.0	2.4	2.5

Peak numbers refer to the numbers labeled in the electrophoregram; W_A is the peak width at half height in terms of time obtained from the electrophoregram; W_B is the baseline peak width in terms of distance; W_c is the baseline peak width in terms of distance at the injection-to-detection distance of 3.71 cm extrapolated from W_B; Peak shape assumed as Gaussian;

The migration times, bandwidths and separation efficiencies for the five peptide peaks obtained from the electrophoregram in Figure 4.5 are listed in Table 4.1. The calculated plate numbers are similar to those reported previously for peptide separation in a PDMS device using similar conditions.[29] To understand the contributions to band broadening for the separation, we compared the individual plate heights calculated according to Golay's equation (4.1) to the total plate height determined by the experimental plate numbers N. The plate height from the Golay's equation is given by;[35-37]

$$H = \frac{\sigma^2_{\text{T}}}{l} = \frac{\sigma^2_{\text{diffusion}}}{l} + \frac{\sigma^2_{\text{injection}}}{l} + \frac{\sigma^2_{\text{detection}}}{l} + \frac{\sigma^2_{\text{turn}}}{l} + \frac{\sigma^2_{\text{adsorption}}}{l} + \frac{\sigma^2_{\text{temp}}}{l} + \frac{\sigma^2_{\text{electrodispersion}}}{l}$$

$$= \frac{2D_m t}{l} + \frac{l^2_{inj}}{12l} + \frac{l^2_{det}}{12l} + \frac{[2\theta w(1 - \exp(-\frac{w^2 v_c r_c}{2D\theta(r_c + \frac{w}{2})^2}))]^2}{24l} + \frac{k' V_{EOF} l}{(1+k')^2 l}(\frac{r^2 k'}{4D} + \frac{2}{K_D}) \qquad (4.1)$$

In employing this equation we included contributions from longitudinal diffusion $\sigma^2_{\text{diffusion}}$, injection $\sigma^2_{\text{injection}}$, detection $\sigma^2_{\text{detection}}$, the turn geometry σ^2_{turn}, an adsorption term $\sigma^2_{\text{adsorption}}$, but neglected other possible contributions such as temperature gradient and electrodispersion. The following parameters were used for the estimate of plate height; a diffusion coefficient of $D_m = 5 \times 10^{-6}$ cm^2/s, a migration time t of 20 s, an injection length l_{inj} of 200 μm, a detector path length l_{det} of 15 μm, which is equal to the laser spot size, a turn angle θ of π/2, a channel width w of 100 μm, the velocity of the analyte v_c = 0.13 cm/s, the radius of curvature along the centerline of the turn r_c of 0.1 cm and the separation length l of 2.55 cm.

The plate height determined from the observed N of 2.4 $\times 10^5$/m is given by $H = \dfrac{l}{N}$. Calculations using the Golay equation show that about 19% of the observed band broadening was contributed by longitudinal diffusion, 7% by the injection, the detection and the turn geometry. The remainder of the observed band broadening is mostly likely due to the adsorption of peptides to the hydrophobic PDMS. This result contrasts with the much smaller band-broadening data reported in glass,[29] but is consistent with reports for PDMS.[29]

To determine the spatial length of the bands in the fractionation zone, we converted from the peak width at half height in terms of time to an estimate of the baseline peak width in terms of distance. Equation (4.2) was used for the conversion;[38, 39]

$$W_B = L_d \times \frac{W_A(s)}{t_m(s)} \times \frac{6\sigma}{2.35\sigma} = 25.5(mm) \times \frac{W_A(s)}{t_m(s)} \times \frac{6\sigma}{2.35\sigma} \qquad (4.2)$$

where W_B is the baseline peak width in terms of distance, W_A is the peak width at half height in time obtained from the electrophoregram, t_m is the migration time, 2.35 σ and 6 σ are the peak width at half height and baseline respectively, assuming a Gaussian peak shape. To extrapolate the baseline peak width in terms of distance in the fractionation and collection zone, we employed the known relationship of peak width and the square root of the length of the separation channel:[39, 40]

$$W_L \propto \sqrt{L_d} \qquad \qquad . \qquad (4.3)$$

where W_L is the baseline peak width at the injection-to-detection distance of L_d. Derivation of the relationship is given in the Appendix A.3. The fractionation and
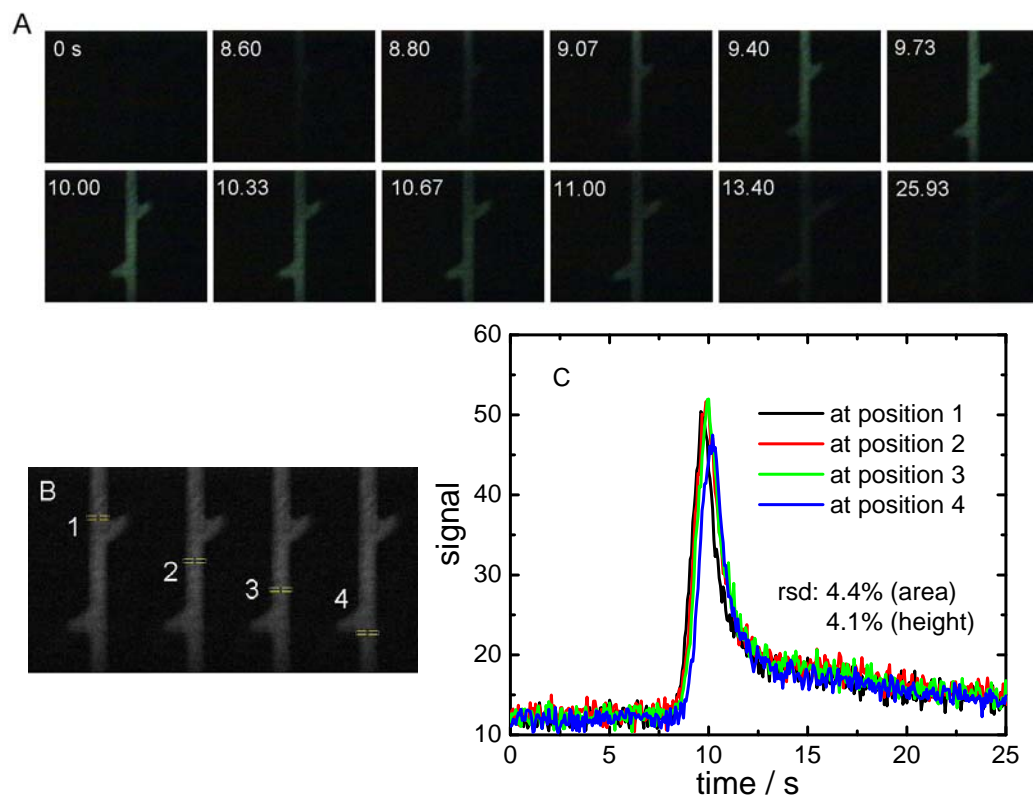
Figure 4.6 Observation on the travelling of a plug of FITC through one section of the fractionation zone (200 μM FITC; Side blocked by valves at 25 psi; about 1 kV/cm): (A) The images showing the travelling with time, sample partially passing through side branches due to the electric field distribution into the side channels; (B) Instensity verus time transferred from the image by ImageJ at different position (B) in the channel, indicated by 1 - 4 small boxes in the images, showing no obvious changes of peak areas/heights before/after branches.

collection zone starts at about 2.55 cm and extends to about 3.71 cm from the injection point. According to equation (4.3), the baseline peak width at 3.71 cm can be calculated by using the baseline peak width at 2.55 cm. When sample travels through the fractionation and collection zone, there may be some band broadening due to the distortion of the electric field in the channel with side

branches[41, 42] (Figure 4.6). So the estimated peak width at baseline in terms of distance may be smaller than the actual one.

The results for the five peptide peaks from the electrophoregram are listed in Table 1, including the peak width at half height in terms of time at 2.55 cm, W_A, the baseline peak in terms of distance at 2.55 cm, W_B, and the baseline peak width in terms of distance at 3.71 cm, W_c. The baseline peak widths in the fractionation and collection zone are in the range of 1.8 mm to 3.3 mm. Since the length of each fractionation section was 1.5 mm, peptides are predicted to be fractionated and collected into one to three beds, based on the quality of CE separation determined by fluorescence detection.

4.4.3 Coupled CE-Fractionation-SPE-ESIMS

An analysis of a cytochrome c digest was performed in the coupled CE-Fractionation-SPE-ESIMS system. The complete process included CE separation for tens of seconds, fractionation and delivery of the separated sample into the SPE beds for 1 min, desalting and rinsing of the beds (15 -30 min), and final sequential elution of each bed with detection by ESIMS (5 - 10 min for each bed). During the CE separation step, 3 to 4.5 kV was applied, and all valves were closed at around 30 psi except the fractionation valves (group three, in Figure 4.1). The fractionation valves were then closed to trap the separated samples and the voltage was turned off, and these valves remained closed for the following analysis. Valves in group two and four were then opened and water was flushed through the SPE beds at 5 psi by operating valve groups one and five. After
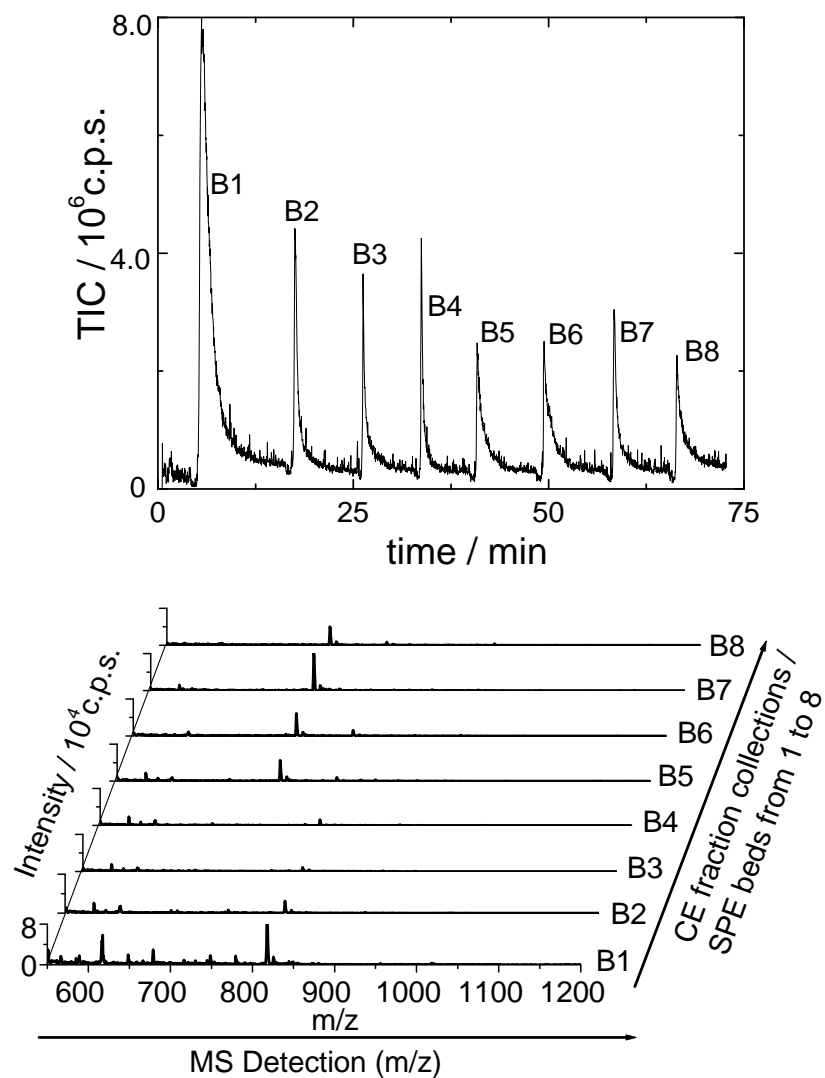
Figure 4.7 The total ion counts (TIC) from the elution of eight channels (top) and the corresponding MS at each peak (bottom) (each peak labeled as to each channel, B1 to B8, the furthest to closest beds away from the double-T injection; 50% methanol + 0.1 M formic acid; ~ 220 fmol cytochrome c digest injected; each MS trace shows the sum of 62 mass scans)

desalting for 15 - 30 min, the solution input was switched to an elution buffer. By operating the valves of group two, the fractionated samples were sequentially eluted to the MS for detection.

Figure 4.7 shows the total ion count (TIC) for detection of the eluent for the eight eluted peaks, and the corresponding MS of each peak. The time scale in the graph corresponds to elution from each bed, not the electrophoretic separation time. The bed labeled B1 was the furthest from the double-T injector, while B8 was closest. Each elution peak came from the elution of one fraction in one bed and each fraction contained different peptides as shown in the MS graph (Figure 4.7, bottom). The elution peaks show a significant tailing effect, which may arise from the large void volume between the particles in the SPE beds. For a well packed column the void volume is in the range of 40% ,[39] and for 30 μm particles in 76 μm deep channels the packing is likely to be inefficient, giving greater void volume. Jung et al.[43] observed that porosity increased with particle diameter
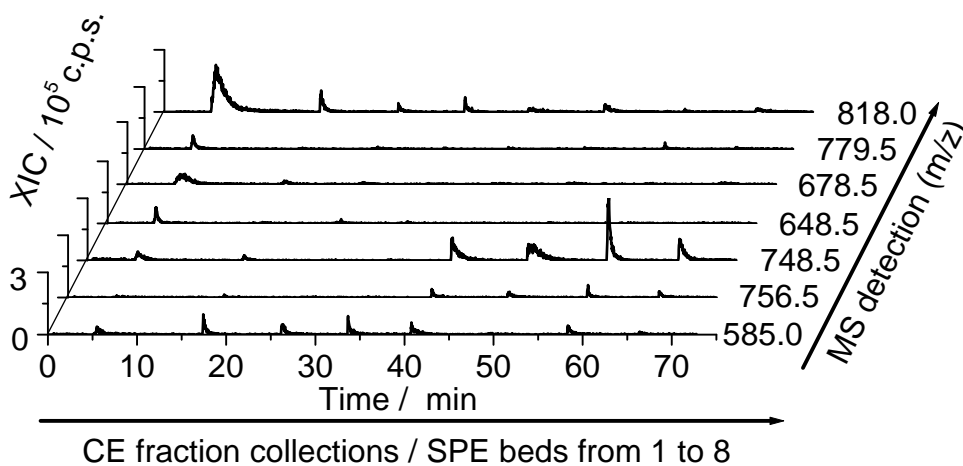
Figure 4.8 The extracted ion counts (XIC) of the peptides (labeled with m/z).

within microchannels, suggesting packing was negatively affected. Other possible tailing sources are post column connections (microchannel, interfacing with capillary, capillary), the adsorptive properties of the beads, and possible adsorption to the post column channel.
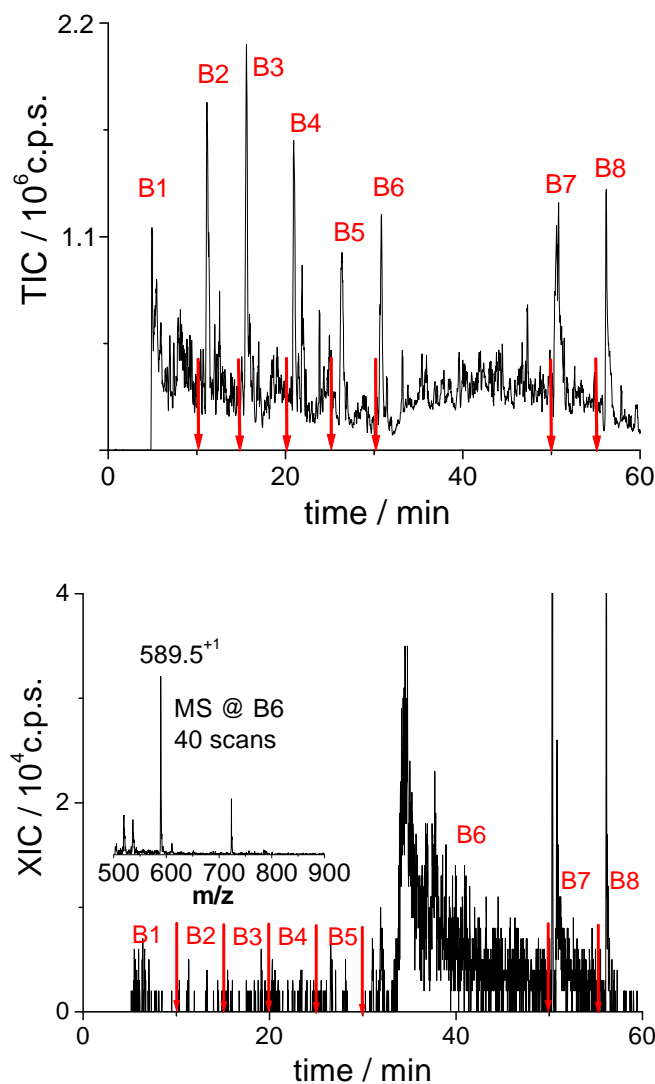
Figure 4.9 TIC from the washing step (top) and XIC (bottom) of the peptide 589.5[+] (arrow indicates the switch point from channel to channel).

Oasis beads have good SPE properties, evidenced by the 7 peptides that were immobilized, as shown in Figure 4.8 for the extracted ion counts (XIC) of the peptides (bead property shown in Appendix A.5). However, given variation amongst peptides, not all will be immobilized. One cytochrome c digest component (m/z 589.5$^+$) was not retained by the SPE beds (Figure 4.9). This small peptide (AcetN-GDVEK) has a 60% hydrophilic content, according to the peptide property calculator from GenScript (https://www.genscript.com/ssl-bin/site2/peptide_calculation.cgi). It was detected primarily from bed 6, and additionally from bed 7 and 8 during the initial washing step. The SPE beds also showed a chromatographic effect during elution. For example (Chapter 2, Figure 2.18), peptide (678.5$^+$) was eluted at a slower rate with a broader elution profile than was peptide (648.5^{2+}). This is probably due to its stronger adsorption on the SPE beads, since peptide (678.5$^+$) has a hydrophobic proportion of 33% and hydrophilic 17%, while peptide (648.5^{2+}) has 25% and 25%.

Peptides were fractionated into one to four beds (Figures 4.7 and 4.8), consistent with the prediction of baseline peak widths from the LIF results (Figure 4.5). Table 4.2 gives a summary of the peptides detected, including the one not captured by the SPE beds. The corresponding sequence coverage is 59%. The m/z, pI, collection beds and peptide sequence are listed, to give information linking the separation and the peptide properties (charge states, hydrophobicity, molecular weight). The pI values were used to give an estimate of the charge state of the peptides, neglecting any post translational modifications. Electrophoretic mobilities of peptides are believed to correlate to peptide charge and molecular

Table 4.2 Summary of the cytochrome c peptides detected

m/z	pI	colle-ction beds	hydro-phobic	hydro-philic	Net charge @ pH 9	$q/MW^{2/3}$	sequence
818.0^{+2}	7.3	1	11	33	-2.3	-0.017	CAQCH TVEK (Heme)
648.5^{+2}	11.7	1	25	25	1.3	0.011	TGPNL HGLFG RK
779.5^{+1}	9.7	1	57	14	0.2	0.0024	MIFAGI K
678.5^{+1}	9.3	1	33	17	0.1	0.0013	YIPGTK
585.0^{+2}	10.6	1-8	27	18	0.2	0.0018	TGPNL HGLFG R
589.5^{+1}	4.2	6-8	20	60	-2	-0.028	AcetN-GDVEK
748.5^{+2}	3.8	5-8	33	42	-4	-0.031	EETLM EYLEN PK
756.5^{+2}	3.8	5-8	33	42	-4	-0.030	EETLM (Met-ox)EYL ENPK

Sequence coverage 59%; The pI and hydrophilicity calculations obtained by using the peptide property calculator from GenScript (https://www.genscript.com/ssl-bin/site2/peptide_calculation.cgi); The pI values are based on the peptide sequence alone without considering the effect of modifications; Structures are shown in Appendix A.2.

weight (one model in a form of $q/MW^{2/3}$).[44-46] Drawings of the peptide structures are shown in Appendix A.2 for reference.

The CE separation peak profile for an analyte fractionated into multiple beds can be examined by comparing the signals from each bed. Figure 4.10 gives the analysis results for peptides fractionated into beds 5 to 8 (peptides with m/z 748.5, and 756.5). The signals (integrated XIC peak area) from each bed were normalized to total signal from eight beds. The signals from the bed were simulated using a Gaussian distribution, and then noise/error is added to each signal based on the bed-to-bed variations (12.3% rsd). As shown in the graph, the peak area distributions fell in the range of a regular Gaussian separation peak profile.

The analyte signals may be complicated by background carryover. In the system, there is possible downstream (after bed) carryover due to insufficient cleaning. During the desalting and rinsing step, all the beds are open and the contaminants washed away from all the beds may accumulate in the connection between the exit of channel B1 and the MS. Other channels downstream of the SPE beds may accumulate contaminants from their own elution and possibly from elutions upstream of that channel. Peptide 589.5^+ can be used to evaluate the rinsing step; since this peptide is unretained on the SPE beds and should be washed away during the cleaning step. As shown in the XIC plots of the elution for this peptide (Figure 4.11), there is a large elution peak from B1 (about 66%), a small one from B2 (about 11%), and minor ones from B3 to B8 (2 − 6%). This indicates that there is downstream carryover due to insufficient cleaning prior to
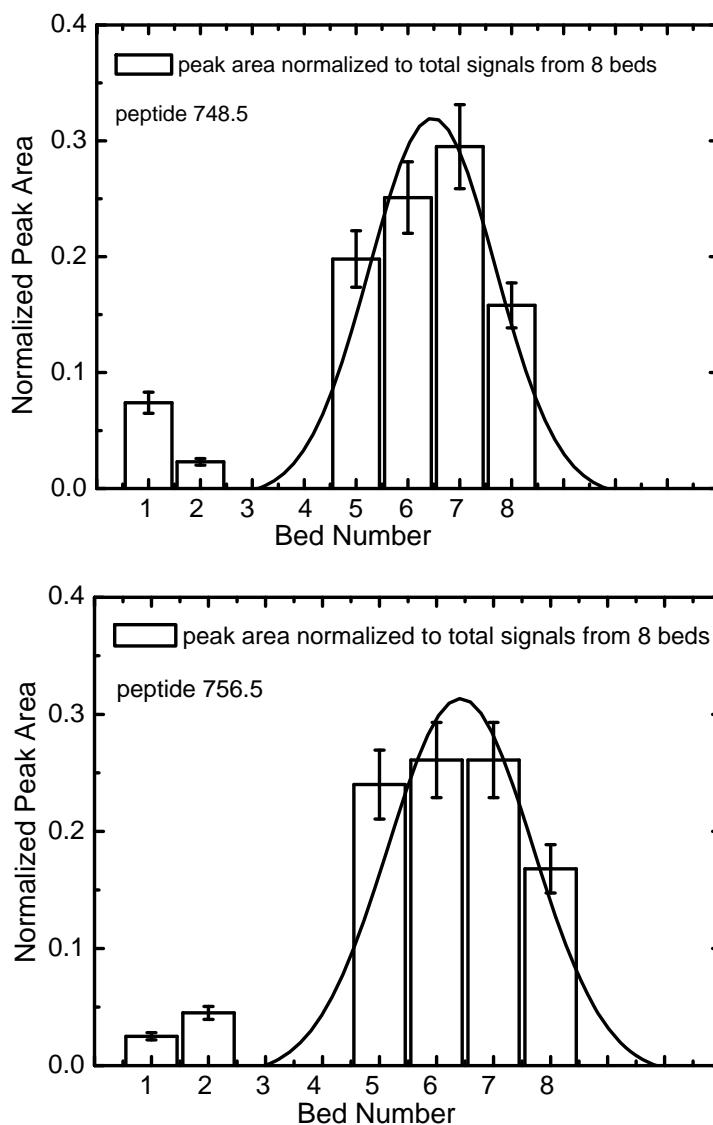
Figure 4.10 the integrated XIC peak areas from each bed for the peptides with m/z 748.5 (top) and 756.5 (bottom) which show the regular Gaussian separation peak profile from bed 5 to 8 (peak area from each bed is normalized to total signal from eight beds; noise is considered according to bed-to-bed variations 12.3% rsd).

elution for this run. Bed B1 is closest to the MS and the first to be eluted into the

MS, so will experience the largest downstream carryover during the bed rinsing

step. Other beds show minor downstream carryover. Therefore, we suggest that
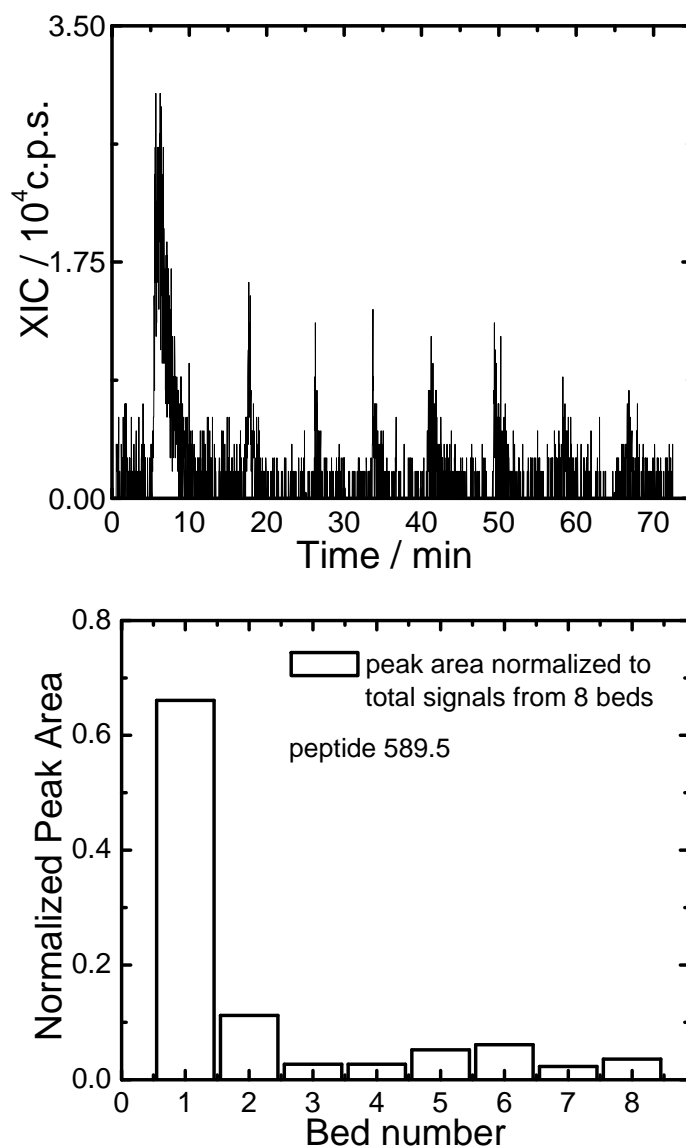
Figure 4.11 The elution profile (top) and the corresponding integrated peak area (bottom) from each bed for the untrapped peptide with m/z 589.5.

small signals observed in B1 and B2 for peptides m/z 748.5 and 756.5 appear to arise from downstream sample carryover. For those peptides fractionated into B1, the minor signals in other channels are due to a possible downstream carryover as well. Peptide (585.0^{+2}) was observed to exist in every bed, probably due to its

strong adsorption in the PDMS channel since this peptide is almost neutral at pH 9 and it has a significant hydrophobic proportion (27%).

After complete elution from each bed, the chip was rinsed with 100% MeOH for three or more hours. This flush was successful, in that there was no observed carry over from previous runs.

The signal detected in B1 is higher than other channels. The peptides detected in each channels approximately following their estimated mobility, so it is reasonable that more peptides with similar mobility are collected into B1. However, the simultaneous closing of all fractionation valves, with no pathway for the volumes under the valves to flow might give an extra big signal at channel B1, if valve B1 happened to be the last valve that closed.

To obtain a good S/N ratio during mass analysis, the amount of the cytochrome c digest sample must exceed 50 fmol. The S/N response is sample dependent. For a specific peptide with m/z 736.0, the measured S/N values were 11, 21, 52 for digest loads of 16, 80 and 160 fmol, correspondingly. The detection sensitivity is reasonable and comparable to the data reported in a regular SPE-ESIMS system by pressure driven flow at several μL/min.[44-46] For example, Oleschuk[46] reported S/N 21 and 115 for 23 and 696 fmol leucine enkephalin with a microsphere entrapped emitters for sample preconcentration before ESIMS (API 3000 triple-Q MS, 3 μm SPE beads, 0.8 μL/min). For the data shown in the figures, about 220 fmol digest (~ 1 mM) gave a good S/N ratio, but this concentration may cause some electrodispersion during the separation step.[47] In the current system, one separation peak starting with 220 fmol may be

fractionated into four channels, averaging 55 fmol for each channel. In an optimized system with less band broadening, lower amounts of sample may be required. Further details and discussion about detection sensitivity are given in Chapter 2 and chapter 5.

From the calculations on band broadening for the separations, we see that PDMS is not a very good material for peptide and protein separation. Strong efforts need to be taken to modify the surface property of the material to obtain a high resolution separation. However, since the separation was acceptable for testing the total system, no effort was applied to coating the PDMS to increase the resolution of the separation. In order to obtain better resolution, one possibility is to change the fractionation segment length in the separation channel, so that each peptide can be fractionated into one or two beds. However, as we extend the length of each segment, we inevitably increase the length of the separation channel and make each peak wider (equation 4.3), which makes this idea less valid. There are some examples on PDMS chips in which a high resolution separation of peptides was achieved using a permanent coating method[25] and also of proteins, using isoelectric focusing (IEF).[48] Recently, a new packing method was developed for packing long stable HPLC columns on a PDMS chip,[34] which provides another way to integrate a separation into our device to improve separation resolution. In addition to the adsorption problem in PDMS, there is a stable background signal from PDMS material in ESIMS. It may be possible to use other materials for device fabrication, as suggested by the development of new soft materials for multilayer soft lithography.[49, 50]

4.4.4 Protein Separations in Single PDMS Channel

Protein separations in a single channel provide useful information for future work on the multiplexed device and are thus presented here. Considering the complexity and difficulty of static coating of PDMS devices, dynamic coating was first tested to eliminate EOF and reduce protein adsorption in PDMS. EOF changes using different coating materials are shown in Appendix A.4, Table A.1 and Figure A.2, measured using a current-monitoring method.[51]

Hydrophilic nonionic surfactant DDM and MC can block a hydrophobic surface and decrease EOF in PDMS channels, while the anionic surfactant SDS can introduce negative charges to surface. DDM might be an efficient coating material to reduce protein adsorption in a PDMS channel.[27, 52, 53] A hybrid dynamic coating with DDM and MC was realized in polymethyl methacrylate (PMMA) chips to minimize analyte adsorption and EOF.[54] Therefore, CZE separation of protein mixtures of TI and BSA with hybrid coating of DDM and MC in single PDMS channel was tried. The two proteins are well separated and give an efficiency of 2.9×10^4 N/m for BSA, as shown in Figure 4.12. However, such efficiency was still not satisfactory for the multiplexing concept if used with capillary zone electrophoresis.

A. Device layout

B. Separation
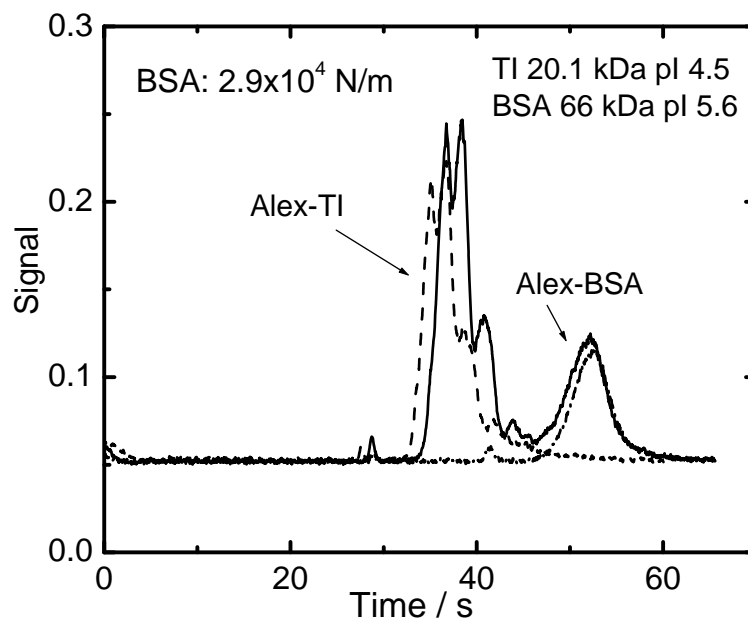
Figure 4.12 CZE separation of proteins: (A) device layout and (B) separation results (dash - Alex-trypsin inhibitor (Alex-TI); dash dot - Alex-BSA; solid - mixture of the two); injector to detector distance 2.4 cm; during separation a voltage of 0.86 kV applied between buffer waste and buffer reservoirs, with an anti-leakage voltage of 0.15 kV applied to sample and sample waste reservoirs; 0.001 mg/mL Alex-TI, 0.001 mg/mL Alex-BSA; 20 mM borate (pH 9.3) containing 0.2% DDM and 0.1% MC.
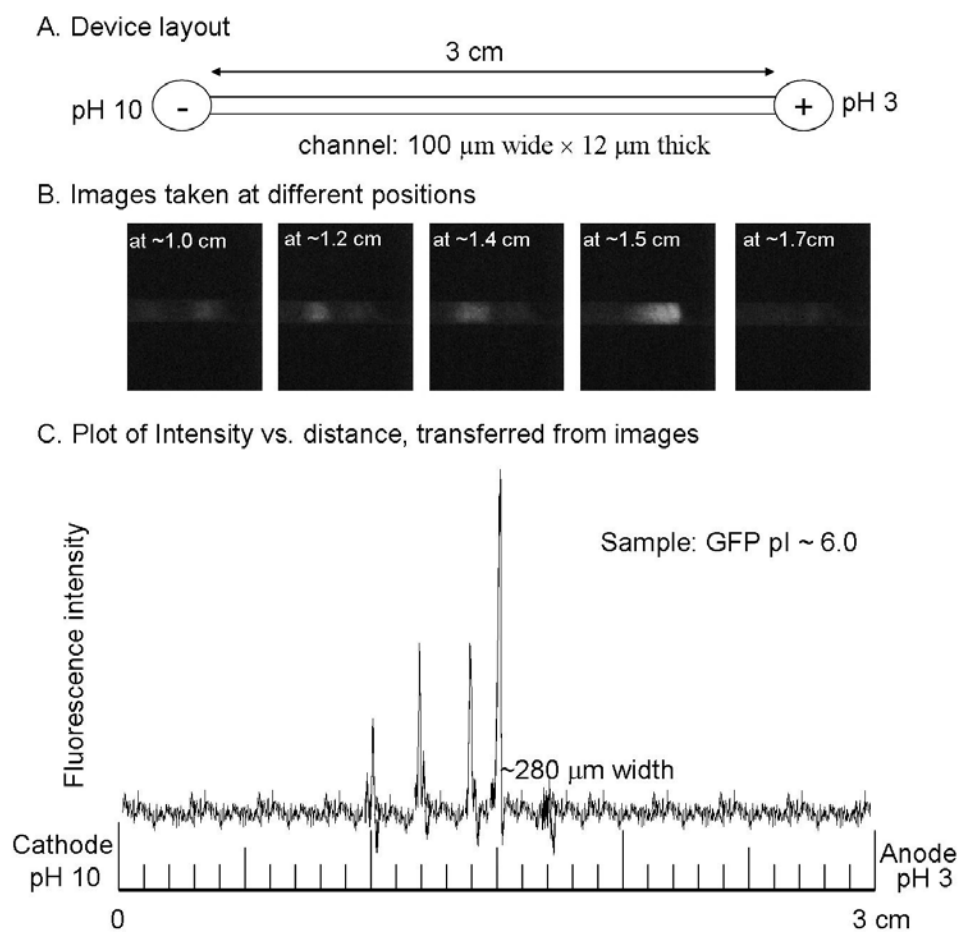
Figure 4.13 IEF separation of GFP in single PDMS channel: (A) device layout showing the dimensions of the channel, cathode solution, 0.02% NH$_4$OH containing 2% MC, anode solution, 50 mM acetic acid containing 2% MC, sample load solution, 2% ampholyte 3 – 10, 0.5% MC, seven times diluted from original GFP solution, voltage, 333 V/cm, images taken at five minutes focusing time; (B) images taken at different positions in the channel; (C) plot intensity vs. distance, using ImageJp to process still images.
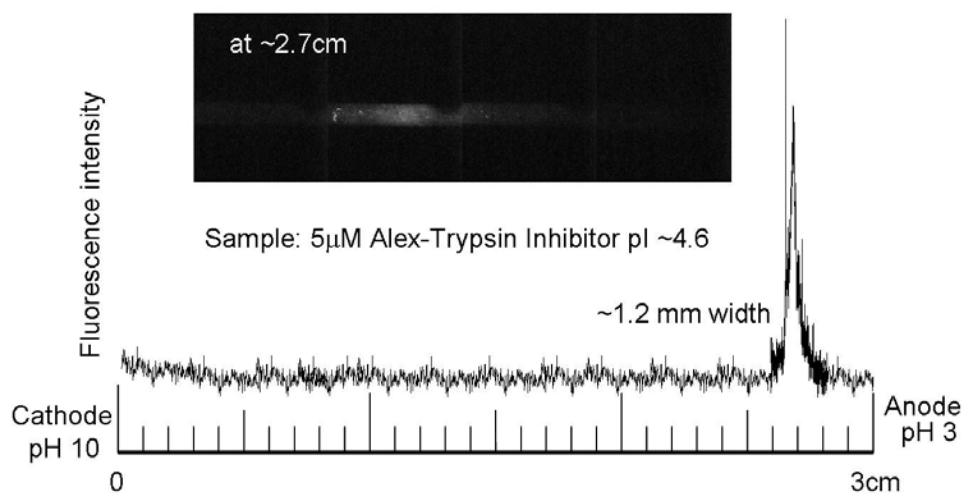
Figure 4.14 IEF separation of Alex-trypsin inhibitor in single PDMS channel: sample load solution, 2% ampholyte 3 – 10, 0.5% MC, 5 μM Alex-trypsin inhibitor, other conditions the same as that in Figure 4.12, inset – several images are binned together based on built-in stage scale since the band was not in the same field of view.

Static IEF separation was carried out in a single PDMS channel, as shown in Figure 4.13 and 4.14, along with the device layout; images were taken at different positions and intensity plotted versus distance. MC was added to minimize protein adsorption, decrease EOF and increase the viscosity of the solution. With addition of MC, EOF in a PDMS channel is depressed to about 0.15×10^{-4} cm^2/V·s with 0.5% MC addition. 2% MC is added to increase the viscosity of the electrode solutions, since it is said such addition can suppress pH gradient drift.[48] Still images were obtained from different positions of the channel. A plot of intensity corresponding to distance is obtained from the pixel intensities of the still images by using ImageJ. When the protein bands were not in the same field of view, several images were binned together, based on a built-in stage scale to estimate the band width. Four GFP peaks were obtained with a base bandwidth of about

280 μm. Another Alex labeled trypsin inhibitor peak of about 1.2 mm. The broadening of Alex-trypsin inhibitor peak comes mainly from labeling band broadening, as discussed in literature,[55] and supported by the CZE separation result (Figure 4. 12) where multiple peaks were obtained from Alex-trypsin inhibitor peak. Theses results indicate that IEF was a very good choice for the multiplexing concept. Using the multiplex device we designed, one to three IEF focused bands will be collected into a single SPE bed, and the estimated limit of detection (LOD) will be about several femtomols. The separation and fractionation are matched.

4.5 Conclusion

A coupled CE-Fractionation-SPE-ESIMS on valve-based device was designed, fabricated and used for peptides analysis. Our device gives the first example to integrate electrophoresis, sample fractionation, packed beds with weir-style trapping, and interfacing to electrospray mass spectrometry in one complex system. The analysis results of cytochrome c digest on the coupled CE-Fractionation-SPE-ESIMS shows that this device is functional, and the given concept is very promising for on-chip multiple sample preparation for proteomics.

4.6 References

(1)   Beranova-Giorgianni, S. *Trac-Trends Anal.Chem.* **2003**, *22*, 273-281.

(2)   Washburn, M. P.; Wolters, D.; Yates, J. R. *Nat. Biotechnol.* **2001**, *19*, 242-247.

(3)   Koster, S.; Verpoorte, E. *Lab Chip* **2007**, *7*, 1394-1412.

(4)   Freire, S. L. S.; Wheeler, A. R. *Lab Chip* **2006**, *6*, 1415-1423.

(5)   Lion, N.; Rohner, T. C.; Dayon, L.; Arnaud, I. L.; Damoc, E.; Youhnovski, N.; Wu, Z. Y.; Roussel, C.; Josserand, J.; Jensen, H.; Rossier, J. S.; Przybylski, M.; Girault, H. H. *Electrophoresis* **2003**, *24*, 3533-3562.

(6)   Fortier, M. H.; Bonneil, E.; Goodley, P.; Thibault, P. *Anal. Chem.* **2005**, *77*, 1631-1640.

(7)   Yin, N. F.; Killeen, K.; Brennen, R.; Sobek, D.; Werlich, M.; van de Goor, T. V. *Anal. Chem.* **2005**, *77*, 527-533.

(8)   Xie, J.; Miao, Y. N.; Shih, J.; Tai, Y. C.; Lee, T. D. *Anal. Chem.* **2005**, *77*, 6947-6953.

(9)   Slentz, B. E.; Penner, N. A.; Regnier, F. E. *J. Chromatogr. A* **2003**, *984*, 97-107.

(10)   Mellors, J. S.; Gorbounov, V.; Ramsey, R. S.; Ramsey, J. M. *Anal. Chem.* **2008**, *80*, 6881-6887.

(11)   Wang, C.; Oleschuk, R.; Ouchen, F.; Li, J. J.; Thibault, P.; Harrison, D. J. *Rapid Commun. Mass Spectrom.* **2000**, *14*, 1377-1383.

(12)   Li, J. J.; LeRiche, T.; Tremblay, T. L.; Wang, C.; Bonneil, E.; Harrison, D. J.; Thibault, P. *Molecular & Cellular Proteomics* **2002**, *1*, 157-168.

(13)   Gottschlich, N.; Culbertson, C. T.; McKnight, T. E.; Jacobson, S. C.; Ramsey, J. M. *J. Chromatogr. B* **2000**, *745*, 243-249.

(14)   Foret, F.; Kusy, P. *Electrophoresis* **2006**, *27*, 4877-4887.

(15)   Wang, C. Ph.D. theses University of Alberta (Canada), Edmonton, 2001.

(16)   Taylor, J. PhD theses, University of Alberta (Canada), Edmonton, 2004.

(17)   Pan, J. Y., VerLee, D., Mehregany, M. *Transducers* **1997**, 817-820.

(18)   Thorsen, T.; Maerkl, S. J.; Quake, S. R. *Science* **2002**, *298*, 580-584.

(19)   Unger, M. A.; Chou, H. P.; Thorsen, T.; Scherer, A.; Quake, S. R. *Science* **2000**, *288*, 113-116.

(20)   Studer, V.; Hang, G.; Pandolfi, A.; Ortiz, M.; Anderson, W. F.; Quake, S. R. *J. Appl. Phys.* **2004**, *95*, 393-398.

(21)   Dodge, A.; Brunet, E.; Chen, S. L.; Goulpeau, J.; Labas, V.; Vinh, J.; Tabeling, P. *Analyst* **2006**, *131*, 1122-1128.

(22)   Chan, J. H.; Timperman, A. T.; Qin, D.; Aebersold, R. *Anal. Chem.* **1999**, *71*, 4437-4444.

(23)   Grover, W. H.; Skelley, A. M.; Liu, C. N.; Lagally, E. T.; Mathies, R. A. *Sens. Actuators B* **2003**, *89*, 315-323.

(24)   Liu, J. K.; Lee, M. L. *Electrophoresis* **2006**, *27*, 3533-3546.

(25)   Hu, S. W.; Ren, X. Q.; Bachman, M.; Sims, C. E.; Li, G. P.; Allbritton, N. *Electrophoresis* **2003**, *24*, 3679-3688.

(26)   Abate, A. R.; Lee, D.; Do, T.; Holtze, C.; Weitz, D. A. *Lab Chip* **2008**, *8*, 516-518.

(27)   Huang, B.; Wu, H. K.; Kim, S.; Zare, R. N. *Lab Chip* **2005**, *5*, 1005-1007.

(28)   Haeberle, S.; Zengerle, R. *Lab Chip* **2007**, *7*, 1094-1110.

(29)   Lacher, N. A.; de Rooij, N. F.; Verpoorte, E.; Lunte, S. M. *J. Chromatogr. A* **2003**, *1004*, 225-235.

(30)   Sung, W. C.; Chang, C. C.; Makamba, H.; Chen, S. H. *Anal. Chem.* **2008**, *80*, 1529-1535.

(31)   Martinez, D. Ph.D. theses, University of Alberta (Canada), Edmonton.

(32)   Ocvirk, G.; Tang, T.; Harrison, D. J. *Analyst* **1998**, *123*, 1429-1434.

(33)   Flemming, J. H.; Baca, H. K.; Werner-Washburne, M.; Brozik, S. M.; Lopez, G. P. *Sens. Actuators B* **2006**, *113*, 376-381.

(34)   Gaspar, A.; Piyasena, M. E.; Gomez, F. A. *Anal. Chem.* **2007**, *79*, 7906-7909.

(35)   Heiger, D. *High performance capillary electrophoresis*; Agilent Technologies, 2000

(36)   Culbertson, C. T.; Jacobson, S. C.; Ramsey, J. M. *Anal. Chem.* **1998**, *70*, 3781-3789.

(37)   Culbertson, C. T.; Jacobson, S. C.; Ramsey, J. M. *Anal. Chem.* **2000**, *72*, 5814-5819.

(38)   Dennis G. Peters, J. M. H., and Gary M. Hieftje *Chemical separations and measurements; theory and practice of analytical chemistry*: Philadelphia, Saunders, 1974.

(39)   Cantwell, F. F. *Analytical separations: Gas Chromatography, Liquid Chromatography and Electrophoresis*; Department of Chemistry, University of Alberta, 2004.

(40)   Miller, J. M. *Chromatography: Concepts and Contrasts*; John Wiley & Sons, Inc., 2005.

(41)   Buch, J. S.; Rosenberger, F.; Highsmith, W. E.; Kimball, C.; DeVoe, D. L.; Lee, C. S. *Lab Chip* **2005**, *5*, 392-400.

(42)   Cui, H. C.; Huang, Z.; Dutta, P.; Ivory, C. F. *Anal. Chem.* **2007**, *79*, 1456-1465.

(43)   Jung, S.; Ehlert, S.; Mora, J. A.; Kraiczek, K.; Dittmann, M.; Rozing, G. P.; Tallareka, U. *J. Chromatogr. A* **2009**, *1216*, 264-273.

(44)   Lindberg, P.; Dahlin, A. P.; Bergstrom, S. K.; Thorslund, S.; Andren, P. E.; Nikolajeff, F.; Bergquist, J. *Electrophoresis* **2006**, *27*, 2075-2082.

(45)   Bonneil, E.; Li, J. J.; Tremblay, T. L.; Bergeron, J. J.; Thibault, P. *Electrophoresis* **2002**, *23*, 3589-3598.

(46)   Koerner, T.; Xie, R. X.; Sheng, F.; Oleschuk, R. *Anal. Chem.* **2007**, *79*, 3312-3319.

(47)   Yassine, M. M.; Lucy, C. A. *Electrophoresis* **2006**, *27*, 3066-3074.

(48)   Cui, H. C.; Horiuchi, K.; Dutta, P.; Ivory, C. F. *Anal. Chem.* **2005**, *77*, 1303-1309.

(49)   Liu, J. K.; Sun, X. F.; Lee, M. L. *Anal. Chem.* **2007**, *79*, 1926-1931.

(50)   Rolland, J. P.; Van Dam, R. M.; Schorzman, D. A.; Quake, S. R.; DeSimone, J. M. *J. Am. Chem. Soc.* **2004**, *126*, 2322-2323.

(51)   Huang, X. H.; Gordon, M. J.; Zare, R. N. *Anal. Chem.* **1988**, *60*, 1837-1838.

(52)   Huang, B.; Kim, S.; Wu, H.; Zare, R. N. *Anal. Chem.* **2007**, *79*, 9145-9149.

(53)   Huang, B.; Wu, H. K.; Bhaya, D.; Grossman, A.; Granier, S.; Kobilka, B. K.; Zare, R. N. *Science* **2007**, *315*, 81-84.

(54)   Dang, F. Q.; Kakehi, K.; Cheng, J. J.; Tabata, O.; Kurokawa, M.; Nakajima, K.; Ishikawa, M.; Baba, Y. *Anal. Chem.* **2006**, *78*, 1452-1458.

(55)   Wang, Y. C.; Choi, M. N.; Han, J. Y. *Anal. Chem.* **2004**, *76*, 4426-4431.

Chapter 5

Conclusions and Future Thoughts

5.1 Summary of the Thesis

Microfluidic platforms made using polymer materials such as polydimethylsiloxane (PDMS) have received more and more attention, since Whitesides *et al.* developed soft lithography for rapid prototyping of PDMS microfluidic devices,[1] and Quake *et al.* realized large-scale-integration of PDMS microfluidic devices using multilayer soft lithography (MSL).[2] In this thesis, valve-based multiplex PDMS devices have been explored for proteomic analyses:

1. Techniques were developed for fabrication and packing multiple beds in a PDMS device in order to be compatible with the integration of multilayered in-line microvalves. The method involves soft lithography to fabricate stable weir traps, and new bead introduction techniques (direct injection and punch-pack-plug (3P) techniques) to eliminate bead introduction channels.

2. Design parameters and the performance of PDMS microvalves as electric switches were studied in detail. The phenomenon of current breakthrough of the valves was presented and the mechanism was discussed. These studies guided the integration of electrophoresis methods with valve-based fractionation.

3. An integrated CE-fractionation-SPE-ESIMS peptide analysis on a valve-based microchip was presented for multiplexed proteomic analysis. The system successfully performs electrokinetic separation, followed by fractionation into

multiple channels, SPE extraction and sample cleanup on packed reaction beds, all performed using a multiplexed, hydraulically valved system, with subsequent mass spectral (MS) analysis.

5.2 Multiple Bead Packing

In Chapter 2, techniques were developed for multiple bead packing in a PDMS device. Weirs consisted of 12 μm deep zones connected to 76 μm or 105 μm deep beds for trapping of large beads. We observed that at pressures above 30 psi, the front edge of the packed beads may be pushed into the large triangular region of the weir interface, since PDMS is very soft and easily shaped. A design using pillars/posts was used in the frontier region as a second trap for bead immobilization.[3] The weirs designed in the thesis are used for large bead packing. Small weirs may also be explored to trap smaller beads.

The 3P technique for multiple bead packing facilitates the building of a multiplexed parallel platform. With this packing method designs with larger densities of bead packed beds can be developed for large scale screening. Direct injection techniques for bead packing provides another promising way to introduce beads into microdevices. A stage controlled operation with a specially optimized needle is worth exploring for future development of this technique.

The connection of the chip to ESIMS was obtained by direct insertion of a capillary into the microfluidic channel, which is not the perfect way to make a connection. As shown in Chapter 2, Table 2.1, the current device has a column porosity of 45.6 nL and post column connection ~ 100 nL. A more compact bed

with smaller bead packing could be used to decrease the column porosity. The length of the transfer lines to ESIMS may be minimized to avoid sample diffusion and obtain rapid sample acquisition. Lots of effort has been put into the integration of in-line ESI tip,[4-6] including in-line PDMS tip.[7] Fabrication of fully integrated HPLC and in-line ESI emitter on polymeric chip has been commercialized by Agilent.[6] It will be beneficial to explore the fabrication method for an in-line PDMS ESI tip in multilayered PDMS devices.

5.3 PDMS Microvalves as Electric Switches

In Chapter 3, the phenomenon of current breakthrough of the valves was presented and the mechanism was discussed with two possible breakthrough pathways. Surface breakthrough may arise from surface conduction or nanochannel conduction. Further study on the relationship of surface roughness and breakthrough may provide interesting information for nanofluidics/double layer system/surface conduction.

The electrical breakdown of PDMS thin membranes in multilayered PDMS devices provides a simple and convenient way to fabricate single nanopores. Nanopore formation and transport is a very interesting field.[8-10] The systematic study of single nanopore formation and study of nanopore transport (such as DNA, protein transport through nanopores) may be interesting.

Table 5.1 Comparison of detection sensitivity by different systems to ESIMS

Work	Device	SPE	MS	Flow rate / μL/min	Sample	Detection
Ours	PDMS chip - CE - multiple SPE-tapered capillary emitter	30 μm Oasis® HLB	API 150EX single quadrupole (Applied Biosystems / MDS Sciex)	Several	8 – 80 nM tryptic digest	S/N 11, 21 52 for 16, 80, 160 fmol
2007[11]	Microsph-ere entrapped emitter at capillary exit	3 μm octadecyl silane	API 3000 triple quadrupole (MDS-Sciex)	0.8	464 nM leucine enkephal-in	S/N 21 and 115 for 23 and 696 fmol
2002[12]	SPE cartridge - tapered capillary emitter	styrene divinyl benzene impregn-ated membr-ane	Quadrupole /time of flight Q-TOF II (Micromas)	0.5	1- 100 ng/mL peptides and tryptic digest	LODs 8–80 fmol
2006[7]	PDMS chip - SPE – in-line emitter	5 μm polysty-rene	Ettan TOF (Amersham Bioscience)	0.7	10 ng/mL peptides	S/N 66 for 430 fmol angiotensin II
2005[6]	polyimide chip - SPE-HPLC-in-line emitter	5 μm ZORB-AX 300SB-C18	Agilent 1100 MSD trap SL	0.1 – 0.4	20 fmol BSA digest	Subfemto-mole
2005[13]	PDMS chip - SPE – CE – in-line emitter	5 μm polysty-rene	Ettan TOF (Amersham Bioscience)	EOF driven		LODs: 0.3 pmol for neurotensin and 0.9 pmol for leucine enkephalin

Continued

150

2002[14]	auto-sampler glass chip - SPE – CE – tapered capillary emitter	mixed 40 / 5 μm C18	Q-Star quadrupole /time-of-flight (MDS /Sciex)	EOF driven	5 nM leucine enkepha-lin, CE injection 10 – 20 nL	LOD: 25 fmol (2.5 fmol detected for MS)
2000[15]	glass chip – sample stacking using polarity switching – CE – tapered capillary emitter		Q-Star quadrupole /time-of-flight (MDS /Sciex)	EOF driven	0.1 – 1000 ng / mL peptides, CE injection 10 nL	LODs: 0.34 – 3.94 nM (3.4 – 39.4 amol)
	without stacking				0.5 nL CE injection	LODs: 8.2 - 24.3 nM (4.1 – 12.2 amol)
2008[4]	glass chip – CE – integrated in-line emitter		Micromass QT of Micro MS (Waters Corp.)	0.04 (electro-kinetic-based hydraul-ic pump)	0.2 mg/mL protein; 5 μM tryptic digest	6 fmol protein, 3 fmol digest analyzed; no report on LOD

5.4 Multiplexed Proteome Analysis Device

A coupled CE-fractionation-SPE-ESIMS peptide analysis system on a valve-based microchip was presented for multiplexed proteomic analysis. The device design needs to be further optimized for application to proteomic analyses.

The following discussion for device optimization was divided into three sections. First, the sensitivity of the current system was evaluated, then compared with other similar systems in the literature, in order to identify the sensitivity-

related parameters that require optimization. In the second section, sensitivity losses from the separation method are specifically discussed, to identify the close relationship between sensitivity and device design for separation and fractionation. Finally, potential ways to optimize the device design for real applications are proposed and summarized.

5.4.1 Comparison of Sensitivity

Proteomic analyses with MS detection usually deals with sub-picomole or even smaller amount of samples. Sensitivity is one of the important parameters involved in determining system performance. As shown in Chapter 2 and 4, measurements in a single SPE-ESIMS channel show that a 16 fmol loading amount is detectable and 80 fmol gives reliable and quantifiable results. In the CE-multiple SPE-ESIMS device, a 220 fmol digest loading, i.e., a maximum amount of 220 fmol for individual peptides, gives a nice spectrum. The system detection limit is obviously in the femtomole range, using a single quadrupole Sciex API 150EX (Applied Biosystems / MDS Sciex, Foster City, CA, USA) with pressure driven flow at several μL/min.

Such detection sensitivity is consistent and comparable to other developed systems, as shown in Table 5.1. Most of the systems developed for ESIMS analysis of peptides have a detection limit in the femtomole range. Enrichment steps can be introduced either prior to the CE/LC step or right before the MS detection. The reports cited vary in term of the devices, SPE characters, flow rate, mass spectrometer, samples and detection sensitivity, but in general detection

sensitivity is sample dependent. The direct coupling of SPE – ESIMS, shows a limit of detection (LOD) of 1 fmol (estimated),[11] 8 – 80 fmol[12] and 20 fmol (estimated).[7] A compact on chip SPE-HPLC-integrated in-line emitter developed by Agilent gives an LOD in the subfemtomole range, with the ability to use very low flow rates of 100 nL/min.[6] A PDMS chip coupling SPE – CE – integrated in-line emitter has an LOD in the subpicomole range.[13] A glass chip coupling SPE – CE – integrated tapered capillary emitter, interfaced with an autosampler, produced an LOD of 25 fmol, where only 2.5 fmol was actually detected by MS considering that only 10% of the sample was injected to the CE step.[14] An attomole detection sensitivity can be obtained by CE – ESIMS with or without sample stacking.[15] Direct integrated chip CE MS can provide a much lower flow rate,[4] resulting in high sensitivity. Our system detection limit is in the femtomole range, which is reasonable and comparable to other reports considering the flow rate (several µL/min) and mass spectrometer (an old single quadrupole) we used. Such sensitivity is good for proteomic analyses and can be further improved, as discussed below.

The mass sensitivity in ESI-MS is closely related to the device design, flow rate, mass spectrometer, and samples. Sensitivity can be improved using lower flow rate and better mass spectrometers.[16] In addition, better sensitivity is expected with smaller bead size than we used in our SPE stage, a more compact stationary phase, and reduced transfer line volume. The extraction and elution in large beds packed with large SPE beads, travelling through long post column connections to MS (Chapter 2, Table 2.1) caused extra band broadening and

sample dilution in our design, which will cause some sensitivity loss. Another

sensitivity loss comes from the separation resolution, as discussed in the next

section.

Table 5.2 Comparison with different separation efficiency

		CZE		IEF
Device	width / μm; depth / μm	100; 12		100; 12
	injector length	200 μm		3 cm
	fractionator to injector / cm	2.55 – 3.71		
	each collection zone length / mm	1.5		1.5
Efficiency		1×10^5 N/m	7×10^5 N/m	0.1 pH
Injection	volume / nL	0.24	0.24	36
	concentration / mM	1	0.25	0.0017
	amount / fmol	240	60	60
Separation	baseline peak band width range / mm	3 - 3.7	1.1 – 1.4	0.43
	volume / nL	~ 4	~ 1.5	0.5
	concentration / mM	0.06	0.04	0.12
Fractionation	volume / nL	~ 1	1.5	0.5
	concentration / mM	0.06	0.04	0.12
	amount / fmol	60	60	60
Sensitivity		reliable detection with 240 fmol injected; estimated LOD 20 fmol	reliable detection with 60 fmol injected; estimated LOD 5 fmol	reliable detection with 60 fmol; estimated LOD 5 fmol

5.4.2 Sensitivity Loss from Separation

In the CE-multiple SPE-ESIMS device, there is some sensitivity loss due to the mismatch of the separation efficiency and the device design. It will be important to evaluate the system sensitivity with improved separation efficiency in future work. A detailed analysis and calculations of the sensitivity issues is given in the following, and shown in Table 5.2.

During the CE injection step about a 200 μm long CE injection plug gives a sample loading volume V_{inj}, concentration $C_{initial}$, and amount n_{total} of;

$V_{inj} = 200\ \mu m \times 100\ \mu m \times 12\ \mu m = 0.24\ nL$

$C_{initial} = 1\ mM$

$n_{total} = C_{initial}\ V_{inj} = 240\ fmol$

After CZE separation, a 200 μm long injection plug may expand to an about 3.5 mm wide peak given the separation efficiency of $1 \times 10^5\ N/m$ obtainable in our uncoated PDMS devices. This volume is large enough to be fractionated and collected in four beds. With a sample concentration $C_{fraction}$, loading an amount to each bed of $n_{fraction}$, with a loading volume to each bed of $V_{fraction}$;

$C_{fraction} = C_{initial} \times (200\ \mu m\ /\ 3.5\ mm) = 0.06\ mM$

$n_{fraction} = n_{total}\ /\ 4 = 60\ fmol$

$V_{fraction} = (3.5\ mm \times 100\ \mu m \times 12\ \mu m)\ /\ 4 = 1\ nL$

As we can see, the CZE separation causes sample dilution. The low-resolution separation and poorly matched fractionation zone lengths lowers the sample amount collected in each channel. For a peak fractionated into four channels, the sensitivity is decreased by 4.

In Chapter 4, CZE separation of peptides without any surface coatings on the PDMS was carried out in the multiplexed proteome device, which gave efficiencies of $1.2 - 2.8 \times 10^5$ N/m. Such efficiencies give baseline peak widths in the fractionation and collection zone (a distance of $2.55 - 3.71$ mm from the injector) in the range of 1.8 mm to 3.3 mm. Peptides were fractionated and collected into one to four beds for MS detection. Thus for some peptides 240 fmol loading gives reliable MS results and the estimated LOD will be about tens of femtomols. However, for most samples the separation efficiency and device design is not well matched. For optimization, one possibility is to change the fractionation segment length in the separation channel, so that each peptide can be fractionated into one or two beds. However, as we extend the length of each segment, we inevitably increase the length of the separation channel and make each peak wider (equation 4.3, Chapter 4), which makes this idea less valid. Another possibility is to make a strong effort to obtain higher resolution by modifying the surface property of the PDMS, using a different separation scheme, or changing the device material.

Using typical plates of 7×10^5 N/m (or higher) obtainable by CZE for separation of peptides in a glass channel[4, 17] or a permanently coated PDMS device[18] for calculation, the baseline peak widths in the fractionation and collection zone (a distance of $2.55 - 3.71$ mm from the injector) are in the range of 1.1 mm to 1.4 mm, as shown in Table 5.2. Since the length of each fractionation section was 1.5 mm, peptides are thus predicted to be fractionated and collected into a single bed or no more than two beds. Thus a 60 fmol CE

loading can give reliable MS results. The estimated LOD will be several femtomols. So CZE separation with high efficiency in a glass or coated PDMS will provide better sensitivity for the multiplexing concept, compared to the results obtained in the uncoated PDMS device. Strong efforts are thus worth making to modify the surface properties of the material to obtain high resolution separations.

By using CZE, the injection volume is limited to subnanoliter, so a high concentration sample is needed. By extending the injection volume using sample stacking,[15] the loading volume may be increased to tens of nanoliters. Even so, only a small portion of sample in the sample reservoir is loaded into the channel, resulting in inefficient sample consumption.

If isoelectric focusing (IEF) is carried out in the device, a large volume of diluted sample can be loaded and focused into narrow bands, as shown in Table 5.2. For a 3 cm long device with a pH gradient from 3 to 10, if the device is theoretically able to separate proteins with a pI difference of 0.1 pH units (reasonable on chip[19]), the base bandwidth is about 0.43 mm. With methylcellulose (MC) to minimize adsorption of proteins and EOF, and increase the viscosity of the solution, four GFP peaks were obtained with a base bandwidth of about 280 μm (Chapter 4, Figure 4.14). Using the device we designed, one to three focused bands will be collected into a single SPE bed, and the estimated LOD will be about several femtomols. So IEF also provides better sensitivity for the multiplexing concept, compared to the results in the uncoated PDMS device.

As we compare the separation by CZE and IEF, there are some major differences: small/large loading volume, low/high efficient sample utilization, dilution/enrichment after separation, wide/narrow separation bands. Thus, IEF based separation provides higher sensitivity for the multiplexing concept and it is worth exploring IEF-based analyses for the multiplexing idea. For the device studied about 1 mM protein concentration is needed. With a coated device this drops to 1/4 mM, and if sample stacking is also used this could drop to ~ 1/40 mM. For IEF a protein concentration of 0.0017 mM could feasibly be studied in our device.

5.4.3 Optimization of the Device

Based on the discussion in the above two sections and the work in this thesis, optimization of the device and potential future work on the device is proposed and summarized below.

To optimize the current device, one effort should explore a compact bed design packed with a smaller bead size, and a minimum post column transfer line, as discussed in Section 5.2. Another important step is to improve the separation resolution and fractionation, as discussed below.

The exploration of permanently coating PDMS device is necessary for high efficiency separation. The hydrophobic surface of PDMS devices causes nonspecific adsorption of hydrophobic analytes to the channel wall. Dynamic coatings were tested to suppress the adsorption, considering their simplicity and convenience. Testing with a dynamic coating such as n-dodecyl-β-D-maltoside

158

(DDM), methylcellulose (MC), or sodium dodecyl sulfate (SDS) in this thesis shows improved efficiency for protein separation. With 0.2% DDM and 0.1% MC coating, proteins Alex-BSA and Alex-trypsin inhibitor were separated, with an efficiency of 2.9×10^4 plates/m for Alex-BSA. With 0.05% SDS, proteins FITC-IgG and FITC-BSA were separated with an efficiency of 9.0×10^4 plates/m for FITC-BSA. However, the separations are still not sufficiently high efficiency or else are not compatible with ESIMS detection due to ionization interference by the surfactants. Permanent coating of PDMS has been demonstrated in the literature. Allbritton's group developed UV induced surface grafting of various hydrophilic homopolymers or copolymers. CE separation of peptides in a modified PDMS device gave an efficiency of $4.8 - 7.4 \times 10^5$ plates/m.[18] Lin's group developed a way to graft epoxy-modified polymers on PDMS, through plasma oxidation of PDMS, adsorption of epoxy-modified polymers based on H-bond interaction, and crosslinking of epoxies of polymer and silanols on oxidized PDMS surfaces by heating at 110 ℃. Satisfactory CE separations of basic proteins, peptides and DNA fragments were obtained, with an efficiency of 10^6 plates/m for lysozyme.[20] Thus, high resolution separation of proteins and peptides in permanently coated PDMS device is possible and can be explored in our group in the future. However, it must be noted that these are relatively complex coating procedures that could lead to difficulties in device yield through non-uniformity of the coatings, clogging during coating, or other problems.

Table 5.3 Fractionation capability of CZE-based and IEF-based device

		CZE	IEF	
Separation	Efficiency	7×10^5 N/m	0.1 pH	
	Length / cm	4	3	
	Baseline band width / mm	~ 1.5 mm at 4 cm separation length	0.43 (with pH gradient 3 to 10)	
Fractionation	Each section length / mm	gradually increased from 0.5 mm to 2.0 mm at 0 to 4 cm separation length	0.93	0.46
	Section number	20 – 40	32	64
	Operation	temporally	spatially	
Collection		Some samples not collected in a single run; flexibility of collecting samples by timing	Almost all samples collected in a single run	

In a second approach, a device with higher fractionation capability needs to be explored. The current device was tested for CZE separation of peptides with eight collection channels. IEF was not done, considering the complexity of coating PDMS and matching the coating demands with ESIMS. To deal with real samples the device will need more collection channels. This exploration can utilize either CZE or IEF separation. A comparison of the fractionation capability of CZE- and IEF-based devices is shown in Table 5.3. A 4 cm long CZE based device with an efficiency of 7×10^5 N/m can result in 20 – 40 fractionation sections, using fractionation section lengths in a range of 0.5 mm to 2 mm. A 3 cm long IEF based device capable of separating proteins with 0.1 pH difference can result in

32 – 64 fractionation sections, using fractionation section lengths of 0.46 to 0.93 mm. Therefore, IEF-based devices provide a higher fractionation capability than CZE based device. With a CZE based device, some samples may not be collected in a single run, although this also gives the flexibility of collecting samples by timing the delivery to the fractionation zone, allowing a shorter zone if multiple runs are employed. With an IEF based device, almost all samples must be collected in a single run, and the fractionation zone should be as long as the separation zone.

Other details can be considered for optimization, as shown in Figure 5.1. For example, double multiplexing valves can be located on each channel prior to the fractionation zone and post to the column zone for controlling channels individually, in order to minimize possible downstream carryover. To minimize electrodispersion during fractionation due to the side branches in the zone, narrower side channels may be used[21] or microvalves may be integrated as close as possible to the main channel to block the side branches. For IEF integration, valve defined channels can be included in the design for better sample loading.[22] Furthermore, the device can be adjusted to do other work, like separation of proteins, SPE extraction proteins, in-situ digestion of trapped proteins, and MS analysis of eluted peptides. The SPE columns can be changed to long HPLC columns to integrate a second separation to improve separation resolution. Alternatively, beds containing trypsin digestion beads can be added before the SPE columns to speed up protein digestion.
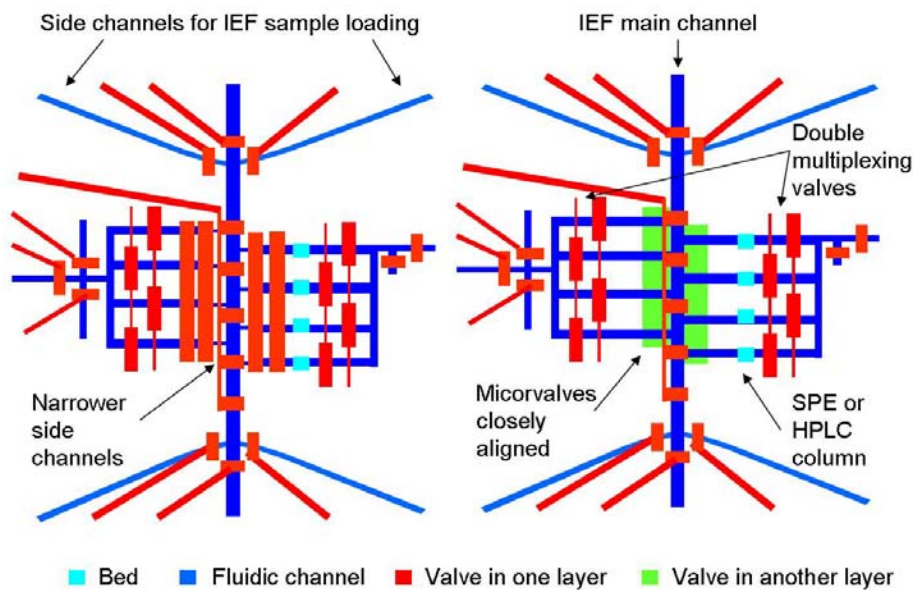
Figure 5.1 Potential designs of IEF-based device with four collection channels for demonstration: (left) a two-layer device with narrower side branches and close microvalves to the main channel; (right) a three-layer device with microvalves closely aligned to the main channel.

In the last stages of drafting this thesis, we realized that the way we closed the fractionation valves might cause leakage and mixing between fractionation zones. As the valves closed the volume under them is forced into the fractionation zones. In the centre zones this effect will cause flow into the outer fractionation zones, possibly causing mixing. The extra big signal seen at channel B1 could arise from this effect, depending on the order in which the simultaneously actuated valves happen to close. Opening the side valve that blocks the SPE beds would provide a path to dump the volume under the valve without causing flow or mixing between fractionation zones. This approach will need to be tested. It might lead to better resolution in the current device. It might also avoid building up of more peptides

in zone B1, should that have occurred because valve B1 happened to be the last one to fully close.

5.5 References

(1)   Xia, Y. N.; Whitesides, G. M. *Annu. Rev. Mater. Sci.* **1998**, *28*, 153-184.

(2)   Thorsen, T.; Maerkl, S. J.; Quake, S. R. *Science* **2002**, *298*, 580-584.

(3)   Flemming, J. H.; Baca, H. K.; Werner-Washburne, M.; Brozik, S. M.; Lopez, G. P. *Sens. Actuators B* **2006**, *113*, 376-381.

(4)   Mellors, J. S.; Gorbounov, V.; Ramsey, R. S.; Ramsey, J. M. *Anal. Chem.* **2008**, *80*, 6881-6887.

(5)   Hoffmann, P.; Eschner, M.; Fritzsche, S.; Belder, D. *Anal. Chem.* **2009**, *81*, 7256-7261.

(6)   Yin, N. F.; Killeen, K.; Brennen, R.; Sobek, D.; Werlich, M.; van de Goor, T. V. *Anal. Chem.* **2005**, *77*, 527-533.

(7)   Lindberg, P.; Dahlin, A. P.; Bergstrom, S. K.; Thorslund, S.; Andren, P. E.; Nikolajeff, F.; Bergquist, J. *Electrophoresis* **2006**, *27*, 2075-2082.

(8)   Smeets, R. M. M.; Kowalczyk, S. W.; Hall, A. R.; Dekker, N. H.; Dekker, C. *Nano Lett.* **2009**, *9*, 3089-3095.

(9)   Howorka, S.; Siwy, Z. *Chem. Soc. Rev.* **2009**, *38*, 2360-2384.

(10)   Talaga, D. S.; Li, J. L. *J. Am. Chem. Soc.* **2009**, *131*, 9287-9297.

(11)   Koerner, T.; Xie, R. X.; Sheng, F.; Oleschuk, R. *Anal. Chem.* **2007**, *79*, 3312-3319.

(12)   Bonneil, E.; Li, J. J.; Tremblay, T. L.; Bergeron, J. J.; Thibault, P. *Electrophoresis* **2002**, *23*, 3589-3598.

(13)   Dahlin, A. P.; Bergstrom, S. K.; Andren, P. E.; Markides, K. E.; Bergquist, J. *Anal. Chem.* **2005**, *77*, 5356-5363.

(14)   Li, J. J.; LeRiche, T.; Tremblay, T. L.; Wang, C.; Bonneil, E.; Harrison, D. J.; Thibault, P. *Molecular & Cellular Proteomics* **2002**, *1*, 157-168.

(15)   Li, J. J.; Wang, C.; Kelly, J. F.; Harrison, D. J.; Thibault, P. *Electrophoresis* **2000**, *21*, 198-210.

163

(16)   Maxwell, E. J.; Chen, D. D. Y. *Anal. Chim. Acta* **2008**, *627*, 25-33.

(17)   Lacher, N. A.; de Rooij, N. F.; Verpoorte, E.; Lunte, S. M. *J. Chromatogr. A* **2003**, *1004*, 225-235.

(18)   Hu, S. W.; Ren, X. Q.; Bachman, M.; Sims, C. E.; Li, G. P.; Allbritton, N. *Electrophoresis* **2003**, *24*, 3679-3688.

(19)   Sommer, G. J.; Hatch, A. V. *Electrophoresis* **2009**, *30*, 742-757.

(20)   Lion, N.; Rohner, T. C.; Dayon, L.; Arnaud, I. L.; Damoc, E.; Youhnovski, N.; Wu, Z. Y.; Roussel, C.; Josserand, J.; Jensen, H.; Rossier, J. S.; Przybylski, M.; Girault, H. H. *Electrophoresis* **2003**, *24*, 3533-3562.

(21)   Buch, J. S.; Rosenberger, F.; Highsmith, W. E.; Kimball, C.; DeVoe, D. L.; Lee, C. S. *Lab Chip* **2005**, *5*, 392-400.

(22)   Shimura, K.; Takahashi, K.; Koyama, Y.; Sato, K.; Kitamori, T. *Anal. Chem.* **2008**, *80*, 3818-3823.

Appendix

A.1 Off-chip Operation for Solution Loading and Pressure

Control

Figure A.1 Schematic drawing of the operating system: 1 - 5, gas cylinder; V1 - V20, valves; R1 – R3, regulator; p1 – p3, pressures.

1. Add chemicals when V_5, V_6, V_7, V_8, V_9, V_{12} and V_{15} are closed;
2. Close all valves.
3. Open gas cylinder (max 30 psi).
4. Open V_1 when V_5, V_6, V_7, V_8 and V_9 are closed.
5. Open V_2.
6. Adjust R_1 to P_1, then lock it.
7. Open V_5, V_6 and V_7.
8. Close V_1.
9. Adjust the cylinder regulator (max 60 psi).
10. Open V_{10} when V_{12} is closed.
11. Adjust R_2 to P_2, then lock it.
12. Open V_{12}.
13. Close V_{10}.
14. Adjust the cylinder regulator (max 60 psi).
15. Open V_{13} when V_{15} is closed.
16. Adjust R_3 to P_3, then lock it.

17. Open V$_{15}$.
18. Close V$_{13}$.

A.2 Sequence Structure for Peptides in Table 4.2

The pKa values are cited from Biophysical chemistry (John T. Edsal and Jeffries Wyman, Academic Press, 1958, chapter 8). The pKa value depends on temperature, ionic strength, and the microenvironment of the ionizable group.

1. 585.0^{+2} TGPNLHGLFGR (Thr-Gly-Pro-Asn-Leu-His-Gly-Leu-Phe-Gly-Arg)
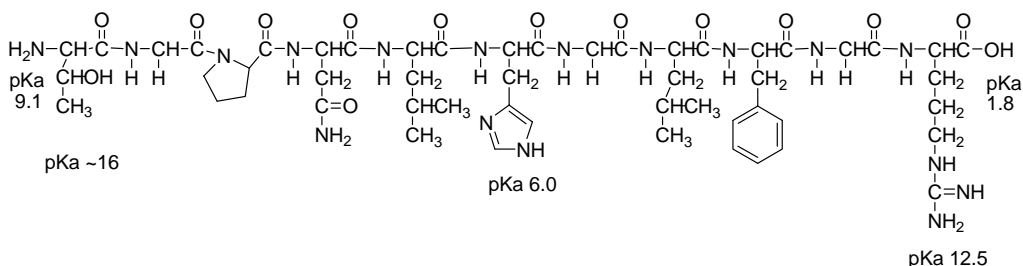
2. 648.5^{+2} TGPNLHGLFGRK (Thr-Gly-Pro-Asn-Leu-His-Gly-Leu-Phe-Gly-Arg-Lys)
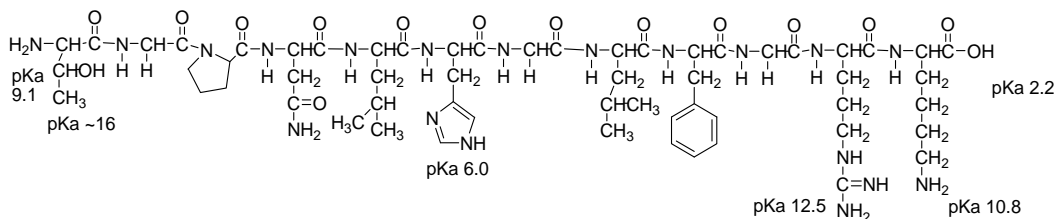
3. 589.5^{+1} AcetNGDVEK (AcetN-Gly-Asp-Val-Glu-Lys)
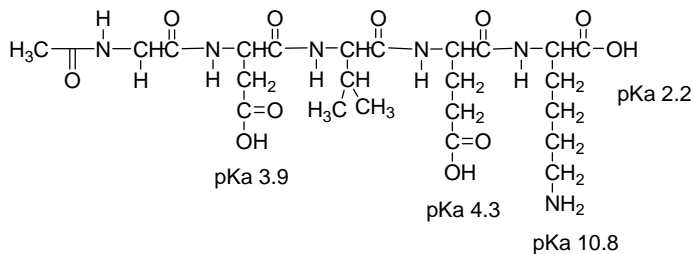
4. 779.5^{+1} MIFAGIK (Met-Ile-Phe-Ala-Gly-Ile-Lys)
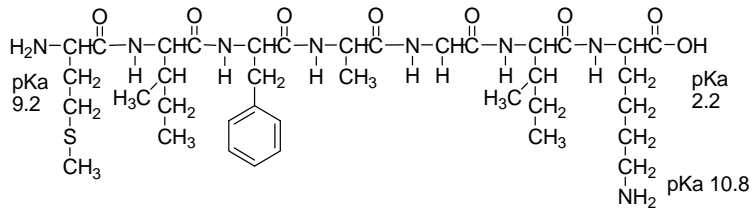
5. 678.5^{+1} YIPGTK (Tyr-Ile-Pro-Gly-Yhr-Lys)
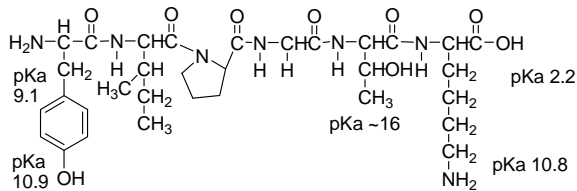
6. 818.0^{+2} CAQCHTVEK(Heme) (Cys-Ala-Gln-Cys-His-Thr-Val-Glu-Lys (heme)
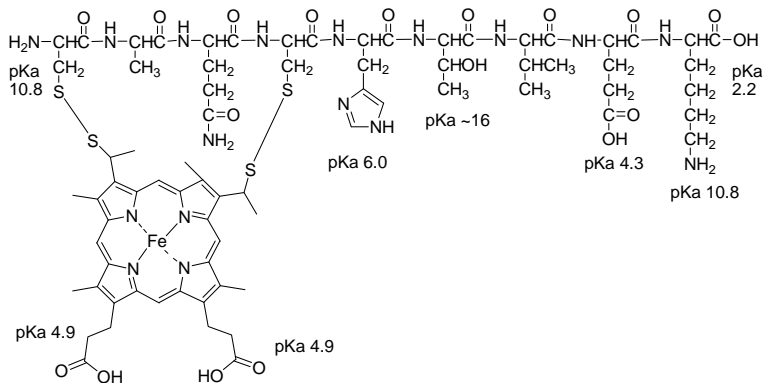
7. 748.5^{+2} EETLMEYLENPK (Glu-Glu-Thr-Leu-Met-Glu-Tyr-Leu-Glu-Asn-Pro-Lys)
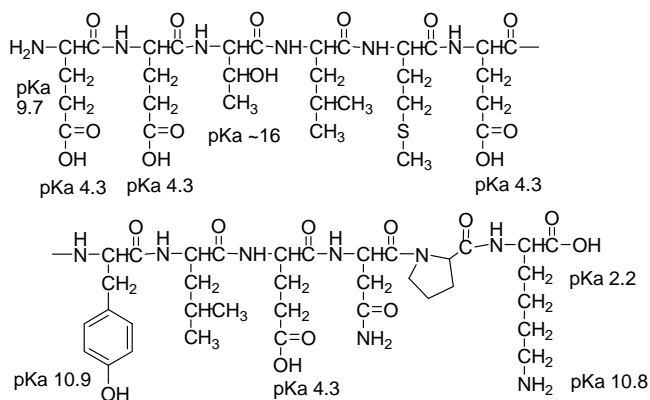
8. 756.5^{+2} EETLM(Met-Ox)EYLENPK (Glu-Glu-Thr-Leu-Met-Met-Ox-Glu-Tyr-Leu-Glu-Asn-Pro-Lys)
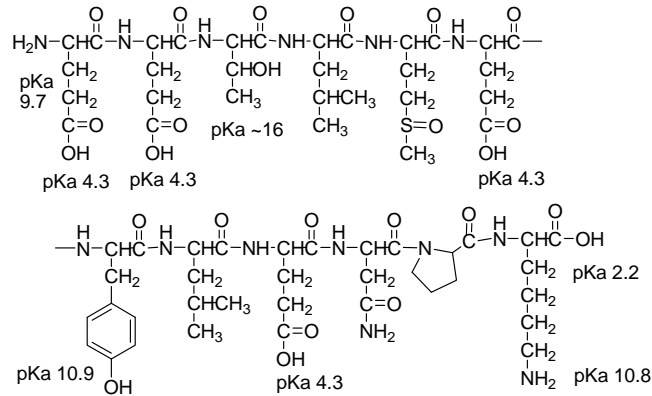
A.3 Derivation of the Relationship between Band Width W and Travelling Length L (Equation 4.3)

Plate height H is constant proportionality between the variance (σ^2) of the band and the distance (L) the band center has migrated:

$$H = \frac{\sigma^2}{L} \tag{A.1}$$

Plate number (N) is given by:

$$N = \frac{L}{H} = \frac{L^2}{\sigma^2} = (\frac{t}{W_t/k})^2 = k^2(\frac{t}{W_x\frac{t}{L}})^2 = k^2\frac{L^2}{W_x^2} \tag{A.2}$$

where t, W_t, W_x, and k is the time, band width in terms of time, band width in terms of distance, and a constant, respectively. For a Gaussian peak, band width W is proportional to σ. The proportionality constants (k) are 2.35 and 6 for the peak width at half height and baseline respectively.

Therefore,

$$W_x = \frac{kL}{\sqrt{N}} = k\sqrt{HL} \propto \sqrt{L}, \tag{A.3}$$

indicating that the band width in terms of distance is proportional to the square root of the distance traveled by the band center. The relationship is true when H is a constant.

Dispersion contributions σ^2 for CE separation follow the equation:

$$\sigma^2{}_T = \sigma^2{}_{diffusion} + \sigma^2{}_{injection} + \sigma^2{}_{detection} + \sigma^2{}_{turn} + \sigma^2{}_{adsorption} + \sigma^2{}_{temp} + \sigma^2{}_{electrodispersion} + \ldots$$

$$= 2D_m \frac{L}{\mu_a E} + \frac{l^2{}_{inj}}{12} + \frac{l^2{}_{det}}{12} + \frac{[2\theta w(1 - \exp(-\frac{w^2 v_c r_c}{2D\theta(r_c + \frac{w}{2})^2}))]^2}{24} + \frac{k' V_{EOF} L}{(1+k')^2}(\frac{r^2 k'}{4D} + \frac{2}{K_D}) + \ldots \tag{A.4}$$

The dominant contributions are column related such as longitudinal diffusion, solute-wall interactions, not other parts such as injection, detection. So it is true that H is a constant. Therefore, we can use the equation $W_x \propto \sqrt{L}$ to estimate the band width at different detection length.

A.4 EOF in PDMS channel with Dynamic Coating
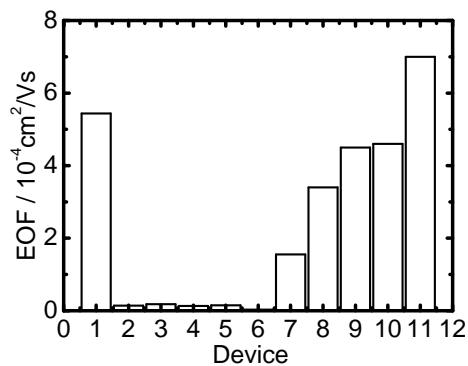
Figure A.2 EOF in PDMS channel with/without coating; device number corresponds to the number listed in Table A.1; *n*-dodecyl-β-D-maltoside (DDM), sodium dodecyl sulfate (SDS), methyl cellulose (MC).

Table A.1 EOF in PDMS device

	Device	EOF ($10^{-4}cm^2$ /V·s)
1	Native PDMS	5.44
2	0.2% DDM + 0.1% MC	0.14
3	0.25% DDM + 0.03% MC	0.18
4	0.25% MC	0.13
5	0.5% MC	0.15
6	1% MC	0.031
7	0.1% DDM	1.55
8	0.1% DDM + 0.025% SDS	3.4
9	0.1% DDM + 0.05% SDS	4.5
10	0.1% DDM + 0.075% SDS	4.6
11	0.05% SDS	7.0

A.5 Oasis® HLB Beads
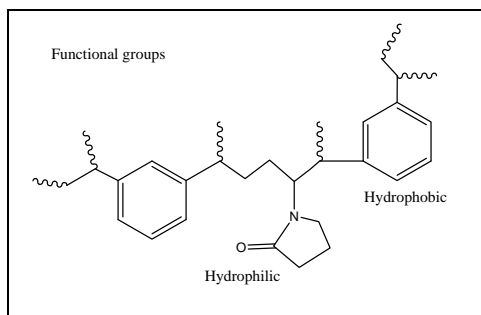
Stability at pH extremes 0-14; Water-wettable; specific surface area, 810 m^2/g, average pore diameter, 80 Å; total pore volume, 1.3 cm^3/g; average particle diameter: 30 or 60 μm.

A.6 Voltage Control
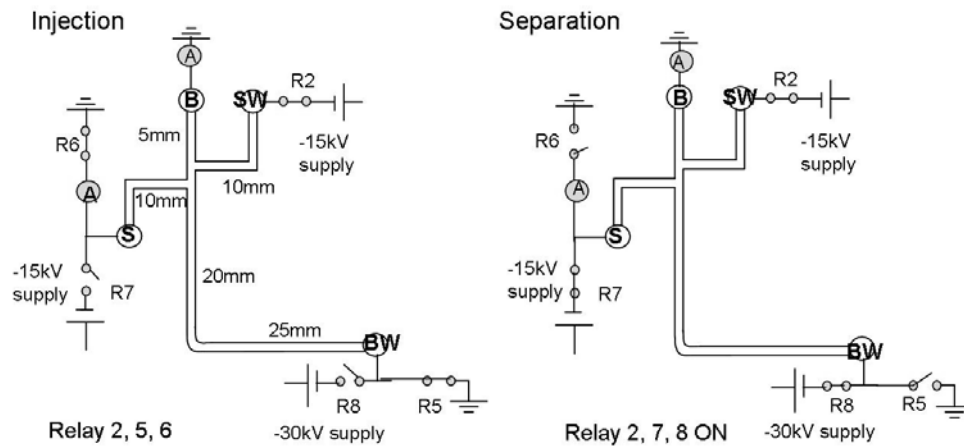
Figure A.3 Voltage control for sample injection and separation (S –sample, SW – sample waste, B – buffer, BW – buffer waste; Injection, S, B, and BW grounded, SW connected to high voltage to set injection voltage; separation, B grounded, S, SW connected to high voltage to set pushback voltages, BW to high voltage to set separation voltage).